



## Scleral structure and biomechanics

Craig Boote<sup>a,b,c,\*,1</sup>, Ian A. Sigal<sup>d,1</sup>, Rafael Grytz<sup>e,1</sup>, Yi Hua<sup>d,1</sup>, Thao D. Nguyen<sup>f,1</sup>, Michael J.A. Girard<sup>b,g,1</sup>

<sup>a</sup> Structural Biophysics Research Group, School of Optometry & Vision Sciences, Cardiff University, UK

<sup>b</sup> Ophthalmic Engineering & Innovation Laboratory (OEIL), Department of Biomedical Engineering, National University of Singapore, Singapore

<sup>c</sup> Newcastle Research & Innovation Institute Singapore (NewRIIS), Singapore

<sup>d</sup> Laboratory of Ocular Biomechanics, Department of Ophthalmology, University of Pittsburgh, USA

<sup>e</sup> Department of Ophthalmology & Visual Sciences, University of Alabama at Birmingham, USA

<sup>f</sup> Department of Mechanical Engineering, Johns Hopkins University, USA

<sup>g</sup> Singapore Eye Research Institute (SERI), Singapore National Eye Centre, Singapore



### ARTICLE INFO

#### Keywords:

Sclera  
Connective tissue structure  
Biomechanics  
Myopia  
Glaucoma  
Ageing

### ABSTRACT

As the eye's main load-bearing connective tissue, the sclera is centrally important to vision. In addition to cooperatively maintaining refractive status with the cornea, the sclera must also provide stable mechanical support to vulnerable internal ocular structures such as the retina and optic nerve head. Moreover, it must achieve this under complex, dynamic loading conditions imposed by eye movements and fluid pressures. Recent years have seen significant advances in our knowledge of scleral biomechanics, its modulation with ageing and disease, and their relationship to the hierarchical structure of the collagen-rich scleral extracellular matrix (ECM) and its resident cells. This review focuses on notable recent structural and biomechanical studies, setting their findings in the context of the wider scleral literature. It reviews recent progress in the development of scattering and bioimaging methods to resolve scleral ECM structure at multiple scales. In vivo and ex vivo experimental methods to characterise scleral biomechanics are explored, along with computational techniques that combine structural and biomechanical data to simulate ocular behaviour and extract tissue material properties. Studies into alterations of scleral structure and biomechanics in myopia and glaucoma are presented, and their results reconciled with associated findings on changes in the ageing eye. Finally, new developments in scleral surgery and emerging minimally invasive therapies are highlighted that could offer new hope in the fight against escalating scleral-related vision disorder worldwide.

### 1. Introduction

Forming around 85% of the outer tunic of the human eyeball, the sclera is a remarkably resilient and structurally complex connective tissue that performs multiple functions critical to vision. Derived from the Greek word “skleros” (meaning “hard”), the sclera's primary role is to provide a firm and stable substrate for the retina and to protect the other mechanically vulnerable internal structures of the eye, while its opacity prevents off-axial light transmission that could otherwise degrade the retinal image. Scleral and corneal geometry are cooperatively regulated to accurately focus light onto the retina. Although under normal conditions the sclera can be considered metabolically quiescent, it is far from inert in a biomechanical sense. Indeed, it is required to maintain optical

stability under highly dynamic loading conditions imposed externally and internally by, amongst other factors, eye movements and a continually fluctuating intraocular pressure (IOP). The sclera's ability to resist deformations that might otherwise impair vision through distortion of the retina or the lens-iris diaphragm relies on biomechanical characteristics imparted by regional specialisations of its connective tissue organisation. In recent years, widening collaboration between clinicians, scientists and engineers has led to significant advances in our understanding of dynamic scleral behaviour. Naturally it follows that we are beginning to perceive with more clarity the central role that the sclera plays in conditions that deteriorate vision. This article aims to summarise and reconcile the findings of these studies as it reviews the state of the art in scleral structure and biomechanics research, considers the

\* Corresponding author. Structural Biophysics Research Group School of Optometry & Vision Sciences Cardiff University, Maindy Road, Cardiff, CF24 4HQ, UK.  
E-mail address: [bootec@cardiff.ac.uk](mailto:bootec@cardiff.ac.uk) (C. Boote).

<sup>1</sup> Percentage of work contributed by each author in the production of the manuscript is as follows: Craig Boote: 50%, Ian A. Sigal: 15%, Rafael Grytz: 10%, Yi Hua: 5%, Thao D. Nguyen: 5%, Michael J.A. Girard: 15%.

<https://doi.org/10.1016/j.preteyeres.2019.100773>

Received 4 June 2019; Received in revised form 7 August 2019; Accepted 8 August 2019

Available online 11 August 2019

1350-9462/ © 2019 Elsevier Ltd. All rights reserved.

**List of abbreviations**

AFM	Atomic Force Microscopy
AI	Artificial Intelligence
CCD	Charge-Coupled Device
CCT	Central Corneal Thickness
CSFP	Cerebrospinal Fluid Pressure
DIC	Digital Image Correlation
ECM	Extracellular Matrix
ESPI	Electronic Speckle Pattern Interferometry
FEM	Finite Element Modelling
GAG	Glycosaminoglycan
IFEM	Inverse Finite Element Modelling
IOP	Intraocular Pressure
LC	Lamina Cribrosa
MPM	Multiphoton Microscopy
MRI	Magnetic Resonance Imaging
OCT	Optical Coherence Tomography
ONH	Optic Nerve Head
OPA	Ocular Pulse Amplitude
PG	Proteoglycan

PLM	Polarized Light Microscopy
PPS	Peripapillary Sclera
PPV	Pars Plana Vitrectomy
PSOCT	Polarization-Sensitive Optical Coherence Tomography
QFDE	Quick Freeze Deep Etch
RGC	Retinal Ganglion Cell
RNFL	Retinal Nerve Fibre Layer
ROI	Region of Interest
SALS	Small-Angle Light Scattering
SAS	Subarachnoid Space
SB	Scleral Buckle
SC	Schlemm's Canal
SEM	Scanning Electron Microscopy
SHG	Second Harmonic Generation
SPLM	Structured Polarized Light Microscopy
SLT	Scleral Laser Trabeculoplasty
TEM	Transmission Electron Microscopy
TPF	Two-Photon Fluorescence
VFM	Virtual Fields Method
WAXS	Wide-Angle X-ray Scattering

implications for ocular ageing and disease, and explores some promising therapeutic avenues in search of novel scleral treatments.

### 1.1. Basic scleral anatomy and function

At its anterior boundary the sclera merges with the corneal

perimeter at the limbus and extends backward to form an approximate sphere of vertical diameter  $\sim 24$  mm. The axial length of the emmetropic adult human eye is 24–25 mm. At the back of the eye, the scleral connective tissue fuses with the dural sheath of the optic nerve, whose entry pierces the sclera about 3 mm nasally and 1 mm downward of the posterior pole. Scleral thickness varies with anatomical position,

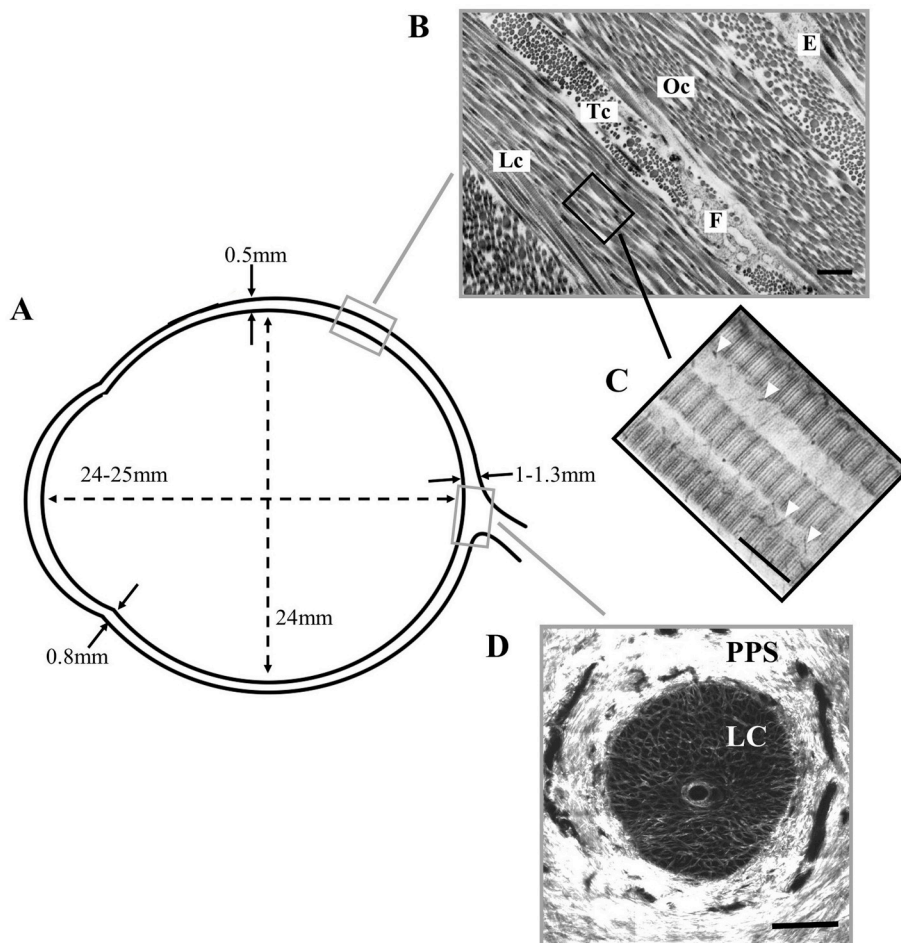


**Fig. 1.** Overview of scleral morphometry and connective tissue structure. **A)** Approximate wall thickness and dimensions of the normal, adult human sclera. **B)** Transmission electron microscopy (TEM) image of the outer scleral stroma, showing lamellar structure formed by collagen fibril bundles in longitudinal (Lc), transverse (Tc) and oblique (Oc) section. A fibrocyte (F) and elastin fibre (E) can also be seen. Bar: 1.5  $\mu$ m. **C)** TEM image of stroma from a different specimen at higher magnification, showing D-periodic banding of individual fibrils in longitudinal section. Proteoglycans are present as fine filaments (arrowheads) associated with the collagen fibrils. Bar: 250 nm. **D)** Second harmonic generation (SHG) image of en-face section through the optic nerve head at mid-stromal depth, showing the fenestrated lamina cribrosa (LC) that supports the exiting retinal nerve axons. The collagen fibril bundles of the neighbouring peripapillary sclera (PPS) adopt a predominantly circumferential orientation in this region. Bar: 0.5 mm. Panel B taken from (Bron et al., 1997) and reproduced with permission of CRC Press Ltd. Panel C adapted from (Watson and Young, 2004) with permission of Elsevier Ltd.

decreasing from 1–1.3 mm at the posterior pole to ~0.5 mm at the equator, before increasing again to ~0.8 mm in the perilimbal sclera. (Fig. 1A).

#### 1.1.1. Tenon's capsule

Tenon's capsule (*fascia bulbi*) is a compact layer of collagen bundles and elastin fibres that lie parallel to the scleral surface. At its anterior origin, Tenon's capsule is anchored firmly to the underlying episclera and the overlying conjunctiva, before becoming more loosely bound to the episclera further back as the capsule coalesces with the perimysium of the recti muscles (Fig. 2). Biomechanically, the Tenon's capsule fulfils an important function in acting as a pulley system to transfer forces from the ocular muscles to the sclera during eye movements (Roth et al., 2002). Accordingly, the collagen bundles and elastin fibres of the anterior Tenon's run broadly perpendicular to the limbus, consistent with the directions of recti muscle force transduction (Park et al., 2016).

#### 1.1.2. Episclera

Lying directly beneath Tenon's capsule, the episclera is a thin but dense layer of connective tissue consisting mainly of collagen bundles sparsely populated with elastic fibres, melanocytes and macrophages (Watson and Young, 2004). The collagen bundles of the episclera run largely circumferentially and render the episclera more difficult to distinguish as a distinct layer by their gradual merging into the connective tissue of the underlying stroma.

#### 1.1.3. Stroma

As the major scleral tissue layer, the stroma (*substantia propria*) dominates the sclera's biomechanical performance. Stromal material properties can be summarised as non-linear viscoelastic, and stem from its collagen-rich extracellular matrix (ECM) composition and organisation. Bundles of parallel-aligned individual collagen fibrils of diameter 25–230 nm, interspersed in places with elastic microfibrils and fibres, form 0.5–6 µm thick lamellae that lie roughly in the plane of the eyeball surface (Fig. 1B). Scleral lamellae overall demonstrate far more branching and interweaving than those of the neighbouring corneal stroma, and the extent of this varies with both tissue depth and anatomical location (Komai and Ushiki, 1991). Superficially, the scleral collagen fibril bundles merge with tendon fibres at the extraocular muscle insertion sites, while in the deepest stromal layers adjacent to the uvea (the *lamina fusca*) they taper and branch to intermingle with the underlying choroidal connective tissue, co-localising with increased numbers of elastic fibres (Marshall, 1995). Unlike the eyes of humans and other primates, the scleral stroma of many non-eutherian vertebrates comprises an inner cartilage layer in addition to an outer fibrous layer (Walls, 1942). Further, the anterior sclera of many birds, reptiles and teleost fish contains a ring of bony plates ('ossicles') (Franz-Ondendaal, 2008) that are thought to provide leverage for the ciliary muscles in facilitating corneal accommodation (Glasser et al., 1994), and into which meridional fibril bundles of the anterior sclera insert (Boote et al., 2008). In the human sclera, regional specialisations of the stromal architecture, as described below, are of particular biomechanical influence.

#### 1.1.4. Perilimbal sclera, scleral spur and trabecular meshwork

On approaching the limbus, the collagen bundles of the deep scleral stroma form a circumcorneal ring-like structure at the scleral spur. Together with the circumferential limbal pseudo-annulus of collagen residing in the posterior one-third of the corneal stroma (Kamma-Lorger et al., 2010; Newton and Meek, 1998), the spur probably helps to maintain the corneal contour in an area of heightened tissue stress imposed by the differing radii of curvature of the cornea and sclera (Boote et al., 2009). Indeed, the use of partial thickness limbal incisions is an established clinical procedure for inducing controlled flattening of the cornea as a means of correcting mild corneal astigmatism. However, not all of the scleral collagen appears to end its forward course at the

limbus, and there is evidence that a significant number of perilimbal scleral collagen bundles continue on into the corneal periphery (Boote et al., 2011), some of which probably originate in the deep sclera (Winkler et al., 2013). At its anterior aspect, the collagen fibrils of the scleral spur taper and become continuous with the connective tissue beams of the corneoscleral trabecular meshwork (Watson and Young, 2004). Here, the innermost layers of the spur, the so-called 'scleral roll', form a bordering substrate for the Schlemm's canal (SC), from whose posterior end an extension of the spur in the direction of the anterior chamber provides an anchor point for attachment of the meridional fibres of the ciliary muscle to facilitate opening of the trabecular beams during aqueous drainage (Hamanaka, 1989). The corneoscleral trabecular beams are further notable for containing significant amounts of elastin (Marshall, 1995; Umihira et al., 1994). These elastic fibres form a tensionally-integrated network that is conserved across species, and appears to be important in tethering the trabecular meshwork to neighbouring tissues - possibly as a design to prevent collapse of out-flow pores during IOP fluctuation (Bachmann et al., 2006; Overby et al., 2014; Rohen et al., 1981; Tektas et al., 2010). The trabecular elastin is probably continuous with the elastic fibre networks observed in the deep limbus (Kamma-Lorger et al., 2010) and the pre-Descemet's stroma of the corneal periphery (Lewis et al., 2016), and the idea of a continuous system of elastic fibres covering the majority of the eye tunic and biomechanically linking the posterior pole to the peripheral cornea is an intriguing possibility that warrants further research.

#### 1.1.5. Peripapillary sclera and lamina cribrosa

On approaching the optic nerve, superficial layers of the stromal connective tissue merge with the dural sheath of the nerve while the remaining deeper scleral fibres become continuous with the lamina cribrosa (LC) - the highly fenestrated stack of interconnected plates that support the exiting retinal ganglion cell (RGC) nerve axons and central retinal artery (Anderson, 1969). The LC and peripapillary sclera (PPS - the 1–2 mm wide region of sclera bordering the nerve canal opening) collectively form the connective tissue of the optic nerve head (ONH) (Fig. 1D) - a region of key biomechanical interest in glaucoma (Downs, 2015). Here the scleral collagen fibrils are more uniform in diameter, show greater spatial order and associate with increased numbers of elastin fibres compared to other regions of the posterior segment (Quigley et al., 1991). A key biomechanical feature of the PPS is the circumferential pseudo-annulus of collagen that surrounds the LC (Gogola et al., 2018b; Pijanka et al., 2012; Winkler et al., 2010) that is probably necessary to limit canal expansion under IOP-loading (Girard et al., 2009a; Grytz et al., 2011).

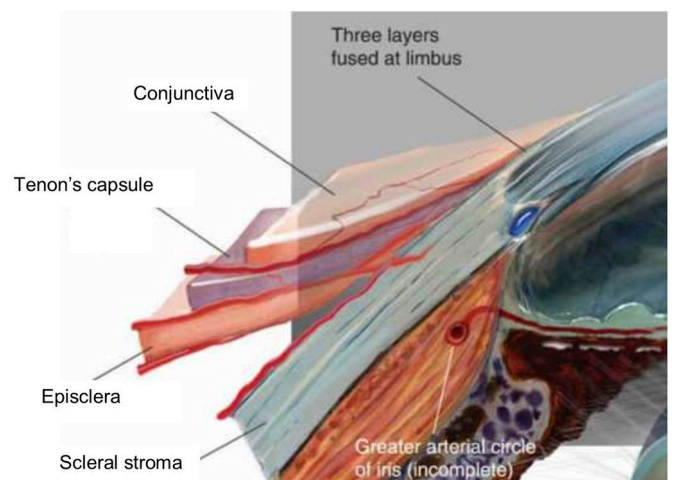


Fig. 2. Anatomy of the anterior segment of the eye, showing the various scleral tissue layers. Adapted with permission from <https://eyeanatomyblog.wordpress.com/2012/10/15/the-limbus>.

**Table 1**  
Approximate composition of the human sclera. Data taken from (Meek, 2008).

Component	% of wet weight
Water	68
Collagens	28
Other proteins (including cell components)	< 3
Proteoglycans	< 1
Elastin	0.6

## 1.2. Scleral composition

The composition of the sclera follows that of other connective tissues in being primarily a scaffold of fibrous collagen in a hydrated inter-fibrillar matrix of proteoglycans and glycoproteins (Table 1). Notwithstanding notable increases in the lamina fusca, perilimbal sclera and PPS, the overall content of elastin fibres in the sclera is small at around 2% of the dry weight (Watson and Young, 2004). Understandably from a metabolic perspective, the quiescent sclera displays low cellularity with transient increases shown in response to pathology or physical insult.

### 1.2.1. Collagens

In the sclera, type I collagen is by far the major contributor at around 95%, with types III, V and VI making up the remaining 5% (Keeley et al., 1984; Thale and Tillmann, 1993). Scleral collagen structure is hierarchical (Fig. 3). Tropocollagen molecules of length ~300 nm are composed of three polypeptide alpha-helix chains of repeating Gly-X-Y amino acid sequences (Bailey et al., 1998). Five such molecules assemble to form ~4 nm diameter collagen microfibrils, in which adjacent molecules are axially staggered by 67 nm (the D-period – see Figs. 1C and 3) (Piez and Miller, 1974). Parallel arrays of microfibrils assemble into fibrils, such that individual microfibrils are slightly inclined (about 5°) to the fibril axis (Yamamoto et al., 2000). Collagen fibrils, in turn, assemble into irregular bundles that ultimately form the scleral lamellae. Scleral collagen fibrils are heterotypic: studies of macular sclera indicated interstitial collagen fibrils of co-polymerised types I/III, with type V residing at the fibril surface and type VI forming inter-bundle filament structures (Marshall et al., 1993). The presence of types V and VI at and between fibril surfaces suggests likely roles in fibril assembly and diameter regulation, as envisaged in other tissues (Izu et al., 2011; Linsenmayer et al., 1993; Wenstrup et al., 2004). In contrast to some other connective tissues, such as tendon, collagen in the sclera does not assemble into discrete structures of a regular size beyond the fibril level. However, the general term “fibre” is used widely

in the biomechanics literature to refer to the suprafibrillar collagen arrangement of the sclera and will also be used in this review. It should also be noted that some techniques that utilise visible light to examine suprafibrillar scleral microstructure (see s2.1.2 and s2.1.4) will contain both collagen and elastin components in their “fibre” signal.

### 1.2.2. Proteoglycans

Proteoglycans (PGs) inhabit the collagen interfibrillar space and help to mediate fibril size and organisation. PGs consist of a protein core with one or more attached glycosaminoglycan (GAG) sidechains of repeating disaccharide units of either chondroitin sulfate, dermatan sulfate, keratan sulfate or heparin sulfate. The main sulfated PGs present in sclera are aggrecan, decorin and biglycan (Rada et al., 1997, 2000). Sulfate residues on the GAG chains impart negative charge that binds water and creates an incompressible “gel” that is ideal for mediating load transfer between the embedded scleral collagen fibrils. Evidence for the importance of PGs in maintaining scleral structure and biomechanics includes findings from research in knock-out mouse models (Austin et al., 2002; Chakravarti et al., 2003) and from enzyme digestion studies in pig (Muriene et al., 2015; Zhuola et al., 2018) and human (Muriene et al., 2016) sclera. The role of aggrecan in the sclera is not well understood. Aggrecan is a large proteoglycan normally found in cartilage. Due to its many attached glycosaminoglycan sidechains, aggrecan provides osmotic properties that produce a swelling pressure. In cartilage, this swelling pressure plays a critical role in withstanding compression forces, but the importance of swelling pressure in the sclera is unclear.

### 1.2.3. Elastic fibres

The elastic fibre network is a proportionately small but functionally important part of the scleral ECM, in particular in the deep tissues of the perilimbal sclera/trabecular meshwork (Marshall, 1995) and throughout the ONH (Quigley et al., 1991) where concentrations are notably increased. Mature scleral elastic fibres consist of an amorphous elastin core sheathed by an aligned scaffold of fibrillin-rich microfibrils. Outside of the trabecular meshwork (see s1.1.4), the significance of scleral elastic fibres to the structural integrity, shape and viscoelastic behaviour of the eyeball is not well understood, but is coming under increasing scrutiny motivated by identified links between systemic microfibril disorders and ocular pathologies such as myopia and glaucoma (Kuchtey and Kuchtey, 2014; Robinson and Booms, 2001).

### 1.2.4. Fibroblasts

With the exception of the lamina fusca, most regions of the sclera are sparsely populated by cells until challenged by pathology, injury or

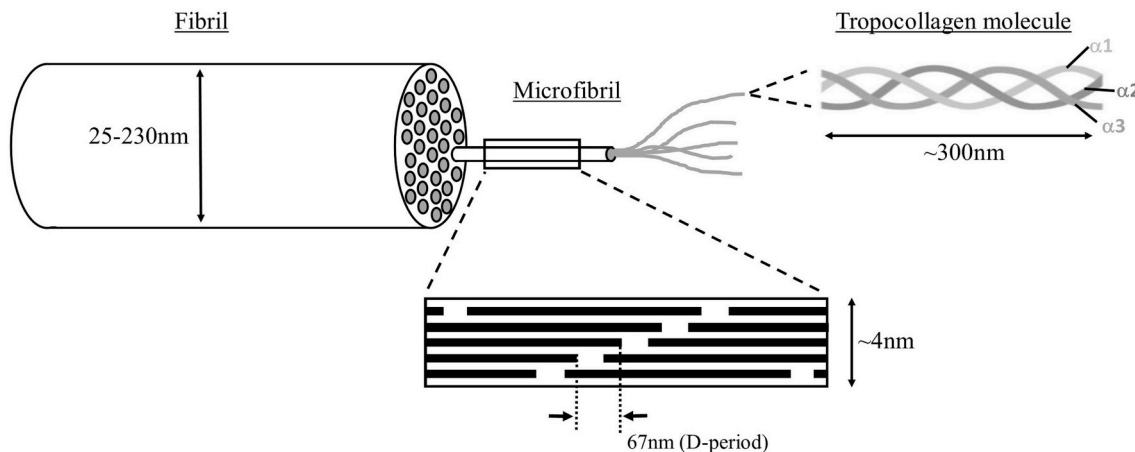


**Fig. 3.** The hierarchical structure of scleral collagen (not to scale). Five triple alpha-chain tropocollagen molecules assemble into microfibrils, in which the axial stagger of individual molecules leads to gap/overlap regions that define the 67 nm axial D-period. Varying numbers of near-parallel microfibrils form collagen fibrils of diameters ranging from 25 to 230 nm. The microfibrils are actually inclined by ~5° to the fibril axis, but this is not shown in this simplified diagram.

infection. The resident cell of the scleral stroma is the fibrocyte, which undergoes transformation into the active fibroblast upon insult. Fibroblasts are responsible for synthesis of all scleral ECM components. They respond to mechanical stimuli from their surrounding ECM and there is growing interest in understanding the extent of the role that fibroblasts might play in dynamically regulating scleral biomechanics via matrix remodelling and contractile responses (Harper and Summers, 2015; McBrien et al., 2009) (see s3.3.2). In addition to mechanical stimuli, fibroblasts control scleral remodelling and alter tissue-level biomechanics in response to a signaling cascade from retina to sclera that is ultimately stimulated by vision. This vision-guided response plays a critical role during eye development, determining the final size of the eye (see s4.3).

### 1.2.5. Scleral hydration and permeability

The ECM structure and biomechanical properties of the sclera depend on the tissue water content. As mentioned, stromal swelling pressure in the sclera is largely determined by the distribution and sulfation level of constituent PGs (s1.2.2). However, there is also believed to be a significant contribution from free chloride binding ligands, which may help to explain the differential swelling of the corneoscleral tunic in response to changes in its ionic environment (Hodson, 1997; Huang and Meek, 1999). In vitro swelling studies (Huang and Meek, 1999) determined the isoelectric point of the sclera (where the tissue swells least) to be at pH 4, with higher tissue hydrations achievable when the ionic strength of the bathing medium was lower. The sclera loses water as its ages (Brown et al., 1994; Rada et al., 2000), an effect which is suspected to be driven by associated changes in PG composition (see s4.1).

Tissue hydration state is also important in determining the permeability of the sclera to exogenous compounds. While molecular size/shape, surface charge and lipophilicity are the dominant predictors of scleral permeability for a given substance (Ambati et al., 2000; Lee et al., 2004; Olsen et al., 1995), diffusion rates in rabbit sclera have been shown to be elevated with increasing hydration across a range of solutes of varying molecular weight (Boubriak et al., 2000). Enhancing scleral permeability is an active area of research in the field of ocular drug delivery, particularly in the management of posterior segment disease where transscleral delivery is especially challenging due to the limited accessibility and increased thickness of the sclera at the back of the eye (Cabrera et al., 2019; Moisseiev and Loewenstein, 2017; Yamada and Olsen, 2016). Moreover, scleral permeability also has important therapeutic implications in the formulation of exogenous chemical agents for scleral crosslinking treatment (see s5.2).

## 2. Scleral ECM structure at multiple scales

### 2.1. Microstructure

Influential studies into the fine structure of the sclera began over eighty years ago with the work of Kokott, who used histological preparations to interpret the gross directions of collagen lamellae across the ocular coat (Kokott, 1934) (Fig. 4). While his methods were undoubtedly crude, Kokott's work has largely stood up to scrutiny by more sophisticated techniques and can be considered something of a landmark in beginning the enduring notion that scleral ECM structure is mechanically adapted to regional tensions in the ocular coat. However, the past decade or so has seen significant progress in the development of more quantitative methods to determine scleral microstructure, driven in large part by advances in numerical simulation of ocular biomechanics and the need to optimise models for clinical use by the inclusion of more physiologically accurate data.

#### 2.1.1. Wide-angle X-ray scattering

Wide-angle X-ray scattering (WAXS) is an ex vivo diffraction-based technique that does not yield an image of the tissue, but instead

produces a Fourier transform (WAXS pattern) from which collagen structure parameters can be extracted (Meek and Boote, 2009) (Fig. 5A). The main collagen WAXS peak from sclera derives from the regular  $\sim 1.6$  nm lateral separation of tropocollagen molecules within the fibrils (Fig. 3). Calibration of the radial position of this peak can be used to detect changes in intrafibrillar scleral collagen packing, for example as occurs in non-enzymatic crosslinking with age (Malik et al., 1992) (see s4.1). Moreover, because the constituent molecules are aligned near-axially within fibrils, WAXS can obtain a thickness-averaged measure of scleral fibril orientation and anisotropy in the tissue plane, without the need for tissue processing (Fig. 5B). Due to its extremely high signal specificity for collagen and tissue averaging capabilities, WAXS has proven highly valuable in supplying extensive amounts of data for use in numerical modelling (Coudrillier et al., 2013; Coudrillier et al., 2015a, b; Coudrillier et al., 2015c; Pinsky et al., 2005).

Pijanka et al., 2012, 2013 used WAXS to quantitatively map collagen fibril orientation in the sclera of human donors. These studies confirmed the major structural features originally identified by Kokott: strong uniaxial fibrillar orientation at the extraocular muscle insertion sites and predominantly circumferential collagen in the PPS. They further identified that the collagen anisotropy of the PPS pseudo-annulus is highly regionally variable and that this pattern is highly conserved between age-matched, normally sighted donors (Pijanka et al., 2012). Inclusion of the WAXS data in inverse finite element modelling (IFEM) indicated that disturbance of the PPS anisotropic structure could significantly impact the ONH's mechanical response to IOP fluctuation (Coudrillier et al., 2013). A further WAXS study using serial cryo-sections (Pijanka et al., 2015) showed that the human PPS pseudo-annulus is located primarily in the outer two-thirds of the stroma (aligning with the normal LC insertion depth range into the scleral flange), with the remaining one-third exhibiting more random orientation and a preference toward radial alignment near the choroid.

While structural evidence and numerical modelling (Coudrillier et al., 2013; Girard et al., 2009b; Grytz et al., 2011) are suggestive of a neuroprotective role in limiting IOP-driven scleral canal expansion and LC strains, the exact functional importance of the PPS structure remains to be established. Gogola et al. (2018b) recently used a polarized light method (see s2.1.4) to show that the PPS circumferential structure is a primary structural component across a range of large animal species. Furthermore, recent work using WAXS indicates that the degree of PPS collagen circumferential alignment varies between species and that eyes from smaller animals generally exhibit a more poorly defined

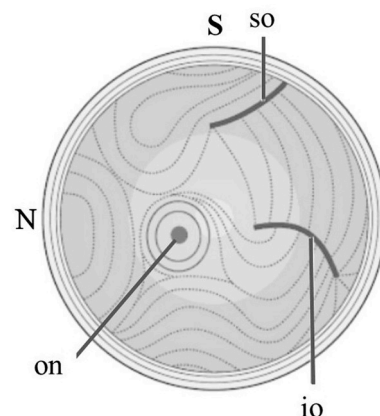
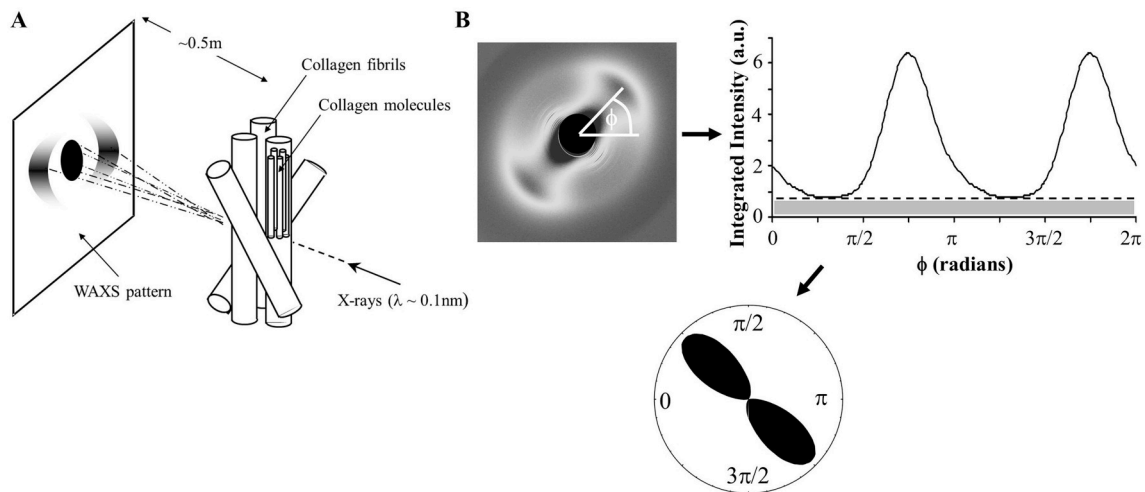


Fig. 4. Gross orientations of collagen lamellae in the posterior human sclera, as interpreted from histological examinations by Kokott (1934). Right eye shown with superior (S) and nasal (N) aspects marked. Notable features are circular orientation around the optic nerve (on) and associations with the superior oblique (so) and inferior oblique (io) muscle insertions. Figure adapted from (Watson et al., 2012) with permission of JP Medical Ltd.



**Fig. 5.** Quantifying scleral collagen orientation using wide-angle X-ray scattering (WAXS). **A)** The constructive interference of forward-scattered X-rays from the regular lateral packing of constituent tropocollagen molecules aligned near-axially within the fibrils produces a Fourier transform (WAXS pattern) that is collected on a detector behind the specimen. **B)** The collagen fibril orientation distribution function is extracted from the WAXS pattern by analysing the angular spread of (radially integrated) X-ray intensity. The scatter from preferentially aligned collagen (clear region of graph above the dotted line) is displayed as a polar vector plot in which the plot shape indicates the preferential fibril orientations (in this case uniaxial), while the plot size is indicative of the degree of anisotropy.

anisotropic structure (Fig. 6). The marked difference between some species further suggests that PPS structure may not be principally determined by IOP-generated scleral wall stress in some eyes, but instead may be more strongly influenced by other biomechanically relevant factors. For example, the wall stress in the tree shrew eye (diameter: 7.8 mm, avg. scleral thickness: 120  $\mu\text{m}$ , IOP: 13 mmHg (Samuels et al., 2018; Siegwart and Norton, 1999)) is predicted to be approximately twice that of the human eye (diameter: 24.2 mm, thickness: 0.9 mm, IOP: 17 mmHg (Bekerman et al., 2014; Kouchaki et al., 2017; Vurgese et al., 2012)), and yet the PPS circumferential structure in the tree shrew (Fig. 6B) is far less evident than in humans (Fig. 6F), despite the two species having similarly well-developed connective tissue LCs (Albon et al., 2007). In considering the above calculation, the reader should be aware that this rough estimate is based upon Laplace's Law for spherical pressure vessels. As such, it makes several simplifying assumptions that include approximating the eye as a perfect sphere of uniform thickness. Further interspecies studies may help to tease out possible physiological, behavioural and anatomical factors that may interact with IOP in influencing posterior scleral collagen microstructure.

### 2.1.2. Small-angle light scattering

Small-angle light scattering (SALS) is another *ex vivo* technique that can be used to quantitatively map protein fibre organisation in collagenous soft tissues. Like WAXS, SALS also produces diffraction patterns from the interaction of light with a tissue patch; but instead of X-rays SALS uses laser light. Because of the higher wavelength (usually 632.8 nm from a HeNe laser), SALS is thought to be capable of mapping the organisation and orientation of larger structures such as collagen fibril bundles ( $\sim 1 \mu\text{m}$  in size), but cannot distinguish between collagen and elastin fibres. For the eye, SALS was first used to map scleral fibre orientation in normal rat sclera. The rat sclera was found to be structurally anisotropic with several consistent features. At the limbus, collagen fibres were highly aligned and organised primarily into a distinct ring surrounding the cornea. In the equatorial region, the fibres were primarily meridionally aligned. In the posterior sclera and PPS, the scleral fibres were mostly circumferential but less aligned than those in the anterior and equatorial regions (Girard et al., 2011a). SALS has also been used extensively to study the microstructure of the human sclera from healthy and glaucoma donors. Interestingly, in humans PPS collagen fibres were also circumferential, consistent with the

aforementioned scheme envisaged to shield the optic nerve, but they exhibited the highest alignment (i.e. degree of anisotropy) not immediately adjacent to, but at a distance (400–500  $\mu\text{m}$ ) away from the scleral canal (Zhang et al., 2015a). Using computational modelling, such an arrangement (i.e. heterogenous collagen fibre organisation) was found to minimise deformations at the scleral canal boundary - a transition zone prone to disinsertion of the LC, focal LC defects, and optic disc hemorrhages in glaucoma (Fig. 7). In humans, SALS was also used to identify key differences in scleral microstructure with age and with glaucoma (Danford et al., 2013; Jones et al., 2015). In one study, collagen fibres in the PPS were found to be more aligned in elderly healthy eyes (average age: 82 years old) than in young healthy eyes (average: 20 years old), and also more aligned than in elderly glaucoma eyes (average age: 82 years old) (Jones et al., 2015) (see also s4.1 and s4.2). Scleral anisotropy was also found to change significantly as a function of depth (Danford et al., 2013). However, it is still unclear how a disrupted collagenous ring in the PPS could predispose an individual to glaucoma.

### 2.1.3. Multiphoton microscopy

Multiphoton microscopy (MPM) is an optical imaging technique that utilises high penetration pulsed lasers (usually infrared) and non-linear optics to achieve fine optical sectioning through biological tissues several hundred microns thick, without the need for exogenous labelling. Second harmonic generation (SHG) imaging exploits the coherent scattering event whereby two incident photons are converted into a single photon of half the original wavelength. SHG signal emission is an intrinsic property of biological materials containing large repetitive, non-centrosymmetric units that include collagen, and indeed SHG has been used extensively to probe the organisation of scleral collagen fibril bundles (Brown et al., 2007; Cone-Kimball et al., 2013; Jones et al., 2015; Keyes et al., 2011; Pijanka et al., 2012; Teng et al., 2006; Zyablitskaya et al., 2018) (see also Fig. 1D). The ability of SHG to image large tissue volumes has enabled full 3D reconstructions of the *ex vivo* human ONH to be built (Winkler et al., 2010), while its application in monitoring real-time pressure-induced LC and PPS deformations (Midgett et al., 2018; Sigal et al., 2014a) is enhancing our understanding of the role of IOP in glaucoma biomechanics. Increasingly, other MPM imaging modalities are being combined with SHG to localise scleral collagen with cells and other ECM components. The most notable example is two-photon fluorescence (TPF), in which the

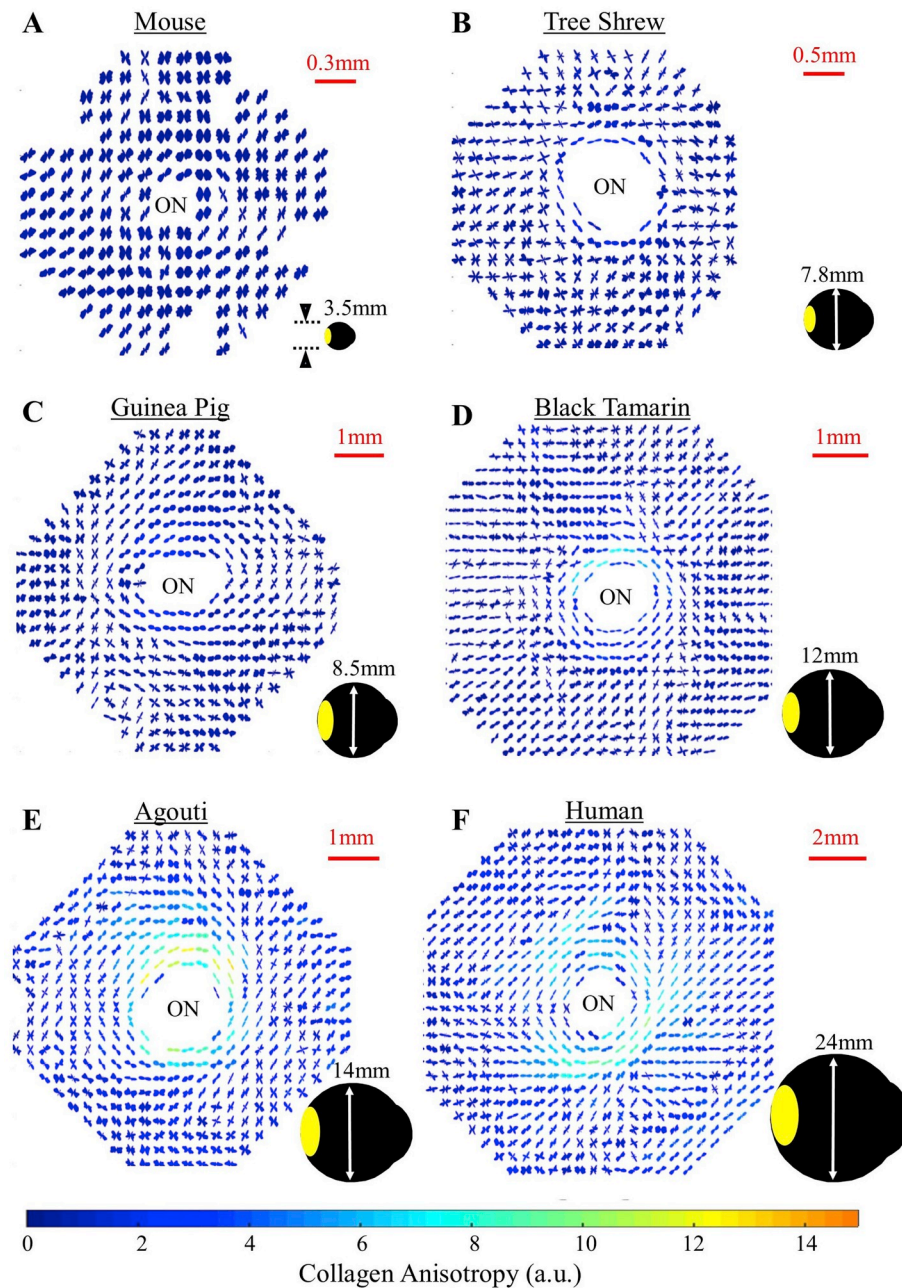


Fig. 6. Collagen microstructure of the posterior sclera across species. Polar vector plots of collagen fibril orientation in various mammal species (A–E) and humans (F), determined using WAXS. The shape of the individual plots indicates the preferred direction of collagen fibrils at that point in the tissue, while the plot colour scaling is indicative of the degree of anisotropy. Note that the circumferential collagen structure of the peripapillary sclera bordering the optic nerve (ON) is poorly defined in smaller mammals, but becomes gradually clearer with increasing eye size. The area covered by the WAXS maps is shown in yellow on the accompanying eye shadow diagrams.

additive absorption of two incident photons results in the emission of an autofluorescence photon of a higher energy. Amongst other structures, TPF can be used to visualise elastin fibre networks over large scleral tissue volumes (Park et al., 2016) (Fig. 8).

#### 2.1.4. Polarized light microscopy

Collagen in the sclera is birefringent (Chakraborty et al., 2016) - the optical property of a material having a refractive index that depends on the polarization and propagation direction of light. Jan et al. have demonstrated that polarized light microscopy (PLM) is a powerful technique for the study of the collagen microstructure in the sclera (Jan et al., 2015). PLM can produce accurate, repeatable, and robust measurements of collagen fibre orientation with  $\mu\text{m}$ -scale resolution over a broad (cm) field of view, unaffected by formalin fixation, without requiring tissue dehydration, labeling or staining. PLM has been shown to be in good agreement with other measurements of collagen, such as those from autofluorescence (Jan et al., 2017b). However current PLM techniques do not measure elastin, and it remains unclear if it is all

possible. Using PLM, Jan et al. identified three distinct regions of scleral collagen fibre organisation, with circumferential, radial (sometimes called meridional) or interweaving fibres (Fig. 9). They reported these first in the sheep (Jan et al., 2017b), then in human, monkey, pig, cow and goat eyes (Gogola et al., 2018b). The consistency in scleral microstructure across species suggests that these three structures (circumferential, radial and interweaving) are primary organisational components whose functions should be better understood.

Although there is consensus that circumferential fibres protect neural tissues by resisting canal expansion, the role of the interweaving fibres remains unclear. Wang and colleagues hypothesized that the fibre interweaving increases tissue stiffness (Wang et al., 2018). Their computational models suggest that a region of sclera with interwoven fibres can be more than twice as stiff as another region with the same amount of collagen organised with the same angular distribution but with no interweaving. This suggests that characterising fibre interweaving may be of critical importance to understanding how the sclera bears loads.

PLM has been further used to characterise the micron-scale

waviness, or crimp, of the collagen fibres in the sclera (Fig. 10). Crimp is important because it is a major determinant of tissue biomechanical behaviour (Grytz and Meschke, 2009). Using PLM, Jan et al. quantified the collagen crimp period in the LC and PPS in sheep eyes at low and normal IOP levels (Jan et al., 2017a). They found that the crimp period

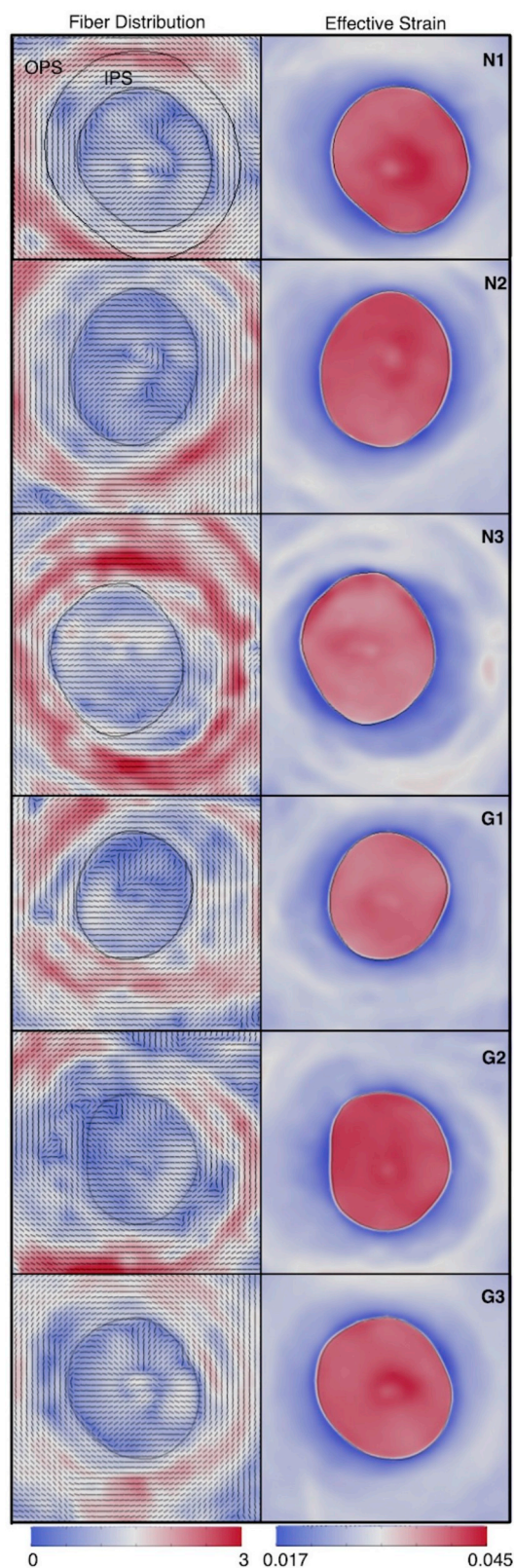


**Fig. 7.** SALS mapping of fibre microstructure in the peripapillary sclera (PPS) and lamina cribrosa. *Left:* Fibre maps for en-face sections from 6 human donors (3 healthy: N1-3; and 3 glaucoma: G1-3). A highly aligned (red colour) fibre ring (black vector) can be observed in the PPS (the LC boundary is shown in black). Contour colour represents the fibre concentration factor. *Right:* Simulated IOP-induced deformations (effective strain). Low deformations (blue colour) can be observed near the scleral canal boundary (a region prone to mechanical defects). Such deformations would be much higher if one were to remove the heterogeneous PPS fibre ring. OPS: outer peripapillary sclera, IPS: inner peripapillary sclera. Contour colour represents the strain magnitude. Figure modified from (Zhang et al., 2015a) with permission of the Association for Research in Vision and Ophthalmology.

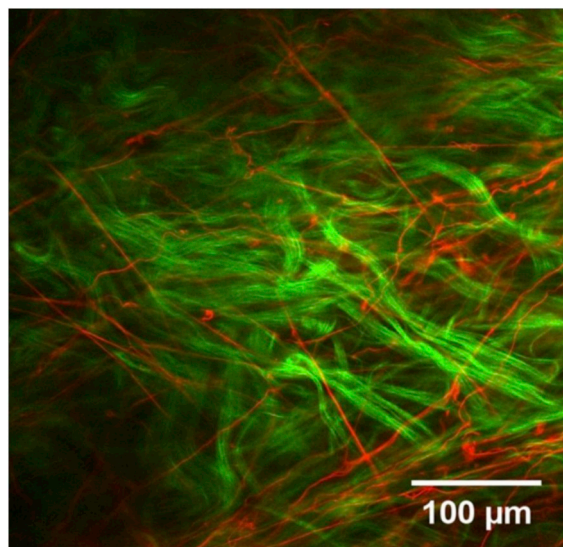


**Fig. 8.** Two-channel multiphoton microscopy image recorded from human episclera. The elastin fibre network (red) is revealed by TPF autofluorescence, and is shown alongside collagen fibril bundles (green) visualised concurrently with SHG imaging. Figure adapted from (Park et al., 2016) with permission of the Association for Research in Vision and Ophthalmology.

was smaller and less variable in the LC than in the PPS (Fig. 11), suggesting a configuration that prevents large or heterogeneous deformations that insult the neural tissues within the canal (Fig. 12). In addition, the crimp period in the PPS increased nonlinearly with distance from the canal, which is believed to provide a smooth transition of mechanical properties that minimizes stress and strain concentrations. This technique was then extended to quantify the collagen crimp morphology across the corneoscleral shell in sheep (Jan et al., 2018) and human (Gogola et al., 2018a) eyes. In these studies, it was found that crimp tortuosity, amplitude and waviness are not uniform over the globe, exhibiting distinct patterns that were similar across species (Fig. 13).

The traditional PLM used in the studies mentioned above shares an important limitation with SALS and WAXS: it only quantifies in-plane fibre orientation (in the plane perpendicular to the light beam). A more advanced technique, 3DPLM, allows quantification of both in-plane and out-of-plane fibre orientation (Fig. 14) (Yang et al., 2018b). This is potentially crucial given the complex 3D architecture of ocular collagen (Komai and Ushiki, 1991), where 2D projections could lead to inaccurate interpretations and conclusions (Yang et al., 2018b). Like SALS and WAXS, traditional PLM is a transmitted signal technique. This means that the measurements obtained are an aggregate of properties across the sample thickness. As mentioned (see s2.1.1), this can offer important advantages in enabling collection of effective structural data for use in numerical simulations. On the other hand, obtaining finely depth-resolved information using transmitted-light techniques requires the use of thin sections which, in turn, precludes or complicates analysis

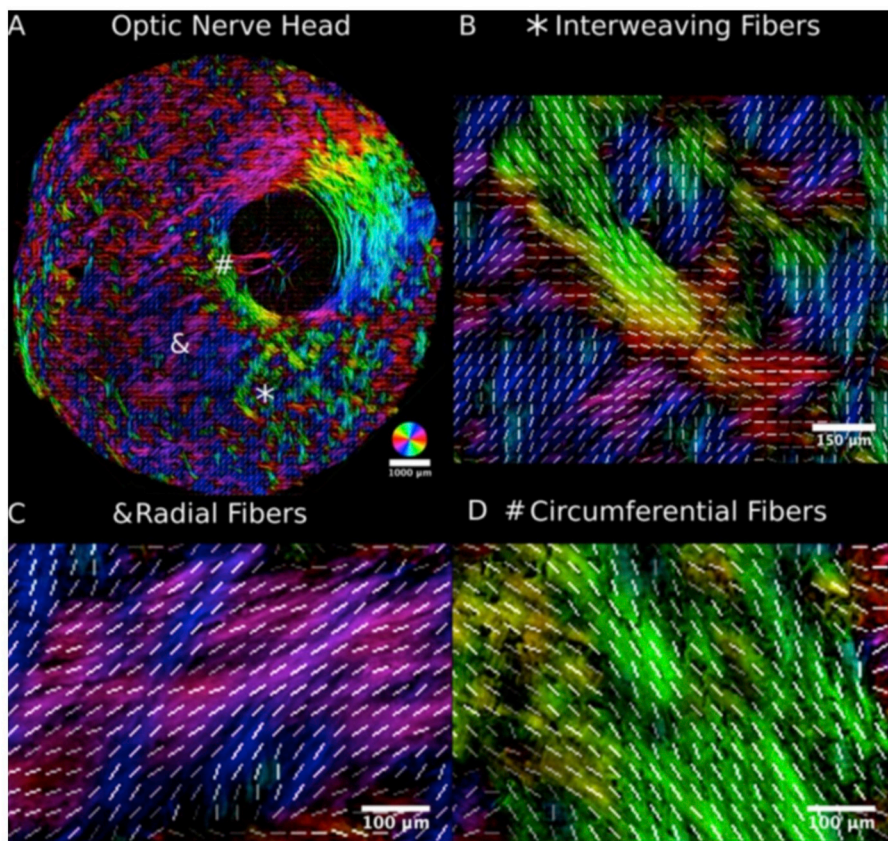


**Fig. 9.** A) The posterior sclera of the sheep eye visualised using PLM. Three major organisational patterns were identified and marked by an asterisk, an ampersand, and a hashtag: i) interweaving fibres that formed a basket-weave pattern ([B] asterisk), ii) fibres oriented radially from the canal ([C] ampersand), and iii) fibres wrapped circumferentially around the canal ([D] hashtag). White lines representing orientation averaged over  $20 \times 20 \mu\text{m}^2$  were overlaid to aid in discerning the fibre organisation. Figure adapted from (Jan et al., 2017b) with permission of the Association for Research in Vision and Ophthalmology.

of dynamic events such as pressure-induced tissue deformations. For PLM, scattering, absorption and retardance limit useable sections to under  $50 \mu\text{m}$  in thickness, and best data to  $30 \mu\text{m}$  or less. To overcome this limitation, Yang et al. introduced structured polarized light microscopy (SPLM) imaging, a reflected light imaging technique that combines structured light illumination with PLM (Yang et al., 2018a). SPLM effectively rejects diffuse background light interfering with the polarization analysis and preserves light encoded with useful tissue birefringence information, thus enabling the visualisation and quantification of collagen fibres of thick tissues while under realistic loading conditions, such as during inflation (Fig. 15).

As a full-field imaging technique, PLM is generally faster than scanning-based techniques. However, it still requires multiple image acquisitions with various filter configurations. This limits the acquisition speed, and thus the range of experiments in which it can be used. To overcome this, Yang and colleagues developed snapshot PLM (Yang et al., 2019), which allows real-time visualisation of the scleral bundles and the constitutive collagen fibres with sub-micron resolution in fresh, unlabeled samples (Fig. 16).

### 2.1.5. Magnetic resonance imaging

Magnetic resonance imaging (MRI) has been used to image the corneoscleral shell and obtain details of the ocular anatomy, such as the globe shape and tissue thickness (Norman et al., 2010a; Voorhees et al., 2017; Wang et al., 2016a). However, MRI studies of the collagen microstructure in the sclera have been limited, partly due to the intrinsically fast transverse magnetic resonance relaxation of the fibrous tissues and the resulting low MRI signal intensities (Luan et al., 2006). Ho et al. demonstrated the use of the magic-angle enhancement effect to improve MRI sensitivity for detecting the collagen microstructure in the ovine sclera (Ho et al., 2014). They found that, at the magic angle (approximately  $55^\circ$  relative to the direction of the main magnetic field), MRI can reveal the distinct lamellae fibres in the ovine sclera, and the

light/dark bands indicative of collagen fibre crimps (Fig. 17). Magic angle-enhanced MRI can also reveal sub-voxel microstructural changes of collagen fibres with IOP elevation. Using diffusion tensor MRI, Ho et al. found that the fractional anisotropy of the ovine sclera increased with IOP, consistent with uncrimping and straightening of microstructural fibres (Ho et al., 2016). Magic angle-enhanced MRI technique has the potential to enable cross-sectional and longitudinal monitoring of the functional microstructures of the eye and their relationship with aging and diseases involving the sclera, such as acute and chronic ocular hypertension, glaucoma, and myopia. However, before this can be realised, important technical challenges remain, particularly the resolution and the long scan times (often over 12 h in the studies mentioned above).

### 2.1.6. Comparison of microstructural techniques

A diverse array of imaging and non-imaging techniques have been developed to resolve and quantify scleral microstructure. Each method has its own particular advantages and disadvantages and, if used in a complementary fashion, these tools can together gain powerful insight into the sclera's complex architecture. Scattering methods (WAXS and SALS) have so far proven the most productive for obtaining representative (i.e. thickness averaged) quantitative information of structure within the scleral plane for modelling applications. This is because scattering methods detect all the fibres in the path of the incident beam, whereas imaging methods (by definition) rely on the visibility of structural features in order to quantify them. In the case of the sclera, fibre paths are often tortuous and interwoven, meaning portions of the structure are essentially hidden from image analysis tools. On the other hand, imaging methods such as MPM and PLM have greater spatial resolution and are, hence, more adept at following the path of individual fibres. Additionally, PLM and (in particular) MPM have greater depth-resolving capabilities for determining 3D structure. A particular challenge is how to reliably distinguish scleral fibre signal

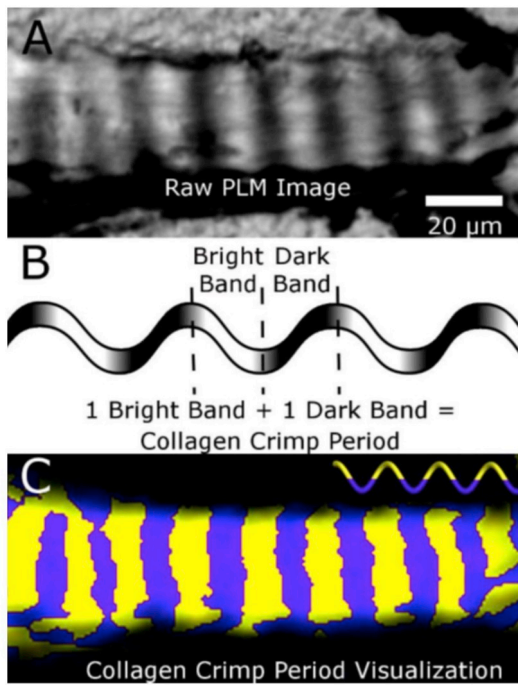


**Fig. 10.** Collagen crimp period visualised using PLM. **A)** An LC beam appears banded when imaged with PLM. **B)** Adding the lengths of one bright band and one dark band makes one collagen crimp period. **C)** Processing several “raw” PLM images with various filter orientations, it is possible to pseudocolour half periods as alternating yellow and purple bands that help visualise the crimp. Note that the crimp bands are fairly uniform and perpendicular to the longitudinal axis of the LC beam. This crimp pattern helps reduce shearing and torsion within the LC beam when loaded longitudinally. Note that crimp period is only one aspect of fibre crimp. Figure adapted from (Jan et al., 2017a) with permission of the Association for Research in Vision and Ophthalmology.

contributions from collagen and elastin. Whereas WAXS has the highest capacity to isolate the collagen signal, TPF is currently the only validated modality for quantifying elastin fibre orientation in the sclera. Finally, obtaining detailed and quantitative views of scleral fibre structure in the living eye remains one of the most important unmet challenges in the ocular biomechanics field. Magic angle-enhanced MRI currently has the greatest potential for in vivo application (albeit at the lower end of the resolution scale), but its possible future adoption in the ophthalmology clinic will very much depend on solutions to existing technical limitations.

2.2. Nanostructure

2.2.1. Scanning electron microscopy

Study of the interaction of incident electrons with the atoms of a target specimen allows the imaging of structure at resolutions beyond 1 nm. For biological specimens this generally comes at the price of invasive tissue preparation involving dehydration, chemical fixation and heavy metal staining/coating to stabilise and preserve tissue structure and enhance image contrast. Scanning electron microscopy (SEM) produces images of a sample surface at < 1 nm resolution by scanning it with a focused electron beam and detecting (usually) the emission of secondary electrons from target atoms excited by the incident beam. Alternatively, an SEM image can be obtained from the reflected/transmitted incident electrons. As documented in several landmark papers (Komai and Ushiki, 1991; Thale and Tillmann, 1993; Yamamoto et al., 2000) SEM has made central contributions to our fundamental knowledge of scleral collagen hierarchical structure and organisation. Reported findings of particular significance include regional, three-dimensional assessments of scleral collagen organisation and its integration with the cornea (Komai and Ushiki, 1991) and immunolocalisation of collagen subtypes and their regional distribution (Thale and Tillmann, 1993). In recent years the advent of volume SEM methods have made it possible to image tissue ultrastructure in 3D over specimen volumes of hundreds of cubic microns (Bushby et al., 2011) and these methods are currently providing insight into how the elastin fibre

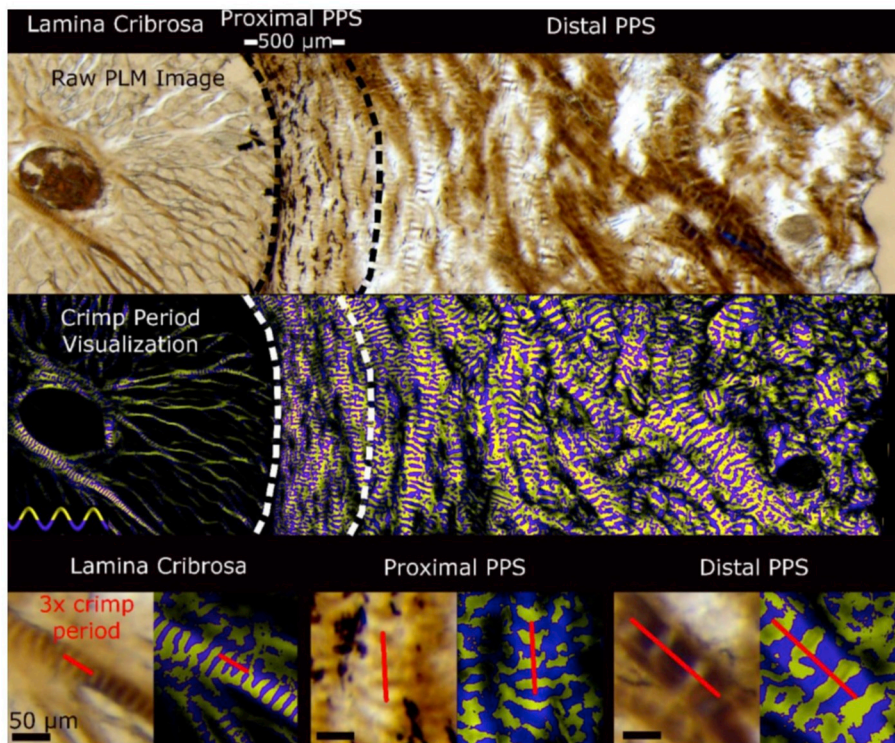


**Fig. 11.** Wide views spanning the LC and sclera under PLM (top) and visualised using the yellow and purple bands as described in Fig. 10 to simplify discerning crimp period independent of the orientation (middle). The bottom shows pairs of raw PLM images and corresponding crimp period visualization images of close-ups of the LC (bottom left), proximal PPS (bottom centre), and distal PPS (bottom right). An example line illustrating three periods is overlaid on each. It is easy to distinguish that the crimp period in the LC was small. In the proximal PPS the period was similar to that of the LC. The period increased with distance from the canal. Figure adapted from (Jan et al., 2017a) with permission of the Association for Research in Vision and Ophthalmology.

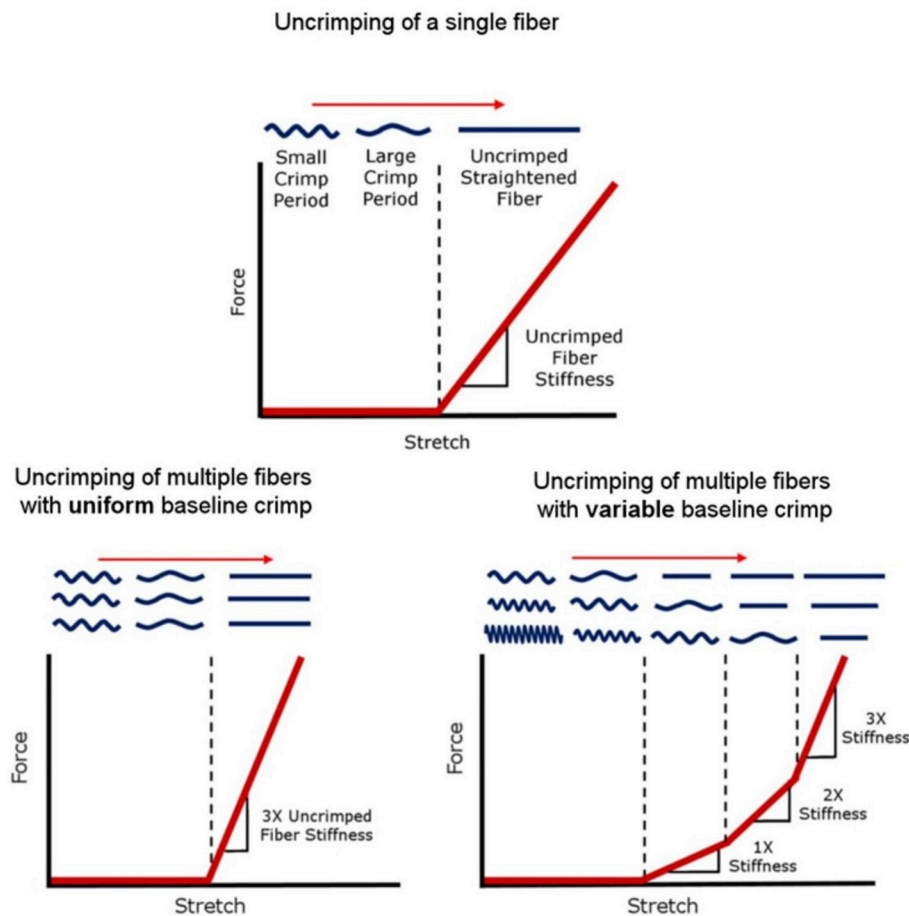


**Fig. 12.** Schematic of how fibre uncrimping contributes to tissue mechanical properties. (Top) As a single fibre stretches, it uncrimps, requiring relatively little force until it loses all crimp. The straightened fibre can only be stretched further by making the fibre longer, which requires an increasing force, and so the fibre appears stiffer. A fibre that has uncrimped and is bearing load is called “recruited”. The macroscopic force or stiffness of multiple fibres depends on the distribution of baseline crimp in the fibres. (Bottom row) In a region with fibres of uniform crimp, stretch leads to a macroscopic step increase in stiffness due to the simultaneous straightening of all fibres. In a region with variable crimp, stretch leads to a gradual increase in stiffness due to the progressive straightening of fibres. Fibres with less crimp are straightened and loaded (recruited) before fibres with more crimp. Figure adapted from (Jan et al., 2017a) with permission of the Association for Research in Vision and Ophthalmology.

network of the anterior sclera might integrate with that of the peripheral cornea (Lewis et al., 2016).

### 2.2.2. Transmission electron microscopy

In transmission electron microscopy (TEM) an electron beam is transmitted through an ultrathin ( $\sim 100$  nm) section of a specimen and can image nanostructure at unparalleled resolution (Fig. 1B and C). With modern aberration corrected electron microscopes, it is now possible to resolve structures of dimensions  $< 0.1$  nm. TEM has made many major contributions in scleral research, in particular in the use of cationic dyes (Quantock and Meek, 1988; Young, 1985) and immunogold particulate markers (Kimura et al., 1995; Marshall et al., 1993) to elucidate collagen-collagen and collagen-PG interactions, and in defining ECM alterations in scleral pathology (Cone-Kimball et al., 2013; Funata and Tokoro, 1990; McBrien et al., 2001; Quigley et al., 1991). These latter studies are particularly noteworthy from a clinical perspective, as they have disclosed important changes in collagen fibril diameter and lamellar organisation that underpin scleral remodelling in myopia (Funata and Tokoro, 1990; McBrien et al., 2001) and glaucoma (Cone-Kimball et al., 2013; Quigley et al., 1991) (see s4.2 and s4.3). Recent years have seen notable progress in tissue cryopreservation methods that significantly reduce structural artifacts induced by post-processing in conventional TEM, allowing high resolution imaging of the sclera that is closer to a physiological setting (Costa et al., 2016; Ismail et al., 2017). Current bioimaging trends towards 3D visualisation of ECM ultrastructure are reflected in recently documented electron tomography (Luesma et al., 2013) and quick-freeze/deep-etch (QFDE) electron microscopy (Ismail et al., 2017) (Fig. 18) studies of the sclera.

### 2.2.3. Atomic force microscopy

In atomic force microscopy (AFM) contact scanning of a sample

surface is performed with a fine mechanical probe. As an imaging technique, AFM can produce topographic surface images of a specimen with in-plane and depth resolutions of respectively  $\sim 2$  nm and  $\sim 0.1$  nm. An advantage of AFM over electron microscopy is that it does not require any artifact-inducing treatments and thus can provide a more physiological view of the tissue. However, the scanning area in AFM (typically a few hundred microns across) is an order of magnitude below that achievable with SEM. AFM has been used to visualise and quantify scleral collagen fibril diameter, D-period (Fullwood et al., 1995) (Meller et al., 1997) and microfibrillar tilt angle (Yamamoto et al., 2000). Importantly, AFM provides a unique link between tissue ultrastructure and mechanics by being able to measure forces between the probe and specimen surface in parallel with imaging. This has been exploited to determine the contribution of different tissue layers (Grant et al., 2011) and ECM components (Zhuola et al., 2018) of the sclera to its mechanical performance. A further strength of AFM is that it can also be used for precision manipulation of the local sample environment. For example it can mechanically stimulate individual cells and monitor the effects in real-time by synchronisation with other imaging modalities (e.g. fluorescence imaging), as demonstrated in work with cultured immune cells (Cazaux et al., 2016). However, the potential for using AFM in mechanotransduction studies of the sclera is yet to be realised.

## 3. Scleral biomechanics

### 3.1. Ex vivo biomechanical characterisation methods

#### 3.1.1. Tensile testing

Much of what we know about the fundamental material properties of the sclera has come from uniaxial tensile testing of scleral stress-strain behaviour. A large body of work using tissue strips from

## Visualizations of Crimp Period and Amplitude Around the Globe

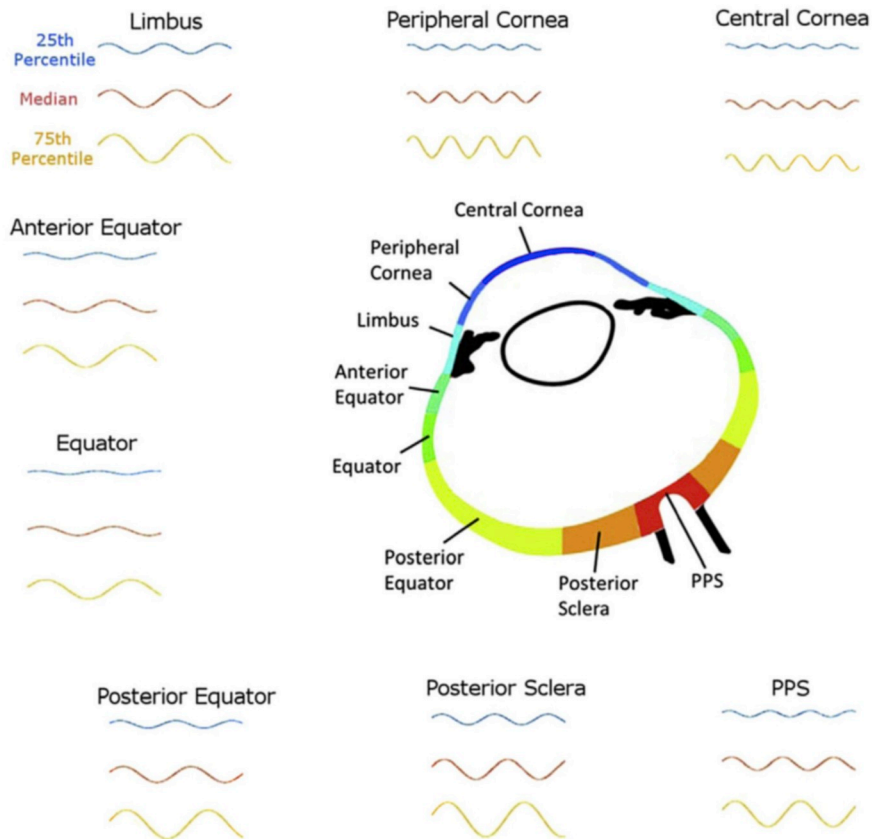


Fig. 13. Crimp characteristics vary around the globe, in consistent ways between individuals. The figure compares crimp period and amplitude across regions of the globe. The 25th percentile, 50th percentile (median), and 75th percentile period and amplitude values were used to generate representative fibres for each region as sinusoids. These visualisations are not intended to represent any specific fibril, fibril bundle or lamellae, but are, instead, intended to visualise how the crimp differs between regions. In regions with more uniform crimp, all three lines would be relatively similar, whereas in regions with highly variable crimp they would vary. Figure adapted from (Jan et al., 2018) with permission of Experimental Eye Research.

enucleated eyes of humans (Eilaghi et al., 2010; Elsheikh et al., 2010; Geraghty et al., 2012; Shin et al., 2018), monkeys (Downs et al., 2005), chicks (Phillips et al., 2000), pigs (Lari et al., 2012), tree shrews (Levy et al., 2018), rabbits (Shin et al., 2018), cows (Shin et al., 2018) and dogs (Palko et al., 2011) have established that the sclera is a non-linear material, exhibiting a strain-stiffening response as crimped collagen fibrils become gradually recruited to bear load (see Fig. 12). These studies have also confirmed that the sclera is a viscoelastic material that displays significant hysteresis. They have shown us that the healthy sclera displays considerable mechanical anisotropy that varies with anatomical position, consistent with the regional microstructural variations in tissue ECM structure discussed in s2.1. Strip testing has been used to uncover important scleral biomechanical changes with ageing, glaucoma and myopia that will be described in Section 4. Moreover, notable recent studies have reported its use to assess the effects of crosslinking treatment for myopia (Levy et al., 2018), and its combination with emergent polarization-sensitive optical coherence tomography (PSOCT) imaging to determine scleral mechanical response to dynamic loading (Shin et al., 2018).

While strip testing has long been a standard method of scleral biomechanical measurement, there are recognised limitations with the technique. Firstly, the scleral tissue strips required for testing are unavoidably curved and demonstrate variations in thickness and structural anisotropy along their length. This can lead to large errors in measured material behaviour that require mathematical back-correction to solve (Elsheikh and Anderson, 2005). Secondly, obtaining repeatable measurements with strip testing requires preconditioning cycles that fundamentally alter the stress-strain response. These limitations have led, in recent years, to a move towards the more physiological techniques of biaxial tensile testing and inflation testing (see s3.1.2), which significantly reduce the above problems (Lari et al., 2012; Tonge et al., 2013). Biaxial tensile testing does not use strips of

tissue, but instead square tissue patches. These are stretched in two perpendicular directions to more closely mimic in vivo loading conditions encountered in the eye wall. Biaxial loading studies on sclera are uncommon in the literature, but notably the method has been successfully employed to observe the non-linear stress-strain behaviour of human (Eilaghi et al., 2010) and porcine (Cruz Perez et al., 2014) sclera.

### 3.1.2. Inflation testing

Although inflation testing cannot measure the stressed state of the sclera directly, it can be used to extract material properties by applying a suitable constitutive model (with some inherent assumptions) to the experimental pressure-displacement data. Scleral inflation studies have been performed across a range of mammalian species from mice to humans (Coudrillier et al., 2012; Cruz Perez et al., 2016; Fazio et al., 2014a; Girard et al., 2009c; Myers et al., 2010a, 2010b; Nguyen et al., 2013; Palko et al., 2016; Tang and Liu, 2012). While the experimental details vary across these studies, the key components of the basic inflation set-up are common to all.

The first component needed is a controllable pressurisation module. A fluid injection system is required that allows adjustment of both target pressure and pressure-rate, usually achieved via a combination of a syringe pump and a pressure transducer with feedback control. The scleral specimen (usually the transected posterior hemisphere, or thereabouts, of the eye globe) is glued/clamped to the pressure chamber with separate inlets for fluid injection and pressure measurement. The second component required is a deformation tracking module. Tracking the surface displacement of the internally pressurised sclera at sufficiently high resolution, and with enough precision, is the most challenging aspect of inflation testing, and researchers have adopted various approaches. Girard et al. (2009c) and Fazio et al. (2014a) used electronic speckle pattern interferometry (ESPI) to track

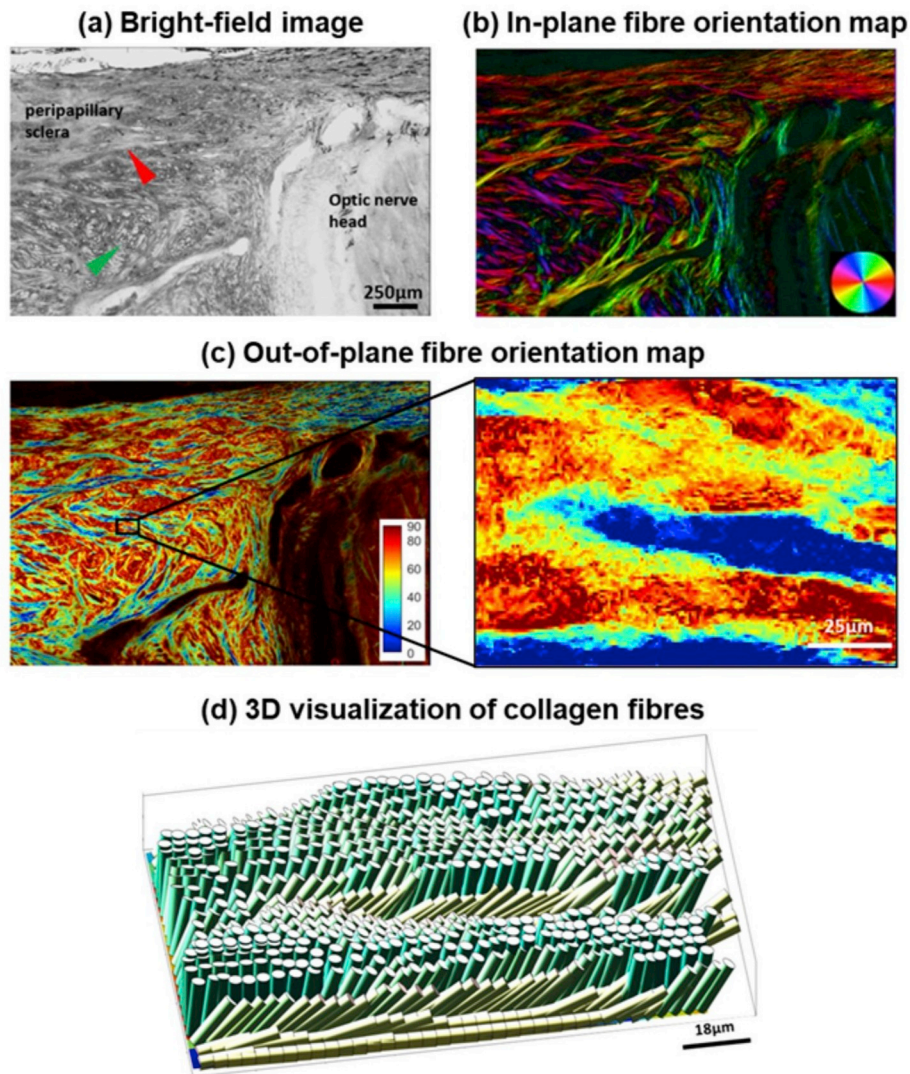


Fig. 14. Application of 3DPLM to the posterior pole of a sheep eye. The 3D orientation of the fibres can be separated into in-plane and out-of-plane orientations, where the plane is that of the section. (a) Bright-field image of a cryosection with red and green arrowheads pointing to long in-plane fibre bundles and out-of-plane fibre bundles, respectively; (b) In-plane fibre orientation map showing both in-plane fibre morphology and orientation. Colours indicate the in-plane fibre orientation; (c) Out-of-plane fibre orientation map highlighting fibre bundles. Colours indicate the out-of-plane fibre orientation, from fully in-plane (blue) to perpendicular to the plane (maroon); (d) 3D visualisation of collagen fibres. Figure adapted from (Yang et al., 2018b) with permission of the Journal of Biophotonics.

posterior scleral surface displacements in monkeys and humans, respectively. ESPI works on the principle that a rough surface illuminated with a coherent light beam (i.e. a laser) creates a random speckle light field. Interference of this field with a reference field then produces an interference pattern that is dependent on the surface displacement and can thus be used to indirectly determine the latter in 3D. Coudrillier et al. (2012) adopted a more direct approach in their inflation tests of human sclera, using graphite powder to create contrast markers on the scleral surface. These markers were then tracked in 3D directly with a combination of CCD cameras and digital image correlation (DIC) software. A DIC approach was also used by Myers et al. (2010a), and developed further by Nguyen et al. (2013) in inflation tests of mouse sclera. However, the small size of the mouse eye facilitated only 2D tracking of the scleral surface profile. Tang and Liu (2012) developed an alternative system, in which ultrasound speckle tracking was used to obtain cross-sectional profiles of scleral displacements in a porcine model. This was subsequently adapted successfully for studies in human (Pavlatos et al., 2016) (Ma et al., 2019) (see Fig. 19) and canine (Palko et al., 2016) sclera. In contrast to DIC methods, ultrasound speckle tracking does not require the application of particulate markers to the scleral surface, but rather generates intrinsic speckle patterns from acoustic interference of sub-resolution scatterers.

Going forward there is likely to be an emphasis on whole eye biomechanical modelling, and there have already been associated developments in inflation testing methods. Lari et al. (2012) developed a

method to test intact eyeballs by using a combination of a skewer and mineral oil bath to support and image cannulated pig eyes under inflation conditions. In a variation on this approach, Pavlatos et al. (2018) and Ma et al. (2019) also tested intact porcine and human eye globes, respectively, by securing them to a holder using thick spinal needles. Whitford et al. (2016) developed a further variation on the whole eye inflation/DIC approach, in which they placed intact eyeballs in a gelatin suspension to further reduce external forces on the sclera (Fig. 20). These kind of approaches have moved inflation testing closer to the in vivo situation by reducing non-physiological stress concentrations and boundary conditions unavoidably imposed when clamping excised scleral specimens in standard inflation regimens (Lari et al., 2012; Whitford et al., 2016).

### 3.1.3. Compression and indentation testing

Indentation testing studies of the sclera are relatively sparse but can be traced back more than three decades to the work of Battaglioli and Kamm. They tested samples of sclera from cow and human eyes in compression and found that the radial compressive stiffness of the sclera (i.e. its ability to resist indentation forces perpendicular to the tissue plane) was approximately 100 times less than its circumferential (i.e. in-plane) stiffness (Battaglioli and Kamm, 1984). In their study, Battaglioli and Kamm used a relatively simple custom-made air piston indenter and optical displacement probe apparatus capable of sub-micron resolution. However, the commercial release of the first AFM

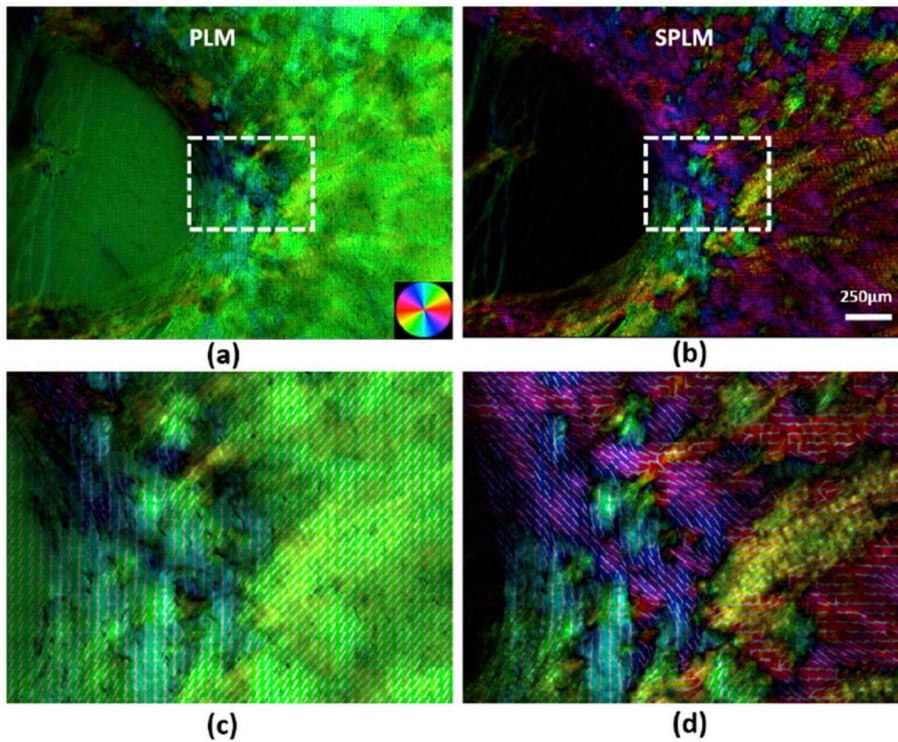


**Fig. 15.** Collagen fibre orientation maps in the PPS and LC region of a pig eye. The images were acquired using either PLM (a, c) or SPLM (b, d) of an uncut thick sample. (a) The PLM images appear green, without much detail of the known architecture of the region. (b) In contrast, SPLM images show a much more heterogeneous arrangement. Both circumferential and radial fibres can be identified, based on colour-coded orientations; (c) and (d) show close-ups of the region marked by the dashed rectangle. Overlaid on the images are locally averaged orientation lines. Figure adapted from (Yang et al., 2018a) with permission of the SPIE.

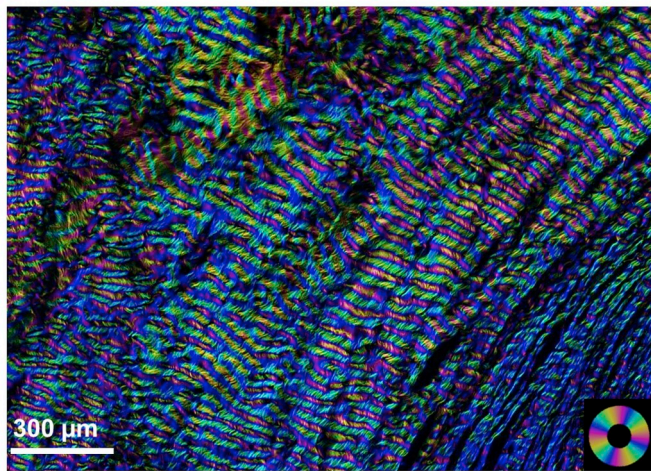


**Fig. 16.** Porcine PPS imaged by snapshot polarized light microscopy (Yang et al., 2019). The colours indicate the local orientation of the collagen fibres and the brightness is roughly proportional to the local collagen density. Note that the colours are obtained through optical means, and the image is not coloured digitally. The scleral canal is slightly out of frame on the bottom right corner. Clearly discernible in the image are collagen fibre bundles circumferential to the canal. The width of the region of circumferential fibres is between 20% and 40% of the canal diameter in both porcine and human eyes (Gogola et al., 2018b). It is also possible to distinguish the collagen fibres that form the bundles. The bands of colour indicate collagen fibre crimp (Jan et al., 2017b). The collagen fibre bundles and the crimp of the fibres increase in size with distance from the canal (Jan et al., 2017a).

instrument some five years later made more sophisticated nanoindentation studies possible. Braunsmann et al. evaluated elasticity alterations in cryosections of LC and PPS in eyes with pseudoexfoliation (PEX) disorder, reporting a marked softening of the ONH tissues in PEX affected eyes that could possibly render them more vulnerable to glaucoma damage (Braunsmann et al., 2012). Later Leung et al. measured ex vivo scleral load-displacement response in porcine eyes as a

function of IOP using a universal indentation testing machine in combination with a DLSR camera fitted with a stereomicroscope (Leung et al., 2014). They found that scleral stiffness correlated positively with IOP. While these studies indicate the possibility for indentation testing technology to perhaps one day provide valuable clinical measures of scleral stiffness in vivo, this potential remains largely unrealised.

### 3.2. In vivo biomechanical characterisation methods

Ex vivo studies have shown that the biomechanical properties of the sclera change with age (s4.1), race (s4.1), glaucoma (s4.2), and myopia (s4.3). In vivo measurements of these properties could therefore potentially serve as valuable biomarkers to detect the earliest stages of glaucoma damage and progressive myopia, helping to profile patients at risk of developing these pathologies. At present, in vivo measurements of scleral biomechanical properties are, in principle, achievable through inverse methods that will be described below.

To fully assess the biomechanical behaviour of the sclera in vivo, one would need to alter one of the known loads acting on the sclera while continuously monitoring the scleral tissue and measuring its resulting local deformations. Only then can the stiffness (or biomechanical properties) of the sclera – roughly speaking the ratio of load changes to deformations – be estimated. It is important to realise that these ‘in vivo biomechanical tests’ need to be performed within a safe physiological range in order avoid further progression of visual field loss. Furthermore, and as for any controlled mechanical test, only one load should be altered at a time while all others should remain constant. This last point represents a significant clinical challenge.

Girard et al. developed a 3D tracking algorithm that can track displacements and strains of the PPS following a change in IOP (Girard et al., 2013). This algorithm requires two optical coherence tomography (OCT) volumes of the ONH: one is captured before a change in IOP (referred to as the ‘undeformed’ volume) and the other is captured after a change in IOP (referred to as the ‘deformed’ volume). Briefly, the tracking algorithm defines regions of interest (ROIs or groups of voxels) in the undeformed OCT volume and then subjects them to mechanical transformations (rigid translation, rigid rotation, stretch/compression

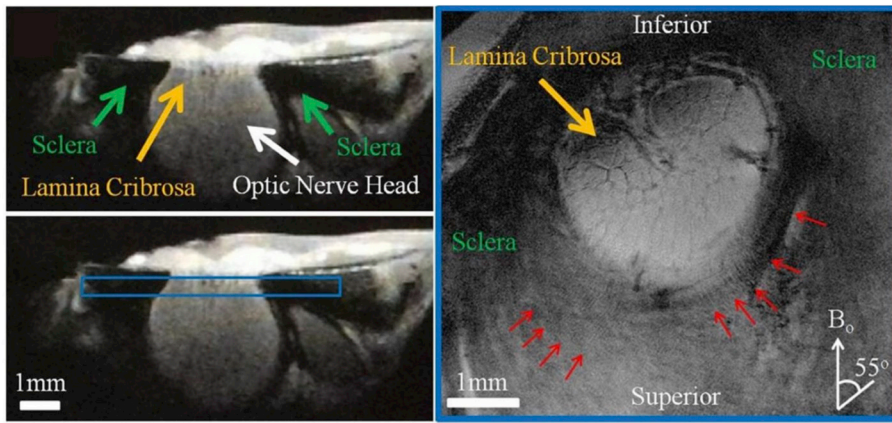


**Fig. 17.** High-resolution T2\*-weighted MR images of the unloaded ovine sclera near the optic nerve head. The left panels show the cross-section of the sclera, optic nerve head, and lamina cribrosa in sagittal view. The right panel shows the coronal T2\*-weighted image oriented as the blue box in the left panel at  $16 \times 16 \mu\text{m}^2$  in-plane resolution and repetition time/echo time = 3000/9.5 m.s. Details of the lamina cribrosa (yellow arrow) within the optic nerve head and the distributions of crimps (red arrows) in the scleral fibres surrounding the optic nerve head were revealed especially at orientations near the magic angle at approximately  $55^\circ$  to the main magnetic field ( $B_0$ ). Figure adapted from (Ho et al., 2014) with permission of the Association for Research in Vision and Ophthalmology.

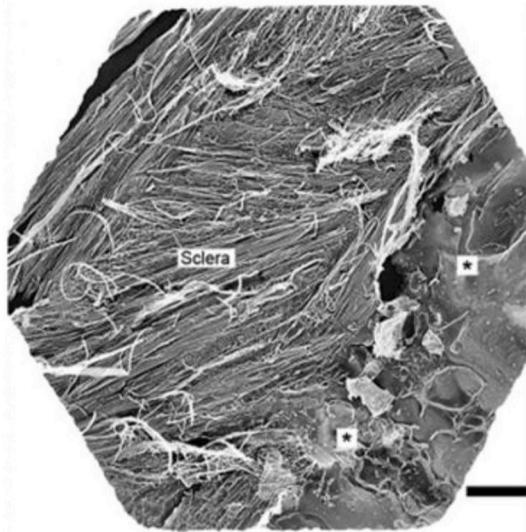


**Fig. 18.** Quick-freeze deep-etch (QFDE) electron microscopy image of mouse posterior sclera, revealing layers of differentially oriented collagen lamellae in 3D. On the right side of the image (\*) can be seen an area of partially etched, vitrified ice - a product of the "freeze-fracture" processing that can preserve native hydrated structure more closely than is possible with conventional electron microscopy sample preparation. Scale bar:  $2 \mu\text{m}$ . Figure reproduced from (Ismail et al., 2017) with permission of Elsevier Ltd.

and shear) until they best match their co-localised ROIs in the deformed OCT volume (Fig. 21). The output is a 3D displacement field from which tensile, compressive, and effective (average) strain components can be derived and mapped. Using such a technique, Girard et al. have reported in vivo local displacement/strain mapping of the PPS following IOP lowering by trabeculectomy in glaucoma subjects (Girard et al., 2016). They demonstrated that the PPS was the tissue that exhibited the highest compressive strain relief (on average 10% for an IOP decrease of 12 mmHg) following IOP-lowering surgery by trabeculectomy. This suggests that trabeculectomy is efficient at relieving a significant amount of PPS stress that may otherwise hasten glaucoma progression.

Once scleral deformations (and the corresponding loads) are measured in vivo, inverse computational approaches can be used to assess the biomechanical properties of the sclera, such as IFEM (Coudrillier et al., 2013), the virtual fields method (VFM) (Zhang et al., 2017), or the pre-fitting method (Sigal et al., 2014b), each having its own pros and cons. However, in vivo scleral biomechanics is still in its infancy, and the most pressing concern is to further demonstrate and validate that the biomechanical properties of the sclera are indeed measurable in vivo with enough sensitivity and accuracy. Full-thickness visibility of the posterior sclera and PPS by OCT is also not always achievable in all patients, and the reported biomechanical measurements with the above techniques may only reflect the scleral portions that are deemed visible. Improvements in OCT hardware (Sigal et al., 2014c), including adaptive optics, swept source, multiple wavelengths, phase-sensitive

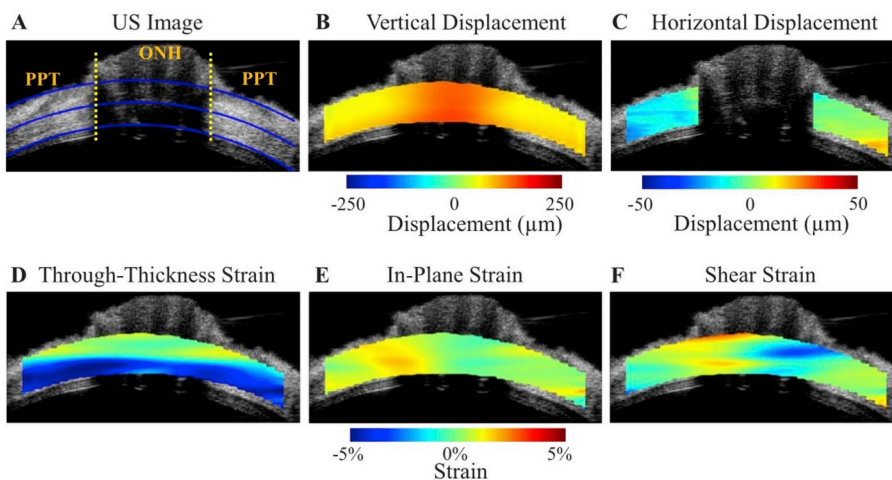


**Fig. 19.** Ultrasound (US) speckle tracking of scleral and ONH deformation under inflation testing. US image (A) and colour maps of vertical displacement (B), horizontal displacement (C), and strains (D-F) for a representative human donor eye at 30 mm Hg. The yellow dotted lines in (A) indicate the boundaries between ONH and peripapillary tissue (PPT), the inner and outer blue lines are fitted curves for demarcation of region of interest (ROI) for strain analysis, and the middle blue line is used to divide the anterior and posterior halves. Note that the retina is largely excluded from the ROI. Positive displacements = upward vertical movement or rightward horizontal movement. Vertical displacements were larger within the ONH. The horizontal displacement of PPT was negative on average on the left side of ONH and positive on the right side of ONH, indicating a small scleral canal expansion. Through-thickness compression was largest in magnitude and concentrated in the anterior half of the ONH and PPT. Reproduced from (Ma et al., 2019) with permission of the Association for Research in Vision and Ophthalmology.

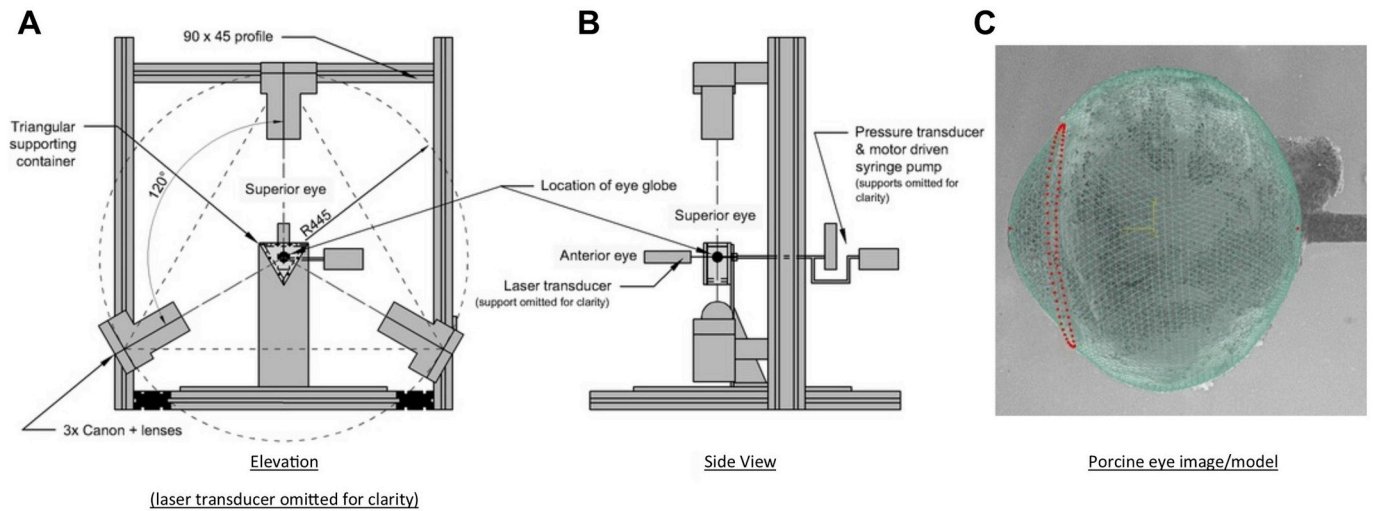


**Fig. 20.** Inflation testing of intact eye globe. **A)** Elevation view diagram of the whole eye globe inflation testing rig set-up. **B)** Side view of the rig set-up. **C)** Match between modelled and imaged topography of the eye globe. The FE nodes representing the corneal apex, posterior pole and limbal ring are highlighted in red. Adapted from (Whitford et al., 2016) under Creative Commons License 4.0.

technology, micro-imaging, and image processing techniques such as compensation (Girard et al., 2011b), are likely to push the quality and availability of in vivo biomechanical measurements to the next level. Furthermore, other new imaging approaches such as Brillouin microscopy (Scarcelli et al., 2012; Yun and Chernyak, 2018) and shear wave elastography (Dikici et al., 2016) may hold great promise if they can be successfully applied to the sclera. Brillouin microscopy can measure the ‘hypersonic longitudinal modulus’ that is thought to be related to the compressive properties of a tissue. It was recently applied to the porcine sclera ex vivo (Shao et al., 2016). The technique provides parameters that are different from those mentioned above but may still prove useful in a diagnostic setting. Shear wave elastography can determine the local shear modulus of a tissue and was recently applied to the PPS in vivo (Dikici et al., 2016). The reported moduli are typically off by several orders of magnitude when compared with traditional methods, however it should be noted that the settings are very different. Shear wave elastography relies on a highly dynamic mechanical stimulus (a shear wave), and more research is required to reconcile shear wave elastography measurements with those obtained from traditional biomechanical methods.

**Key points:**

- OCT-based technologies to measure scleral strains and stiffness in vivo have been developed.
- Such technologies are currently being applied and validated in various settings, and are likely to benefit from future improvements in OCT hardware.
- Other technologies (e.g. Brillouin microscopy, shear wave elastography) to measure scleral stiffness in vivo show great promise, however further validation is required.

**3.3. Scleral response to IOP**

**3.3.1. ECM response**

Studies of the scleral ECM response to IOP can be divided into two groups: response to acute and chronic IOP elevations. Following acute IOP elevations, posterior bowing of the PPS and expansion of the scleral canal were observed in human (Ma et al., 2019; Pavlatos et al., 2018), monkey (Girard et al., 2009a; Yang et al., 2009), porcine (Pavlatos et al., 2018) and sheep (Voorhees et al., 2017) eyes. The effects were non-linear, with larger deformations at normal or sub-normal IOPs than at

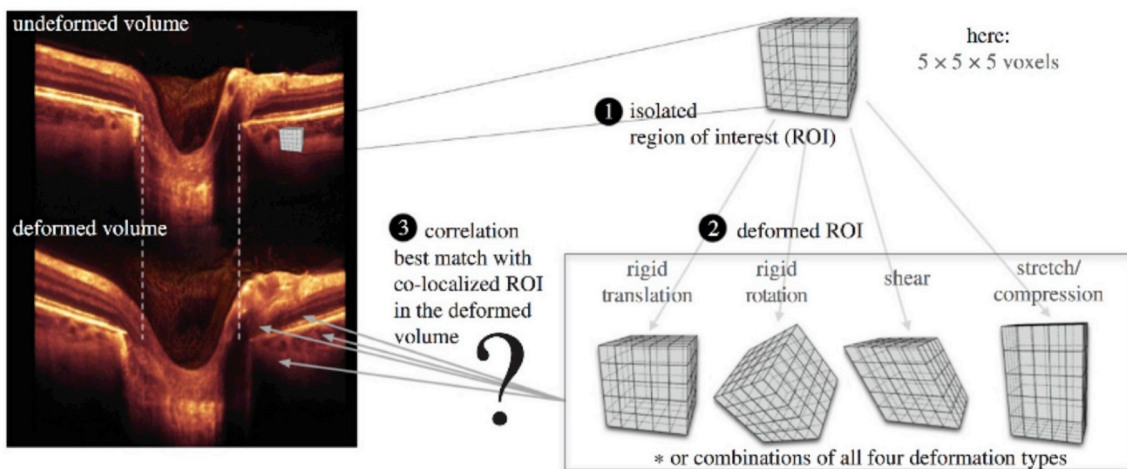


**Fig. 21.** Steps to track IOP-induced displacement of a single scleral point in vivo. 1) an ROI is created in the undeformed OCT volume; 2) The ROI undergoes a combination of affine transformations (translation, rotation, shear and stretch); 3) a displacement vector can be extracted when the deformed ROI best matches a co-localised ROI in the deformed volume. Adapted from (Girard et al., 2013) with permission of the authors.

elevated IOPs, consistent with a non-linear deformation-induced stiffening resulting from inhomogeneously crimped collagen fibres (Fig. 12). Although crimp had been postulated as the microstructural basis of the non-linear mechanical behaviour of sclera (Grytz and Meschke, 2009), it is only recently that it has been confirmed experimentally (Jan and Sigal, 2018). Jan et al. used PLM to quantify and characterise how the collagen fibre crimp waviness (standard deviation of the fibre orientation along a fibre bundle) of the LC and PPS in sheep eyes changes with IOP (Jan and Sigal, 2018). It was found that the crimp waviness decreased with IOP. Interestingly, at a normal IOP of 15 mmHg, both LC and PPS had about 75% recruited fibres, with 25% ostensibly in reserve. Whether this also applies to human eyes remains unknown.

Posterior bowing of the PPS and expansion of the scleral canal were also observed in monkey eyes exposed to chronic IOP elevations (Bellezza et al., 2003; Yang et al., 2007). Girard et al. estimated the scleral tangent modulus (a measure of scleral stiffness) of monkey eyes in which chronic IOP elevation was induced. They found that the tangent modulus decreased at the earliest stage of IOP elevation but increased at moderate stages (Girard et al., 2011). Age-related decreases in collagen crimp are likely one of the mechanisms underlying age-related stiffening of the sclera. Using PLM, Gogola et al. quantified collagen crimp morphology (waviness, tortuosity, and amplitude) in 20 normal eyes of 20 human donors, ranging in age from 0.08 (1 month) to 97 years (Gogola et al., 2018a). They found that all crimp parameters decreased significantly with age, with significantly different age-related decreases between regions. The crimp morphology of the limbus changed the most drastically with age, such that it had the largest crimp in neonates, and among the smallest in the elderly, suggesting that crimp in this region may play a role in eye development. Stiffening of the sclera may also be caused by alterations in the content of scleral glycosaminoglycan (Murienne et al., 2015, 2016). The scleral ECM response to chronic IOP elevation in glaucoma has also been studied from both a biomechanical and microstructural perspective by groups using scattering methods and inflation testing in various combinations (Coudrillier et al., 2012, 2013; Danford et al., 2013; Jones et al., 2015; Pijanka et al., 2012). These studies are described in detail in s4.2.

### 3.3.2. Cellular response

In comparison to ECM, less is known of the response of cells to eye pressure fluctuation, yet scleral mechanotransduction is an area of

growing interest, driven in major part by the need to clarify the sclera's dynamic role in myopia and glaucoma development. Fibroblasts have the potential to impact tissue-level mechanics by two routes: (i) a slow, indirect route via their expression of ECM molecules (tissue remodelling), and (ii) a faster, direct route through force-transduction to ECM from intracellular cytoskeletal protein networks. Cultured human scleral fibroblasts have been shown to be sensitive to their mechanical environment. Applied load alters the expression levels of ECM molecules (Cui et al., 2004; Shelton and Rada, 2007) and promotes phenotypic changes (Qu et al., 2015) in vitro. Notably, high-magnitude and/or high-frequency load was shown to promote differentiation of cultured human PPS fibroblasts into contractile myofibroblasts (Qu et al., 2015), indicating that IOP fluctuations may have an important impact on fibroblast activity in vivo (Fig. 22).

Meanwhile, in vivo animal studies have reported increased myofibroblast cell numbers in the sclera of mice with experimental glaucoma (Oglesby et al., 2016) and tree-shrews with induced myopia (Phillips and McBrien, 2004). It has been suggested that the latter observation could explain recovery from axial elongation in the shrew eye that is too rapid to be attributable to matrix remodelling (Phillips and McBrien, 2004). A role for scleral myofibroblasts in regulation of eye size through tissue-level mechanical influence is further supported by the identification of collagen-binding integrins in human (Hu et al., 2011) and tree shrew (McBrien et al., 2006) derived scleral cell lines, and their demonstrated modulation of tissue creep in collagen gels seeded with human fibroblasts in vitro (Hu et al., 2011). In light of these observations, it is interesting to note that, in contrast to the adult eye, there is an absence of contractile scleral cells in primate eyes undergoing ocular growth (fetal and neonatal stages) (Poukens et al., 1998).

There is a growing consensus that fibroblast numbers in the sclera are probably greater than previously accepted, at least under pathological conditions. For example, recent work by Oglesby et al. (2016) demonstrated up to 6-fold increases in cell proliferation in the sclera of mice following experimental pressure elevation (Fig. 23). Altering the biochemical pathways that control scleral fibroblast number and contractile status could be one route to therapeutically modulating tissue level mechanics (Quigley and Cone, 2013). For example, it has been recently shown that rho-kinase inhibition can suppress cell proliferation and myofibroblast differentiation in cultured primary human PPS

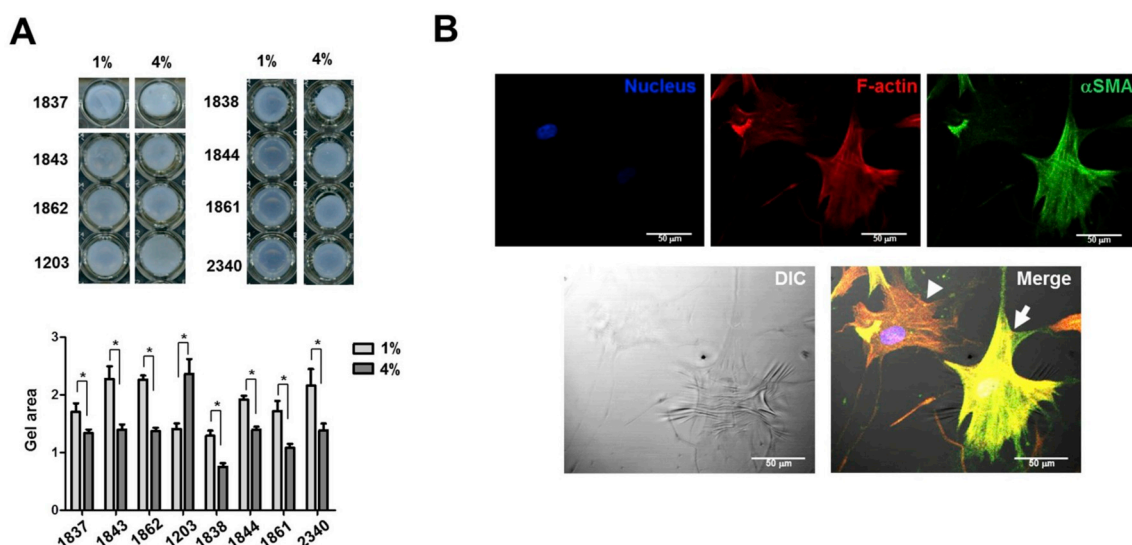


**Fig. 22.** Simulated IOP promotes contractility in cultured human scleral fibroblasts. **A)** Fibroblast contractility in response to 1% or 4% cyclic strain at 5 Hz for 24 h, assessed by a 3D collagen gel-based assay. The numbers refer to cell quantities, while the vertical graph axis denotes relative gel area (a.u.) as measured in ImageJ. **B)** Phase-contrast and confocal immunofluorescent images overlaid to show the correlation between expression of intracellular contractile apparatus ( $\alpha$ SMA and F-actin) and wrinkle formation. Arrow indicates a wrinkle-forming myofibroblast. Arrowhead indicates a non-wrinkle-forming fibroblast. Red: F-actin, Green:  $\alpha$ SMA, Blue: DAPI. Scale bar: 50  $\mu$ m. Reproduced from (Qu et al., 2015) with permission of the Association for Research in Vision and Ophthalmology.

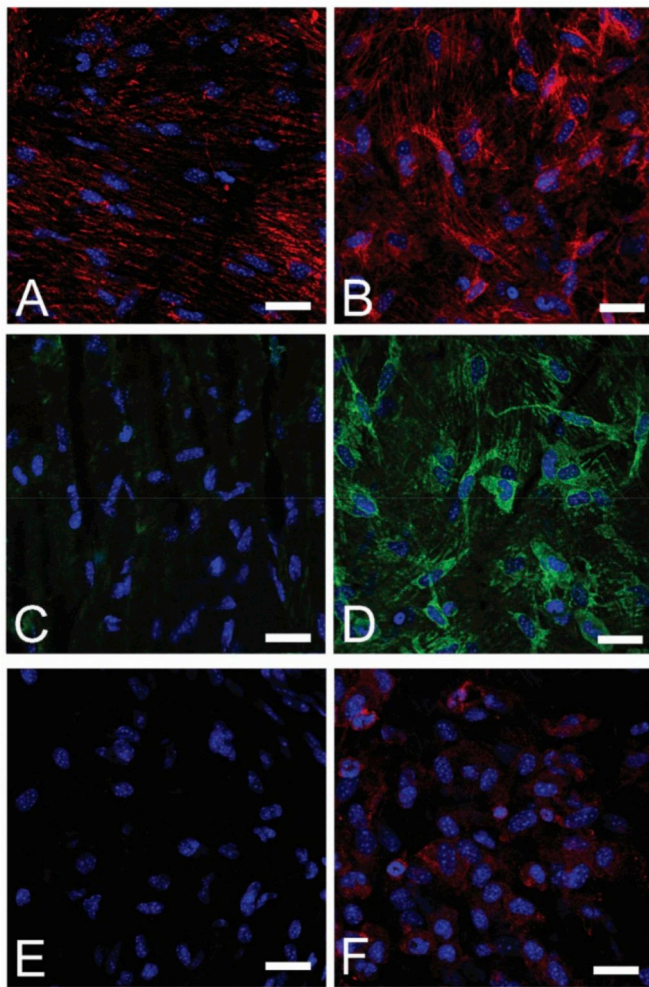


**Fig. 23.** Experimental glaucoma increases cell proliferation and myofibroblast differentiation in mouse sclera. *Top row:* Immunohistochemical labelling of vimentin (red) in A) control and B) 3-day glaucoma scleral wholemounts. *Middle row:*  $\alpha$ -SMA labelling (green) in C) control and D) 3-day glaucoma. *Bottom row:* cell adhesion molecule  $\alpha$ -actinin labelling (red) in E) control and F) 3-day glaucoma. DAPI nuclear counterstain is shown in blue in all panels. Scale bars = 20  $\mu$ m. Reproduced from (Oglesby et al., 2016) with permission of Molecular Vision.

fibroblasts (Pitha et al., 2018). It will be interesting to see whether the translational potential of these findings in glaucoma therapy can be realised going forward.

### 3.4. Scleral influence on ONH biomechanics

The scleral influence on ONH biomechanics has been studied using both generic and specimen-specific models. An example of early generic numerical modelling is the work of Bellezza et al., who studied the effects of the scleral canal size and shape and scleral thickness on the biomechanical response of the ONH (Bellezza et al., 2000). They found that, for a given level of IOP, a thinner sclera with a larger and more elliptical canal induced higher stresses within the load-bearing connective tissues of the ONH. Expanding on this early work, Sigal et al. developed a more realistic generic model that incorporated pre- and post-laminar neural tissues, as well as the central retinal vessel and the pia mater (Sigal et al., 2004). They found that the mean laminar strain was more sensitive to the scleral stiffness than to the laminar stiffness and was only weakly dependent on the stiffness of the neural tissues and pia mater. A schematic illustration of how the stiffness of the sclera affects the IOP-induced ONH deformations is shown in Fig. 24 (Sigal

et al., 2011b).

To determine which anatomic and biomechanical factors most influenced the biomechanical response of the ONH to acute changes in IOP, Sigal et al. parameterized the generic model into 21 factors representing ONH tissue anatomies and material properties (Sigal et al., 2005). The biomechanical response of the ONH tissues was quantified through a set of 29 outcome measures, including peak and mean stress and strain within each tissue, and measures of geometric changes in ONH tissues, such as the cup-to-disc ratio. The five most important determinants of ONH biomechanics (in rank order) were identified as: the stiffness of the sclera, the size of the eye, IOP, the stiffness of the LC, and the thickness of the sclera. This study was the first to highlight the importance of scleral stiffness on ONH stress and deformation. However, it was performed with the simple, but limited, method of varying one parameter at a time. Sigal et al. then extended this work by varying the geometric and material parameters simultaneously (Sigal et al., 2009). They found that independently increasing either the stiffness or thickness of the sclera leads to reduced deformations being transmitted to the ONH. However, if the sclera is already quite stiff, then changing its thickness has relatively little effect on ONH biomechanics and vice versa.

Girard et al. developed a generic model to investigate the effects of scleral collagen fibre alignment on scleral and ONH mechanics (Girard et al., 2009b). The influence of the fibre concentration factor, a parameter used to describe collagen fibre alignment along a preferred fibre orientation, was also evaluated. Results showed that a circumferential fibre organisation in the sclera reduced scleral canal expansion, whereas the opposite was observed with a meridional fibre organisation. Perez et al. developed a generic model of the corneoscleral shell to simulate the viscoelastic responses of the eye during micro-volumetric changes (Perez et al., 2013). The viscoelastic properties of the cornea and the sclera, including the instantaneous modulus, equilibrium modulus, and relaxation time constants, were parameterized to examine their effects on IOP elevations at different rates of volumetric changes. Results showed that all viscoelastic properties influenced the profile of the dynamic IOP due to volumetric changes, and the relative significance of a specific parameter was highly dependent on the rate of change. From this, they concluded that it is necessary to better characterise the viscoelastic properties of ocular tissues. Ayyalasomayajula et al. developed a porohyperelastic model of the ONH to discern the effects of interstitial and intracellular fluid pressure on the biomechanical response to IOP (Ayyalasomayajula et al., 2016). A generic model of the human eye was constructed and the fluid permeabilities of the retina-Bruch's-choroid complex, sclera, uveoscleral pathway, and trabecular meshwork were parameterized. IOP, translaminar pressure gradient and strains in the lamina were considered as computational outputs. As tissue permeability increased, both IOP and translaminar pressure gradient decreased, resulting in decreased strains in the lamina.

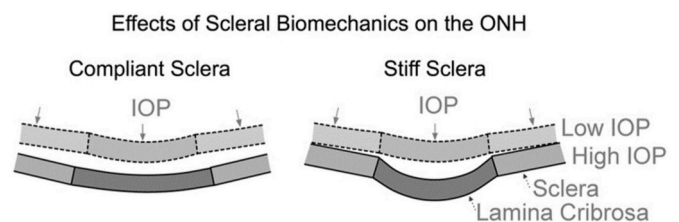


**Fig. 24.** A schematic illustration of how the stiffness of the sclera affects the IOP-induced ONH deformations. In the case of a compliant sclera (left), an increase in IOP induces large scleral deformations, which are transmitted to the scleral canal, resulting in a large scleral canal expansion that pulls the lamina taut. Conversely, a stiff sclera deforms little under IOP (right), with a small scleral canal expansion, allowing the lamina to be displaced posteriorly by the action of IOP on its anterior surface. Figure adapted from (Sigal et al., 2011b) with permission of the Association for Research in Vision and Ophthalmology.

Specimen-specific models, which are based on the geometry and/or mechanical properties of an individual eye, have been developed to more accurately evaluate ONH biomechanics. Sigal et al. developed models of human posterior poles with specimen-specific geometries to explore the IOP-induced deformation of the ONH (Sigal et al., 2007, 2010, 2011a, 2009). They found that the scleral stiffness was the most important material parameter in determining the biomechanical insult to the lamina, matching the findings from generic models (Sigal et al., 2004, 2005, 2009). Norman et al. developed human globe models that combined specimen-specific corneoscleral shells and generic ONHs to determine the effects of globe shape and size on ONH biomechanics (Norman et al., 2010b). They found that the PPS thickness was the largest determinant of ONH biomechanics, with decreased thickness resulting in increased maximum strains in the LC and increased scleral canal radial displacement.

The state of the art in eye models now includes experimental measurements of collagen microstructure. Coudrillier et al. developed a model with human specimen-specific scleral geometry including specimen-specific details of sclera collagen anisotropy derived from WAXS

data, but with a generic lamina (Coudrillier et al., 2013). The non-linear material stiffness used in this study was also specimen-specific and was determined through inverse modelling. This model implemented a distributed fibre-based constitutive equation that allowed them to study the influence of collagen fibre alignment and anisotropy through an elegant parametric variation. They found that increasing fibre anisotropy in the PPS resulted in a decrease in LC strains and scleral canal expansion, but also resulted in a posterior deformation of the LC. Campbell et al. created a finite element model with a generic geometry but non-linear and anisotropic material properties based on specimen-specific measurements of connective tissue volume fraction and collagen beam orientation obtained from a  $\mu$ CT scan of a porcine eye (Campbell et al., 2015). They compared their full model to a model of a homogenous isotropic lamina and an inhomogeneous isotropic lamina. They found that the structure of the LC homogenises the strain field within the lamina and that the anisotropy of the collagen beams had little influence on the lamina strains. Zhang et al. incorporated fibre organisation information from postmortem human eyes within the ONH models (Zhang et al., 2015a). The models predicted that the

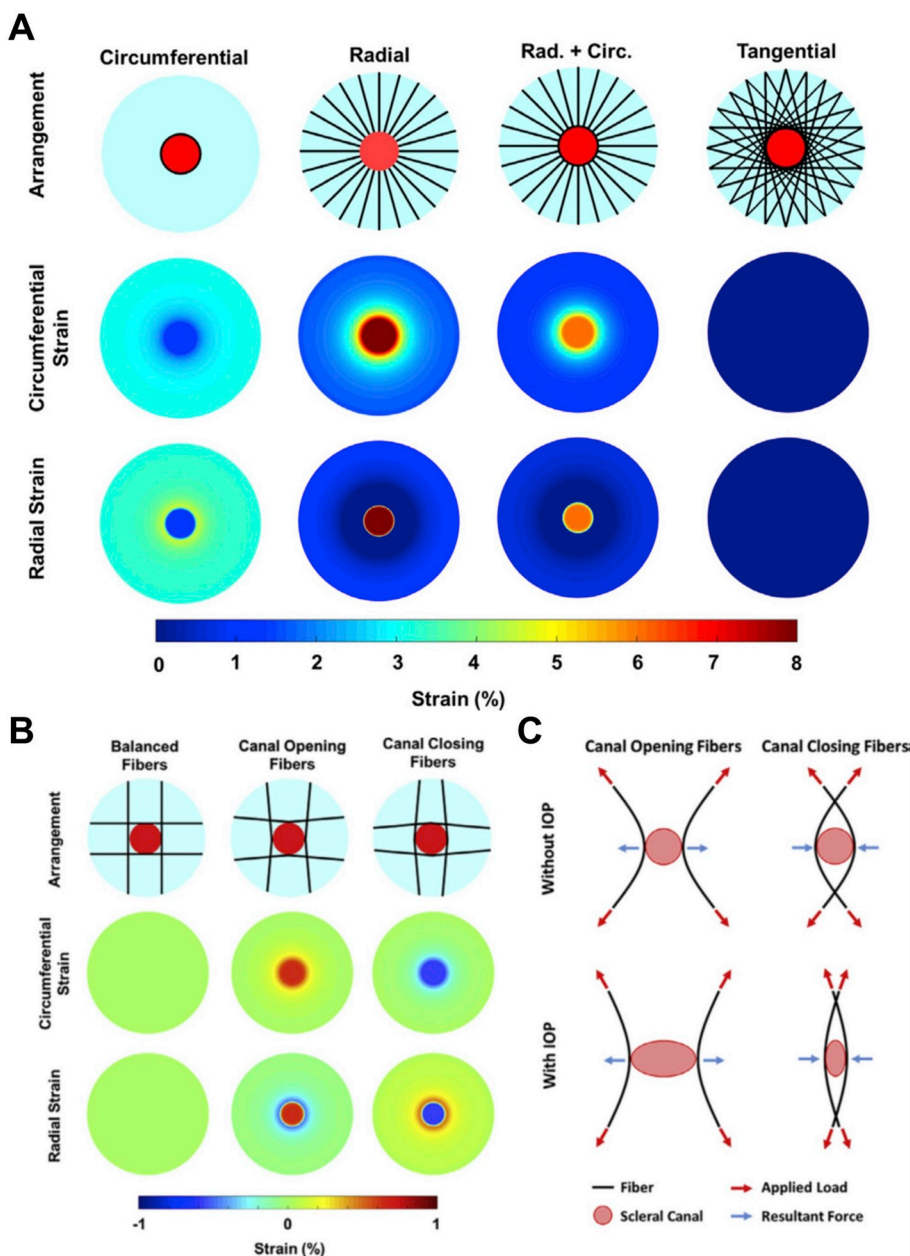


**Fig. 25.** A) Computational models used to simulate the biomechanical behaviour of four theoretical collagen fibre arrangements (top row). Shown in light blue is the posterior sclera, with the scleral canal as a red disc. The black lines represent the collagen fibres. On the middle and bottom row are shown contour levels of the magnitude of the deformations (strain) due to an IOP elevation of 50 mmHg. A simple reinforcement of the canal with circumferential fibres limited the strain in the lamina due to IOP but did provide support to the sclera. Conversely, a radial arrangement of fibres reduced the strain in the sclera, but lead to high strains within the lamina. The combination of radial and circumferential fibres still caused high strains in the lamina. A tangential arrangement of fibres provided the best reinforcement for both the sclera and the lamina, reducing the strains to near zero-levels. Depending on the fibre curvature, long fibres tangential to the canal can have substantially different responses to IOP increases. B) Maps of IOP-induced strain for three different fibre curvatures. When the fibres were concave to the canal (Canal Closing Fibers), increased IOP caused the canal to close, and lamina compression. When the fibres were convex (Canal Opening Fibers), increased IOP caused the canal to open and the lamina to stretch. Note that the models incorporated many fibres. For simplicity, only a few are shown. C) Diagram of the mechanism of action of long tangential fibres. For concave fibres, the load from IOP results in an outward tensile force at the canal boundary as the fibres straighten. For convex fibres, the load from IOP results in an inward compressive force at the canal boundary as the fibres straighten. Figure adapted from (Voorhees et al., 2018) with permission of Acta Biomaterialia.

circumferential collagen fibres in the PPS were effective in limiting LC strains and was able to reduce strain levels at the scleral canal boundary. Instead, Voorhees et al. proposed an alternative fibre architecture for the PPS, in which the scleral canal is supported primarily by long-running fibres oriented tangentially to the canal (Voorhees et al., 2018). They found that the theoretical tangential arrangement of fibres afforded better mechanical support to the tissues within the scleral canal as compared to a simple circumferential ring of fibres (Fig. 25A).

Importantly, the long fibre arrangement may also explain clinically observed behaviours of the ONH that otherwise have found no explanation in other theories of PPS mechanics and behaviour, such as a contraction of the scleral canal under elevated IOP (or its counterpart, an expansion under a decrease in IOP) (Poostchi et al., 2010; Strouthidis et al., 2011; Yang et al., 2009, 2011). A mechanism by which long tangential fibres can have these effects is presented in Fig. 25B and C. Mechanically, the distinction between canal opening and closing under elevated IOP is important, as they likely have different effects on the flattening and lateral stretching or compression of the lamina (Sigal et al., 2011a, 2011b). In turn, from a mechanobiological standpoint, these would have distinct effects on the axons and glial cells within the canal.

An important element of the model developed by Voorhees et al. is that they considered the tangential fibers as long bundles spanning several millimeters. This is different from the traditional approach taken by the other biomechanical studies mentioned above. Those studies acknowledge that the collagen in the sclera is in the form of fibres. The fibres, however, are only considered as part of a continuum material with short fibres spanning each finite element, and which do not interact with one another. This is a simplification of the scleral structure in which the collagen fibre bundles are interwoven and carry loads over scales much larger than the finite elements.

The precise nature of the PPS fibre organisation remains an issue of debate and intense study. However, some consensus may be found across recent studies. For example the presence of a subpopulation of long straight fibres (as postulated by Voorhees et al.), that co-contributes to ONH canal support together with annular or shorter tangential fibres, would be consistent with previous WAXS studies that reported tangential linear “bands” emanating from the PPS pseudo-annulus into the mid-posterior sclera (see s2.1.1) (Pijanka et al., 2012). Interestingly, more than a decade earlier Meek and Boote had envisaged a similar linear tangential model as one possible explanation of the circumferential collagen fibrils in the corneoscleral limbus (Meek and

Boote, 2004), although its biomechanical implications were not studied. The model by Voorhees et al. suggests that long tangential fibres in the limbus would play a major role in anterior segment mechanics.

#### Key points:

- Experimental, computational and analytical studies all support the notion that the sclera plays a central role in ONH biomechanics.
- The sclera's influence on the ONH is highly complex. It is not easy to predict accurately how a specific ONH and sclera pair will behave mechanically, or how this may affect susceptibility to mechanically-related pathologies such as glaucoma.

### 3.5. Scleral response to optic nerve traction

The ‘standard’ biomechanical theory of glaucoma hypothesizes that elevated (or fluctuating) IOP deforms the ONH tissues, including the LC, and that these deformations drive RGC injury and death (resulting in blindness). However, IOP is not the only load deforming the eye tissues. Studies that used OCT (Chang et al., 2017; Sibony, 2016; Wang et al., 2016a), finite element modelling (FEM) (Wang et al., 2016c, 2017b) and MRI (Demer, 2016) all converge to the conclusion that horizontal eye movements considerably deform/shear the ONH tissues (through the “strong” optic nerve [including its sheath] traction imposed on the ONH). These studies also indicate that such deformations can be as large (or significantly larger) than those induced by a substantial IOP elevation (Wang et al., 2016a, 2016c) (Fig. 26). Using FEM, Wang et al. were able to predict relatively large optic nerve traction forces during eye movements, i.e. between 90 (abduction) and 150 mN (adduction), in the same order of magnitude as extraocular muscle forces (Wang et al., 2017b). These forces are directly transmitted to the PPS and scleral flange via the dura, and may have important consequences on the growth and remodelling behaviour of the posterior sclera and surrounding tissues. For instance, optic nerve traction forces may partially explain: 1) the development and progression of myopia; 2) the development of staphylomas (i.e. weak spots within the scleral shell); 3) the presence of tilted discs in myopia; 4) intrachoroidal cavitations; and 5) peripapillary atrophy (Jonas et al., 2016a; Wang et al., 2016b). Interestingly, these findings may also relate to recently reported microstructural alterations found in the PPS of human high myopia eyes (Markov et al., 2018) (see s4.3). Further, Wang et al. showed using simulations that the presence of a stiff sclera (or a weaker, or more tortuous, optic nerve) would, in theory, considerably

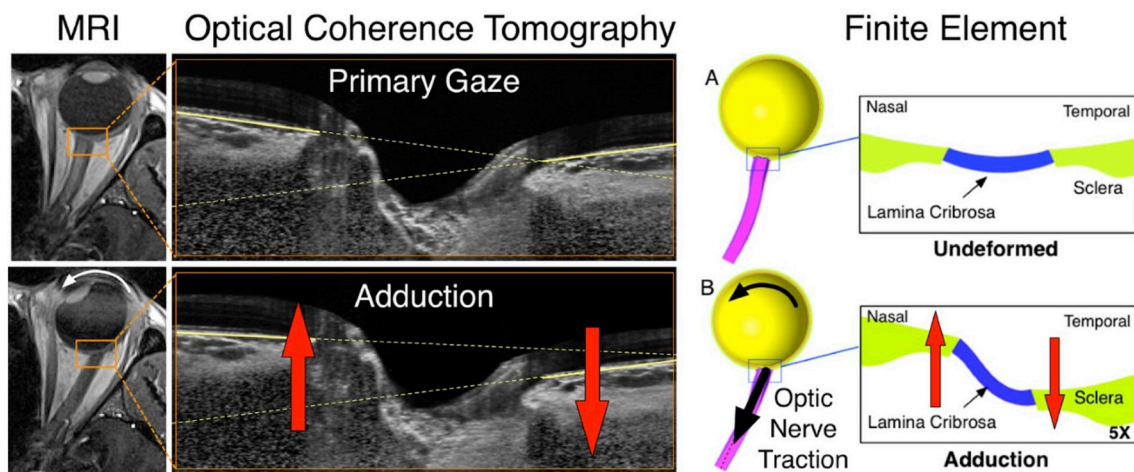


**Fig. 26.** Magnetic resonance imaging (left), optical coherence tomography imaging (centre), and finite element modelling (right) all strongly suggest that the optic nerve applies a traction force onto the back of the eye during eye movements. The net result is shearing of the optic nerve head tissues (red arrows). Note that deformations were magnified 5 times in the finite element models to aid visual interpretation. Adapted from (Wang et al., 2016a, 2016b, 2017) with permission of the Association for Research in Vision and Ophthalmology.

reduce gaze-induced ONH deformations, and may thus limit the development of such conditions. This idea awaits experimental support.

### 3.6. Scleral influence on the ocular pulse during the cardiac cycle

IOP is not a constant value, but instead is pulsatile in nature. The difference between systolic and diastolic IOP defines the ocular pulse amplitude (OPA), that ranges between 0.9 and 7.2 mm Hg in healthy subjects (Kaufmann et al., 2006). Generally, it has been well accepted that the OPA is mainly caused by acute choroidal expansion due to pulsatile blood flow, and changes in the mechanical properties of the sclera could strongly influence the OPA, which might, in turn, have implications for the development and progression of glaucoma. To better understand how the sclera could influence the OPA, Jin et al. built a comprehensive FEM of the eye that took into account blood pressure and choroidal swelling during the cardiac cycle (Jin et al., 2018). The authors found that, during the cardiac cycle, a change in arterial pressure resulted in choroidal expansion which, in turn, induced a change in IOP (the OPA) and ONH deformations. From diastole to systole, they found that choroidal expansion made the peripapillary retina move anteriorly, but both choroidal expansion and the OPA made the prelamina and LC move posteriorly. The net result was shearing of neural tissues in the neuroretinal rim. Interestingly, a stiffer sclera was shown to result in a higher OPA, smaller pulse volume, larger diastole-to-systole ONH strains, and larger neural tissue shear in the neuroretinal rim. In order to estimate how scleral stiffness could influence IOP spikes, several studies used rapid microvolumetric PBS injections in the posterior chamber of porcine eyes and modelled the process computationally (Clayson et al., 2017; Morris et al., 2013; Perez et al., 2013). These studies showed that a stiffer sclera (induced with crosslinking agents) could significantly increase IOP spike magnitudes for a given volumetric change. Increasing the baseline IOP (and hence making the sclera stiffer) also resulted in significantly higher IOP spikes. In summary, experimental and computational studies converge to the idea that a stiffer sclera will generate higher IOP spikes (i.e. greater OPA) and, counter-intuitively, has the potential to generate higher neural tissue deformations.

### 3.7. Scleral response to cerebrospinal fluid pressure

While several studies have addressed the effects of cerebrospinal fluid pressure (CSFP) on the biomechanical environment within the scleral canal and the LC (Feola et al., 2016, 2017; Hua et al., 2017; Jonas, 2011; Morgan et al., 1995; Sibony et al., 2011; Wang et al., 2017a), little is known about the scleral response to CSFP. Fazio et al. used OCT angiography to image and quantify the CSFP-induced ONH deformations in the living human eye (Fazio et al., 2018). They found

that the CSFP-induced strains in the PPS were higher than those in the LC and retina. In addition, their results showed that the PPS strain was negatively correlated with the retinal nerve fibre layer (RNFL) thickness. Hua et al. extended a previously published numerical model of the ONH (Sigal et al., 2005) to include CSFP and 23 other factors representing IOP, central retinal artery blood pressure, tissue anatomy and mechanical properties, and constraints on the optic nerve (Hua et al., 2018). A total of 8340 models were studied to predict factor influences on ONH deformations. The models predicted that IOP and CSFP were the top and sixth most influential factors on ONH biomechanics, respectively. However, IOP and CSFP had different effects. For instance, the strongest effect of CSFP was on the rotation of the PPS, where its influence was more than twice as large as that of IOP. This suggests that the translaminar pressure, computed as the difference of IOP and CSFP, may be too simplistic as a parameter to predict biomechanical insult to the ONH. Fig. 27 illustrates how increases in CSFP cause deformation of the ONH. Several studies have also reported that the flattening of the posterior sclera in space flight-associated neuro-ocular syndrome (SANS) is linked to CSFP elevation in micro-gravity environment (Kramer et al., 2012; Lee et al., 2017; Mader et al., 2011).

## 4. Scleral changes with ageing and disease

### 4.1. Ageing

Numerous studies have shown that the structure and composition of the sclera change with age, though the findings are sometimes conflicting depending on the experimental methods, age range, and animal species examined. Thickness measurements of fresh enucleated monkey eyes (Girard et al., 2009c), mouse eyes older than 1 year (Nguyen et al., 2013) and human donor eyes (Coudrillier et al., 2012) have shown that the sclera thins with age. However, other histological thickness measurements of fixed human eyes did not show variation with age (Vurgese et al., 2012). In the human sclera, the number of elastin fibres decreases after 20 years of age (Watson and Young, 2004), while decorin and biglycan levels decrease after age 40 (Rada et al., 2000). The cross-sectional area of scleral collagen fibrils increases with age (Malik et al., 1992), which may be caused by age-related accumulation of advanced glycation end-products (AGEs) (Schultz et al., 2008). Moreover, the mean collagen fibril radius and intermolecular lateral spacing in the sclera is also larger in older eyes (Daxer et al., 1998). Taken together, these findings point to both an accumulation of intermolecular, non-enzymatic crosslinks and an increase in the number of tropocollagen molecules per fibril as important mechanistic determinants of the stiffening of the sclera as it ages. WAXS measurements of the collagen fibre structure by Coudrillier et al. in the posterior sclera of human donor eyes measured a significant degree of collagen fibre alignment, but no changes in the

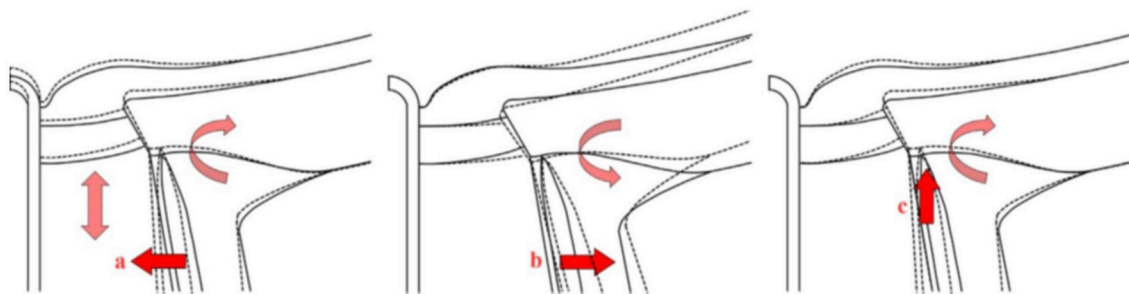


Fig. 27. A schematic description of three mechanisms by which increases in CSFP cause ONH deformations. Undeformed ONH is shown with continuous lines, and deformed ONH with dashed lines. (a) CSFP acts inwardly compressing the pia mater and the retrolaminar neural tissue within. Due to the Poisson effect, lateral compression may cause expansion in the axial direction, increasing retrolaminar pressure (Morgan et al., 1995) “pushing” anteriorly on the lamina and causing clockwise rotation of the PPS. (b) CSFP acts outwardly on the dura mater away from the pia mater, causing the known distension of the dural sheath (Killer et al., 2003), rotating the PPS counterclockwise, and displacing the periphery of the lamina posteriorly. (c) CSFP “pushes” the PPS anteriorly, causing flattening of the globe and clockwise rotation of the PPS, and displacing the periphery of the lamina anteriorly. Figure adapted from (Hua et al., 2018) with permission of the Association for Research in Vision and Ophthalmology.

dominant collagen fibre orientation, of the tissue with age (Coudrillier et al., 2015b) (Coudrillier et al., 2015a). In contrast, SALS measurements by Vande Geest and coworkers did not find age-related variations in the fibre structure of the human sclera (Danford et al., 2013; Yan et al., 2011). The contrasting results may be associated with differences in the way that these studies defined the degree of fibre alignment and in the specific regions of the sclera they examined. Moreover, as mentioned, unlike WAXS measurements using SALS are not specific to collagen and may include the alignment of elastin fibres.

The gross shape of the sclera is also altered by ageing. Recently, using OCT, Tun et al. found that the shape of the sclera at its boundary with the ONH changes as a function of age (Tun et al., 2019). On average, the anterior surface of the PPS had a characteristic v-shaped configuration with its peak pointing towards the orbit. The range, however, varied from an inverted v-shaped (but with a relatively flat profile) to a more pronounced v-shaped configuration. Interestingly, the v-shaped configuration was more prominent with increasing age, worse vision, thinner cornea, greater axial length, thinner peripapillary choroid, and deeper anterior LC (Fig. 28). Such changes in PPS shape with age could have a significant impact on the overall biomechanical environment of the ONH, and therefore warrant further investigation.

The mechanical behaviour of the sclera has been measured using a variety of methods in human, monkey and mouse eyes, and the studies have consistently found a stiffening effect with age. Uniaxial strip tests of human sclera reported that the elastic modulus increased with age and was different in the anterior and posterior regions (Friberg and Lace, 1988) (Geraghty et al., 2012). Inflation tests of the posterior scleral shell of monkey eyes (Girard et al., 2009c), canine eyes (Palko et al., 2016) and human eyes (Coudrillier et al., 2012; Fazio et al., 2014a) all observed a stiffening of the pressure-strain response with older age. Interestingly, scleral stiffness increases more rapidly with age

in eyes from donors of African descent (Fazio et al., 2014b). If and how this latter observation might link to racial differences in susceptibility to scleral-related diseases such as myopia and glaucoma remain important unanswered questions. Pressure-displacement response, measured in inflation tests of mouse eyes, was also significantly stiffer in older compared to younger mouse eyes (Myers et al., 2010a).

Various studies have applied computational modelling and inflation testing to estimate the mechanical properties of the sclera and collagen fibres and their alterations with age. The stress-strain relationship of the sclera was described by anisotropic hyperelastic models that represent the tissue as a distribution of stiff collagen and elastin fibres in a more compliant isotropic matrix. The latter represented contributions from non-fibrous components of the tissue, such as PGs, and the effects of crosslinking. Girard et al. (2009c) and Grytz et al. (2014) applied such models to fit the elastic properties of the fibres and matrix, and parameters for the distribution of fibre orientation, to full-field inflation scleral data of monkey and human eyes. Coudrillier et al. (2013) applied experimental WAXS measurements directly to describe the collagen fibre structure and fit the elastic properties of the collagen fibres and matrix to the inflation tests of human eyes. All three studies showed that the shear modulus of the soft matrix material increased with age. The increase in matrix stiffness may be caused by the accumulation of AGEs with age and other age-related changes in the matrix microstructure that may affect collagen interfibrillar interactions. For example, Murienne et al. (2016) showed that removing glycosaminoglycans in the posterior sclera of human donor eyes decreased the scleral thickness and increased its stiffness under inflation testing. Grytz et al. (2014) also reported that the collagen crimp angle decreased with age. Both a larger matrix stiffness and a smaller collagen crimp angle lead to a stiffer stress-strain response in the low-pressure region of an inflation test, resulting in a more linear stress-strain response. The findings for

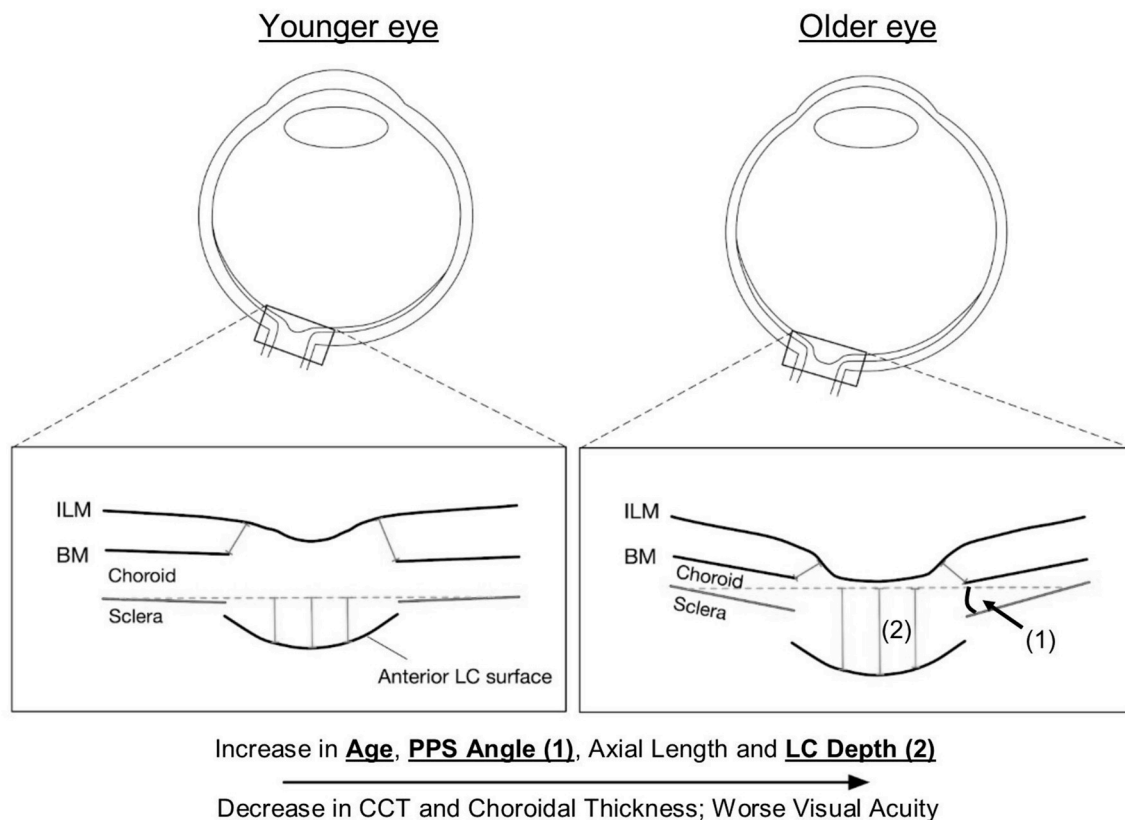


Fig. 28. Determinants of the peripapillary sclera (PPS) angle in healthy eyes. An increase in the v-shaped configuration of the peripapillary sclera (PPS) is associated with increasing age, longer axial length, thinner central corneal thickness (CCT), thinner choroidal thickness, worse vision and an increase in lamina cribrosa (LC) depth. Adapted from (Tun et al., 2019) with permission of the Association for Research in Vision and Ophthalmology.

the collagen fibre stiffness were more varied. Girard et al. (2009c) found that the strain-stiffening behaviour of the scleral collagen fibres in monkeys increases with age, indicating that the sclera stiffens more quickly with strain in older animals. Grytz et al. (2014) reported that the collagen fibre modulus decreased with age in European-derived donor eyes, while there was no statistically significant age effects in fibre modulus in African-derived donor eyes. Furthermore, Coudrillier et al. found that the fibre modulus increased with age in human diabetic donors but not in those without diabetes (Coudrillier et al., 2015a, b). However, despite these advances in our knowledge, the precise relationship between ageing, diabetes and glaucoma remains to be established. Notably, experiments thus far have probed the equilibrium and pseudo-elastic behaviour of the sclera, while the age-dependent viscoelastic scleral properties remain poorly characterised. Importantly, viscoelastic properties determine the deformation response of the sclera and ONH to IOP fluctuations and optic nerve traction, and may impart toughness to the interfacial interactions between the retina and sclera. This has clinical implications not only for glaucoma, but also macular degeneration.

#### Key points:

- The stress-strain response of the sclera becomes stiffer and more linear with age.
- Age-related mechanical changes are likely due to an accumulation of intermolecular collagen crosslinks and a reduction in glycosaminoglycan content that alters collagen fibril morphology and interactions.
- Age-related alterations in scleral material behaviour may be important in glaucoma and macular degeneration.

#### 4.2. Glaucoma

Multiple studies have shown that the collagen structure and mechanical behaviour of the PPS is different in glaucoma human donor eyes and in animals subjected to long-term IOP elevation. Significant regional differences have been measured in the collagen fibre organisation of human eyes using WAXS (Coudrillier et al., 2015c; Pijanka et al., 2012) and SALS (Danford et al., 2013). Using WAXS, Pijanka et al. reported a decrease in the degree of fibre alignment in the superior/temporal and inferior/nasal quadrants of the human PPS, while the remaining two quadrants showed an increase (Pijanka et al., 2012). A later study with a larger number of specimens showed that the collagen structure in the PPS overall becomes more uniform as the eye's glaucoma status (based on axonal loss) changed from normal to glaucoma undamaged to glaucoma damaged (Coudrillier et al., 2015c). SALS measurements showed that a parameter related to the degree of collagen alignment of the PPS of glaucoma eyes was higher than in

normal eyes in the nasal region, but smaller in the superior region (Danford et al., 2013). The collagen structure of the PPS also became less organised in mouse eyes with glaucoma. Pijanka et al. measured a lower degree of collagen alignment in bead-injected glaucoma mouse eyes compared to the contralateral control eye (Pijanka et al., 2014). Meanwhile, Cone-Kimball et al. performed detailed TEM evaluation of the collagen structure in bead-glaucoma mouse eyes and reported an increase in the number and cross-sectional area of collagen fibrils. There was also an increase in the number and cross-sectional area of collagen fibrils. There was also an increase in the number smaller diameter fibrils and fewer larger diameter fibrils (Cone-Kimball et al., 2013).

The mechanical behaviour of the PPS becomes stiffer with glaucoma. Nguyen et al. developed an inflation test method for mouse eyes that used two-dimensional DIC to track the deformation of the scleral edge (Nguyen et al., 2013). They observed a stiffer pressure-strain response in the PPS, in both the meridional and circumferential directions, in bead-glaucoma mouse eyes compared to contralateral controls. Downs et al. used uniaxial strip tests to measure the stress relaxation behaviour of the PPS of normal and early-glaucoma monkey eyes and found a stiffer equilibrium (long-time) elastic modulus in the early-glaucoma group (Downs et al., 2005). The increased scleral stiffness in early-glaucoma monkey eyes was later confirmed by Girard et al. in more detailed inflation tests with ESPI to measure the full 3D deformation field of the posterior sclera (Girard et al., 2011). The authors applied IFEM to fit the parameters of a hyperelastic distributed fibre model to the surface deformation field and reported a larger elastic modulus and structural stiffness. Coudrillier et al. applied inflation testing with DIC to measure the full-field deformation response of the posterior sclera of human donor eyes and found that diagnosed glaucoma patients, both with and without optic nerve damage, exhibited a stiffer pressure-strain response in the meridional direction and a smaller ratio of meridional to circumferential strain in the PPS (Coudrillier et al., 2012). These findings were consistent with WAXS measurements indicating a less aligned fibre structure in the various regions of the PPS (Pijanka et al., 2012). IFEM showed that, on average, the matrix shear modulus and collagen fibre stiffness increased as the level of optic nerve damage changed from undamaged to glaucoma undamaged and finally glaucoma damaged (Coudrillier et al., 2015c). However, the effect was not statistically significant because of the large inter-specimen variability.

The pressure-strain inflation response of the PPS is stiffer in C57BL/6 mice compared to the albino CD1 strain, which has a longer and wider eye and thinner PPS. In bead-injection glaucoma experiments, the optic nerve of CD1 mice was more susceptible than C57BL/6 to RGC axonal death, while the sclera of bead-glaucoma CD1 eyes exhibited a significantly larger stiffening effect than that of C57BL/6 eyes (Cone et al., 2010). However, modelling studies have not definitively determined whether a stiffer scleral response to pressure is indicative of a stiffer scleral material behaviour (i.e. a larger elastic modulus) because of the large variability in the inflation response of individual glaucoma eyes.

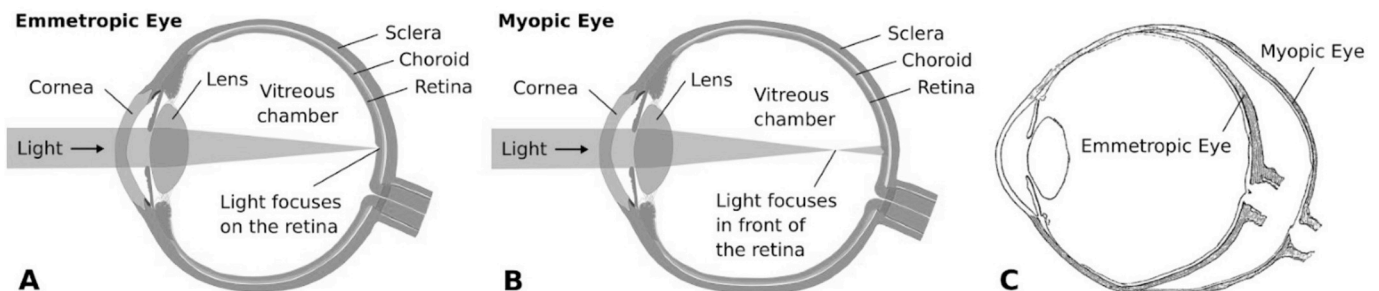


**Fig. 29.** Effect of myopia on eye shape. **A)** Emmetropia is the visual condition of the normal eye with clear vision. This condition is achieved when the axial length of the eye matches the refractive power of the cornea and lens, such that light rays are focused exactly on the retina. **B)** A myopic eye is too long for its optical components and light focuses in front of the retina causing faraway objects to appear blurry. **C)** Overlaid histologic sections of the emmetropic eye and the contralateral, highly myopic eye of the same donor showing the extended posterior segment of the myopic eye. The anatomy of the anterior segment is nearly identical in both eyes. In contrast, the posterior segment of the myopic eye is elongated compared to the emmetropic eye, causing the typical increase in axial length seen in myopia. Reproduced from (Grytz, 2018) with permission of Kugler Publications.

Moreover, it remains unclear whether a stiffer response to pressure is protective of glaucoma. Mice with a mutation in collagen 8A2 exhibited a larger eye and stiffer scleral response to IOP, and were less susceptible to RGC axon death than the wild-type B6 control (Steinhart et al., 2012). However, stiffening the sclera of CD1 mice by collagen crosslinking with glyceraldehyde led to greater susceptibility to RGC damage (Kimball et al., 2014). Efforts to directly measure ONH deformation in mouse models may show the combined effects of variations in eye length, regional scleral thickness and scleral stiffness on the observed strains (Nguyen et al., 2017, 2018). More detailed modelling is needed to evaluate the combined effects of these factors on the stresses experienced by the glial and axonal tissues of the ONH (Myers et al., 2011).

#### Key points:

- Chronic IOP elevation causes remodelling of PPS collagen structure and a stiffer pressure-strain response, that occurs concurrently with optic nerve damage.
- The effects of IOP increase are individually variable and may be influenced by the homeostatic baseline structure and mechanical properties of a given eye.

### 4.3. Myopia

Myopia is the most common refractive condition, affecting about 22% of the current world population (Holden et al., 2016). In a normal emmetropic eye with clear vision, light rays entering the eye focus precisely on the retina (Fig. 29A). However, in a myopic eye light rays focus in front of the retina, causing the typical blurry vision in myopia (Fig. 29B). Generally, myopia first occurs in school-age children and typically progresses until age 20. Juvenile-onset myopia is typically characterised by an elongated posterior scleral shell (Fig. 29C).

Human and animal studies have confirmed the existence of a common mechanism across species that uses visual cues to actively match the axial length of the eye to its focal length (Howlett and McFadden, 2007; Norton and Siegart, 1995; Siegart and Norton, 2011; Wallman and Winawer, 2004; Wildsoet, 1997). This vision-guided, active process is called emmetropization. Like humans, many animals are hyperopic at birth (i.e. the light focuses behind the eye) and the refractive error diminishes as the eye emmetropizes. In animals, eye size can be experimentally modulated by shifting the focal plane posterior or anterior to the retina using negatively or positively powered lenses, making the eye respectively myopic or hyperopic (Norton et al.,

2010; Schaeffel et al., 1988; Siegart and Norton, 2010). Increasing evidence from animal studies suggests that the emmetropization process relies on a feedback mechanism that alters scleral remodelling to match the axial length of the eye to its optical system. Fig. 30 illustrates the emmetropization process as a mechanism involving the detection of visual stimuli at the retina, signaling from the retina to the sclera and modulation of scleral remodelling and axial elongation; which in turn modulates the visual stimulus and closes the loop.

The prevalence of myopia has dramatically increased over the past 60 years and has risen from 20% to nearly 90% in some Asian populations (Dolgin, 2015). Several visual stimuli have been identified to alter the refractive development of the eye including axial defocus, peripheral defocus, form deprivation, light intensity, contrast and light chromaticity (Ashby et al., 2009; Gawne et al., 2017; Liu and Wildsoet, 2011; Ohlendorf and Schaeffel, 2009; Rucker and Wallman, 2012; Sherman et al., 1977; Wallman et al., 1978). While the exact cause of the epidemic increase in myopia is still unclear, accelerated scleral remodelling is thought to be a common factor across all visual stimuli that may cause myopia (Grytz, 2018).

Several changes in scleral composition and structure have been identified in human myopia and experimental animal myopia. In terms of composition, notable changes reported include lower hyaluronan and sulfated glycosaminoglycan levels (Moring et al., 2007), upregulated enzymatic degradation (Guggenheim and McBrien, 1996; Guo et al., 2013), downregulated collagen type I synthesis (Gentle et al., 2003) and downregulation of aggrecan (Siegwart and Strang, 2007). While myopia occurs early in life and is characterised by an elongated eye size, accelerated tissue growth is not the cause of myopia. Scleral growth ceases very early during axial development of the eye. Scleral volume increases from birth to the end of the second year of life but remains unchanged thereafter in both normal eyes (Shen et al., 2016) and eyes that develop myopia (Jonas et al., 2014, 2016b). Similar to human myopia, the amount of sclera changes little (3–5% reduction in dry weight) during experimental myopia in tree shrews (McBrien et al., 2000, 2001; Moring et al., 2007). In human eyes, scleral thickness decreases significantly with increasing axial length (Shen et al., 2015a). In severe cases of high myopia, the sclera thickness was reported to be only 31% of a normal sclera (Cheng et al., 1992). Severe scleral thinning in high myopia can lead to the formation of posterior scleral staphyloma. Animal studies have confirmed that the sclera thins during experimental myopia (McBrien et al., 2001; Norton and Rada, 1995). These tissue-level observations suggest that not accelerated scleral growth, but another distinct mechanism underlies axial elongation in myopia: scleral

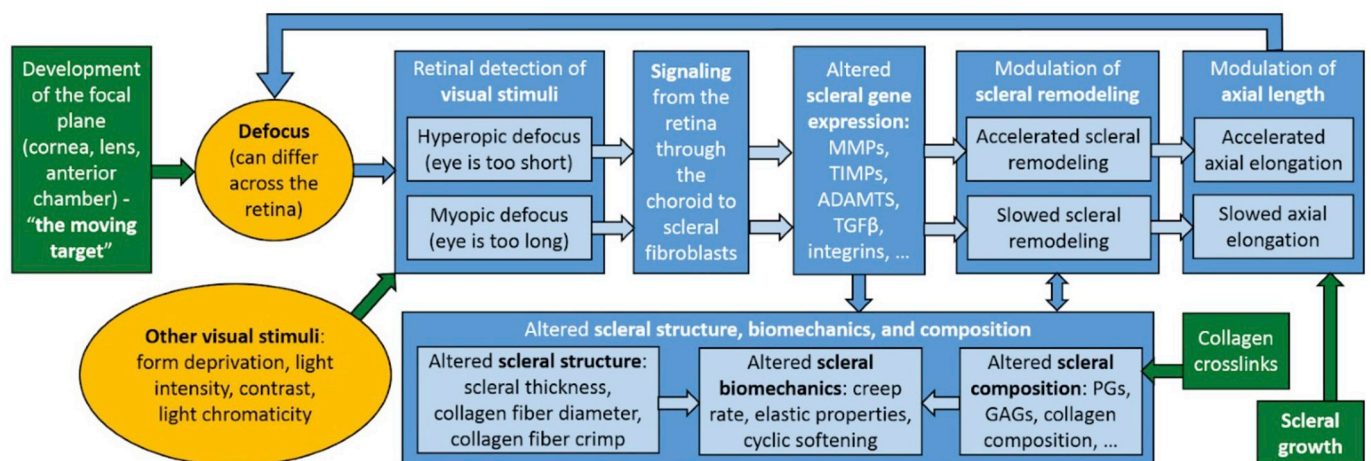


Fig. 30. The emmetropization process and factors that impact the refractive development of the eye. Mechanisms highlighted in yellow represent visual stimuli and environmental factors that impact the refractive development of the eye. Mechanisms highlighted in blue are thought to be involved in the feedback mechanism. Mechanisms highlighted in green are believed to impact the refractive development of the eye without modulation by the feedback mechanism. Reproduced from (Grytz, 2018) with permission of Kugler Publications.

remodelling. Scleral remodelling is a mechanism that involves the re-arrangement of existing material due to micro-deformations that are (nearly) volume-conserving at the tissue-scale, whereas scleral growth is a mechanism that changes the amount (volume) of the sclera.

Animal studies have revealed changes in scleral ultrastructure during myopia development. After experimental myopia induction, a significant diameter thinning of scleral collagen fibrils has been observed in rabbits (Lin et al., 2018) and tree shrews (McBrien et al., 2001). While these ultrastructural changes occur quickly (2 weeks) in rabbits with lens induced myopia, no significant changes were seen in a similar time frame in tree shrews. Instead, only after prolonged lens-induced myopia (~3 months) was a significant reduction in collagen fibril diameter seen in the shrew. This reduction in collagen fibril diameter is consistent with ultrastructural observations in highly myopic human eyes (Curtin et al., 1979). Based on inverse computational models, Grytz and Siegwart reported that the crimp of scleral collagen fibres increases during the development of myopia (Grytz and Siegwart, 2015). Meanwhile, experimental evidence of changes to the bulk fibre organisation of scleral collagen in human high myopia has recently come from WAXS studies. Markov et al. reported changes in the posterior collagen fibre alignment, in which the normally well-conserved circumferential PPS fibre structure unravels towards a more meridional alignment (Markov et al., 2018) (Fig. 31). Further studies are required to ascertain whether these changes reflect tissue remodelling relating directly to myopic lengthening of the sclera. A further possibility is that they could point to a mechanical adaption to elevated scleral tension in highly myopic eyes, that will be greater at a given IOP due to globe enlargement and posterior thinning of the eye wall (Markov et al., 2018). If and how such scleral microstructural changes might relate to optic nerve traction forces (see s3.5) and increased risk of retinal atrophy and staphyloma in highly myopic eyes is unknown.

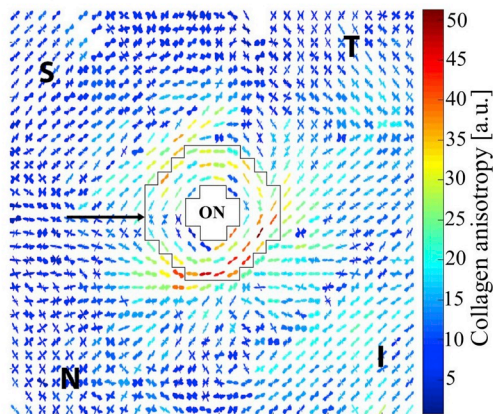
Siegwart and Norton reported the first vision-induced change in

scleral biomechanics, showing that the scleral creep rate increases during experimentally induced myopia (Siegwart and Norton, 1999). The creep rate represents the rate by which the sclera stretches while it is subjected to a constant load. The creep rate was found to respectively increase/decrease while the axial elongation rate was experimentally increased/decreased, and myopia induced/recovered (Fig. 32). Similar to the changes in scleral creep rate, the so-called ‘transition strain’ or ‘locking strain’ was found to increase/decrease during myopia development/recovery (Grytz and Siegwart, 2015). The transition strain is directly related to the collagen fibre crimp and represents the strain level at which the scleral collagen fibres straighten (Jan and Sigal, 2018) (see Fig. 12). Interestingly, a similar increase in scleral transition strain was found by Murienne et al. after digestion of glycosaminoglycans in pig sclera (Murienne et al., 2015). Collectively, these findings illustrate the tight connection between changes in tissue composition, structure, biomechanics and scleral remodelling. More recently, Levy et al. identified a profound cyclic softening effect in tree shrew sclera after inducing experimental myopia (Levy et al., 2018). They also reported that scleral crosslinking using genipin inhibits the process, providing support for the notion of scleral crosslinking as a potential myopia control therapy (see s5.2).

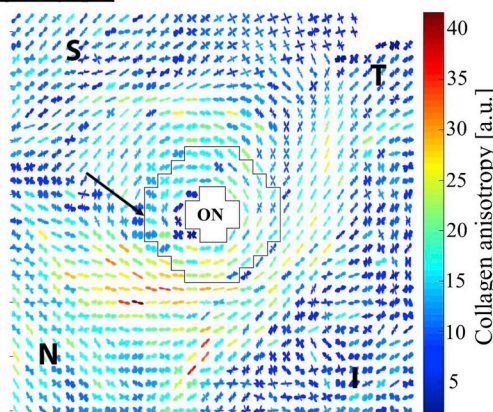
#### Key points:

- The emmetropization process involves a vision-guided feedback mechanism that alters scleral remodelling to match the axial length of the eye to its optical system.
- Accelerated scleral remodelling, and not scleral growth, underlies myopia development.
- Scleral composition, structure and biomechanics are changed during myopia development.

#### Normal



#### High Myopia



#### PPS fibres: Difference from circumferential

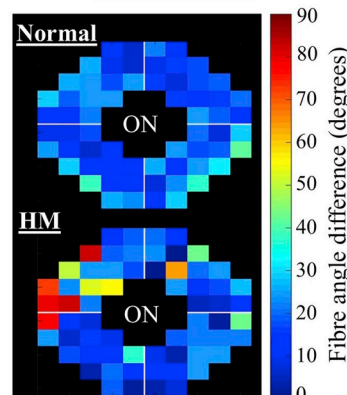


**Fig. 31.** Bulk collagen microstructural changes in human high myopia. *Left panel:* WAXS polar vector maps of collagen orientation in (top) a normal and (bottom) a high myopia flat-mount human posterior sclera. The peripapillary sclera, bordering the optic nerve, is shown bounded in black. Note myopic alteration to collagen directions in this region. The normal sclera features a predominantly circumferential pattern, with only a slight interruption in the superior (S)-nasal (N) aspect. However the S-N interruption is far more widespread in the highly myopic eye (arrows), suggesting an unravelling of the normal structure in high myopia. *Right panel:* fibre displacement angle from perfect circumferential alignment in (top) average of 7 normal specimens and (bottom) the high myopia specimen. ON: optic nerve. Figure adapted from (Markov et al., 2018) with permission of Molecular Vision.

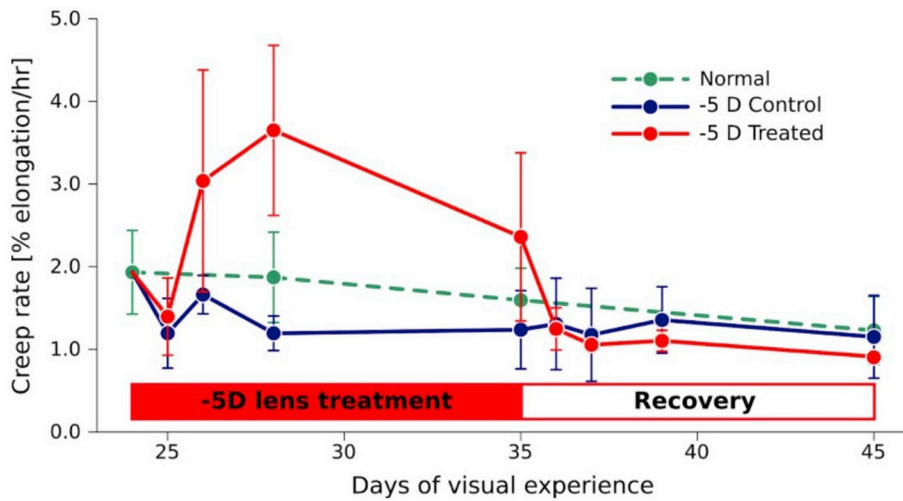


**Fig. 32.** Regulation of scleral creep rate in tree shrews during experimentally induced myopia (-5D lens treatment) and recovery. Axial elongation was accelerated in the treated eye during monocular -5D lens treatment and slowed during recovery from -5D lens wear (lens removal). Creep rate increased/decreased in the treated eye during lens treatment/recovery. The creep rate of the control eye and normal animals without lens treatment are shown for comparison. Reproduced from (Grytz, 2018) with permission of Kugler Publications.

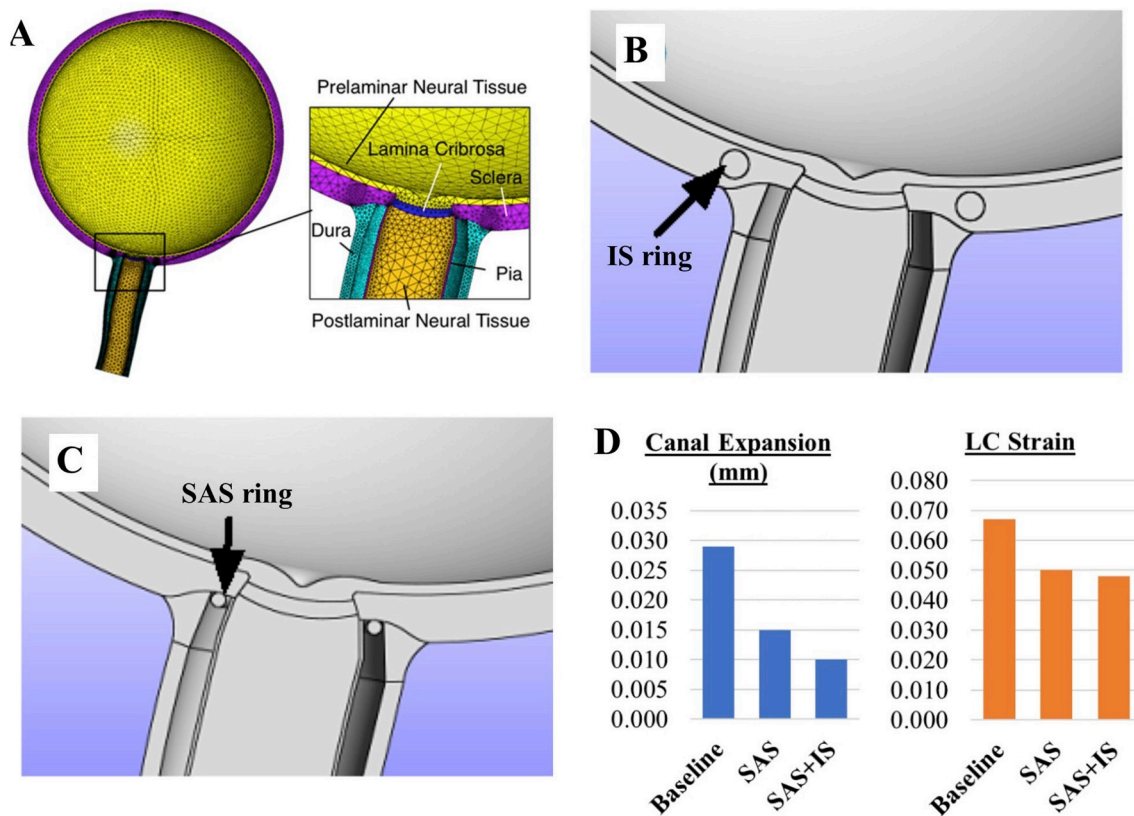


**Fig. 33.** Computational modelling of theoretical posterior segment ring implants as a potential glaucoma therapy. A) Generic human eye model geometry and FE mesh. B) Proposed intrascleral (IS) ring implant (implant material stiffness = 200 GPa). C) Alternative ring implant (200 GPa stiffness) located in the subarachnoid space (SAS). D) Effect of SAS and IS + SAS combination implants on calculated ONH deformation behaviour, under a simulated IOP of 50 mmHg. A maximum 66% reduction in scleral canal expansion and a 28% reduction in LC strain are predicted by the model under the double ring combination implant strategy. Adapted from (Soh, 2016) under Creative Commons License 4.0.

## 5. Scleral therapies

### 5.1. Surgical treatments

In the context of this review, relevant surgical treatments may be broadly divided into two groups: (i) those that justify surgery of the sclera as a means to access and/or biomechanically alter neighbouring ocular structures for clinical benefit (referred to here as ‘collateral scleral surgeries’); and (ii) those involving deliberate and targeted mechanical alteration of the sclera itself (classified here as ‘primary scleral surgeries’).

#### 5.1.1. Collateral scleral surgeries

Scleral surgery to treat presbyopia (loss of focal range) has been explored over more than two decades (reviewed in (Hipsley et al., 2018)). Surgical approaches include anterior ciliary sclerotomy (radial incisions in the sclera overlying the ciliary muscle) (Hamilton et al., 2002), implantation of scleral expansion bands (Davidson et al., 2016; Malecaze et al., 2001), and anterior scleral laser ablative surgeries (Hipsley et al., 2017; Lin and Mallo, 2003). All these approaches have been shown to be effective in reversing presbyopia to various degrees by increasing the elasticity of the eye’s accommodative apparatus.

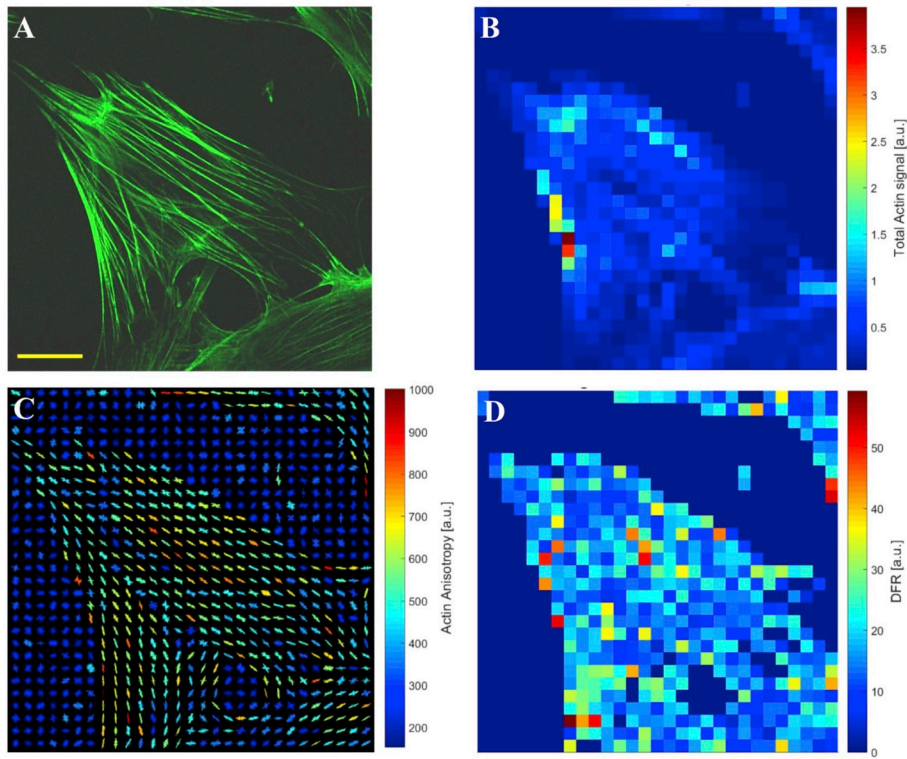


**Fig. 34.** Fourier analysis of mechanical load-induced F-actin stress fibre networks in cultured bovine scleral fibroblasts. **A)** Confocal image showing green cytoskeletal stress fibres of F-actin, stained with Alexa-488® phalloidin (bar = 25 µm). **B)** Map of integrated actin signal, sampled every 5 µm. **C)** Polar vector map of actin fibre orientation from analysis of Fourier power spectrum. **D)** Map of degree of fibre recruitment (DFR) around the principal fibre direction. Reproduced from (Pijanka et al., 2019) with permission of the Journal of Biophotonics.

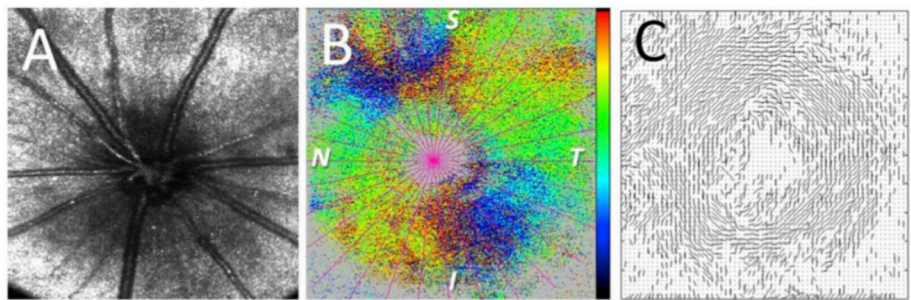


**Fig. 35.** **A)** Fundus image of the rat ONH. **B)** Collagen fibre orientations (colour map) in the peripapillary sclera about 160 µm posterior to the retinal pigment epithelium. Colour scale: -90 to 90°. S, T, I, N: superior, temporal, inferior, nasal. **C)** Preferred collagen fibre orientations in the peripapillary sclera showing a ring pattern. Adapted from (Baumann et al., 2014) with permission of the Association for Research in Vision and Ophthalmology.

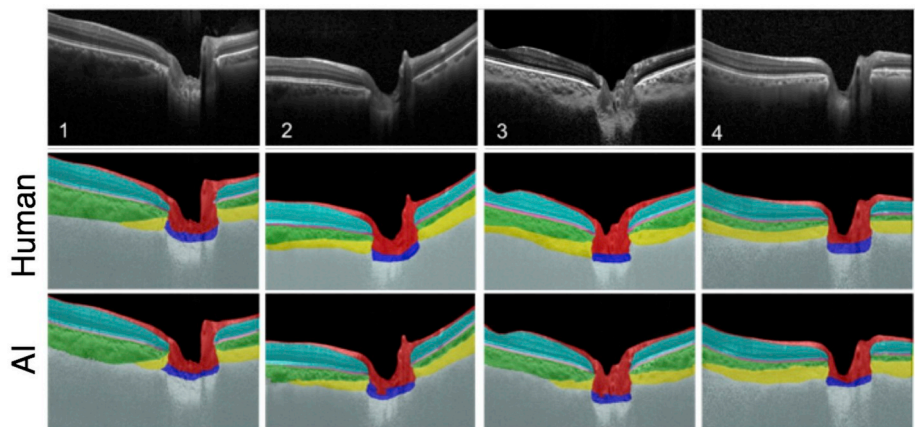


**Fig. 36.** Automated segmentation of ONH connective and neural tissues using artificial intelligence (AI) computing. The peripapillary sclera is shown in yellow. The performance of AI is now similar to that of a human expert.

However, inconsistent clinical outcomes, treatment effect regression and incidences of anterior ischemia have led to the justification of scleral surgery as a presbyopia treatment being called into question. Nevertheless, while controversial, it remains an active area of research

(Glasser, 2008; Hipsley et al., 2018). Scleral buckle (SB) treatment to repair retinal detachment is another example of an enduring scleral surgical procedure that continues to evolve. A silicon sponge, rubber or plastic “buckle” element is strapped to the eyeball to indent the sclera at

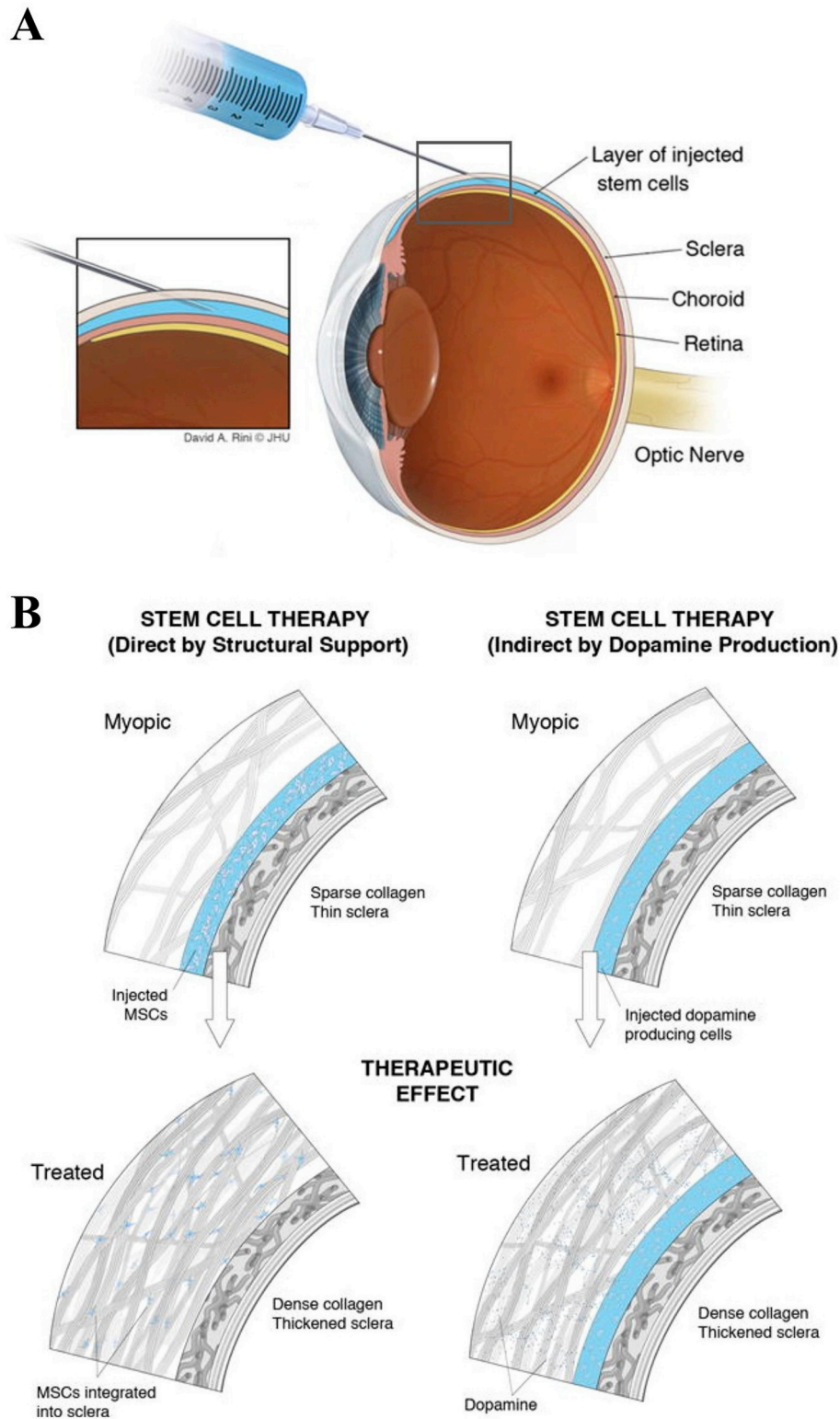


**Fig. 37.** Potential stem cell treatment for progressive myopia. **A)** Injection of a mesenchymal stem cell suspension into the subscleral space. **B)** Dual mechanisms for the possible prevention of myopic eye elongation. *Left:* Integration of stem cells into the scleral stroma for direct mechanical support. *Right:* Indirect stimulation of the scleral tissue via dopamine production. Adapted from (Janowski et al., 2015) with permission of AlphaMed Press.

the retinal detachment site, promoting reattachment and healing (Park et al., 2018). Over the past decade, the burgeoning of ocular biomechanics as a scientific discipline has positively impacted SB technique development. For example, computational modelling approaches are continuing to guide surgeons on buckle design and use by helping to identify factors (e.g. buckle size/shape, strap tightness, ocular

biometry, IOP) that most strongly influence the clinical outcome (Ge et al., 2017; Lanchares et al., 2016; Wang et al., 2007). Increasingly, SB is being combined with pars plana vitrectomy (PPV), a procedure where a small number of scleral holes (typically three) are created to facilitate vitreous removal (Park et al., 2018).

Anterior scleral surgery in the form of trabeculectomy, scleral laser

trabeculoplasty (SLT) and drainage shunt implantation has long been a clinical mainstay of IOP reduction in the treatment of medically uncontrolled glaucoma (Bovee and Pasquale, 2017), and here too techniques are progressing. The recent adoption of micro-pulse lasers for SLT (Ma et al., 2019), new shunt implant designs and materials (Chen and Gedde, 2018) and adjunct tools such as collagen matrix implants, fibrin adhesives, and amniotic membrane transplants (Lu et al., 2018) are all examples of emerging strategies to suppress fibrosis, scarring and other side-effects of glaucoma drainage surgery.

### 5.1.2. Primary scleral surgeries

Surgical reinforcement of the posterior sclera is a viable but highly debated option to manage pathological myopia, and is usually indicated in eyes with associated macular changes and/or staphyloma (Ohno-Matsui and Jonas, 2018). The procedure involves inserting a strip of (usually) donor sclera material under the separated extraorbital muscles and pushing it down deeply towards the posterior pole. The ends of the strip are then crossed over the medial rectus muscle and sutured to the sclera on the medial aspect of the superior and inferior recti (Thompson, 1990). One source of controversy stems from difficulty in obtaining and storing donor tissue, and this is driving current efforts to develop biocompatible artificial materials and devices (Yuan et al., 2016). Meanwhile, established and emerging adjunct procedures such as patching therapy (Shen et al., 2015b) and collagen crosslinking (Xue et al., 2018) (see s5.2) are being combined with surgical reinforcement in an effort to improve efficacy and safety. Mechanical alteration of the posterior sclera is also being considered as an alternative neuroprotective strategy for glaucoma patients who respond poorly to IOP lowering (Quigley and Cone, 2013; Strouthidis and Girard, 2013). One possible surgical approach could be to locally stiffen the scleral tissue around the ONH, for example by the insertion of a biocompatible (e.g. titanium) ring implant into the PPS and/or adjacent tissues. While there is not yet any experimental evidence to support the viability of such an approach, recent computational modelling results (Soh, 2016) show that, theoretically at least, it could be one effective route to reducing IOP-driven scleral canal expansion and LC strain (Fig. 33).

### 5.2. Scleral crosslinking

Collagen crosslinking has been used in multiple settings to mechanically stabilise collagenous tissues and hydrogels (Lima et al., 2009). It is thought that biomechanical weakening of the cornea is the underlying cause of keratoconus (Hayes et al., 2007). Corneal crosslinking using riboflavin and ultraviolet A light has been proposed and successfully used to mechanically stabilise the cornea in keratoconus patients since 1998 (Raiskup et al., 2015; Wollensak et al., 2003). A single treatment session of corneal crosslinking has been shown to slow or arrest keratoconus progression and achieve long-term stabilisation of the condition (10 years) with a good safety profile (Raiskup et al., 2015). In section 4.3 we discussed several structural and biomechanical changes that occur during the development of myopia, including scleral creep rate, collagen fibre crimping and re-alignment, and cyclic softening (Grytz and Siegwart, 2015; Levy et al., 2018; Markov et al., 2018; Siegwart and Norton, 1999). These changes suggest that the sclera is biomechanically weakened during the development of myopia. Collagen crosslinking has therefore been proposed as a potential treatment for myopia and, in particular, for progressive myopia (Wollensak and Iomdina, 2008a). Progressive myopia is one of the leading causes of blindness worldwide without an accepted treatment option that can slow or halt progressive scleral remodelling (Buch et al., 2004; Cotter et al., 2006; Green et al., 1986; Krumpaszy et al., 1999; Munier et al., 1998). Given the lack of treatment options available and the morbidity of progressive myopia, an effective clinical solution is becoming increasingly necessary.

Collagen crosslinks accumulate naturally in the sclera throughout life (Schultz et al., 2008). Based on computational model predictions,

Grytz and El Hamdaoui proposed that the natural accumulation of collagen crosslinks decreases the eye's susceptibility to scleral remodelling and myopia with age (Grytz and El Hamdaoui, 2017). McBrien and Norton have shown that preventing natural collagen crosslinking doubles the axial elongation rate during lens-induced myopia in juvenile tree shrews, suggesting that collagen crosslinks modulate scleral remodelling in myopia (McBrien and Norton, 1994). Wollensak and colleagues reported that the biomechanical changes introduced by scleral crosslinking remain effective for up to 8 months in rabbits (Wollensak and Iomdina, 2008b, 2009). Scleral crosslinking was shown to reduce collagen fibril crimping (Zyablitskaya et al., 2017) supporting the idea that crosslinking can counteract biomechanical changes seen in experimental myopia (see s4.3). Wang and Corpuz demonstrated that weekly scleral crosslinking using sub-Tenon's injections of genipin can slow experimental myopia over 21 days in guinea pig eyes (Wang and Corpuz, 2015). However, that study did not incorporate a sham injected group. Garcia et al. have shown that sham injection behind the sclera can have a significant effect on axial development and should, therefore, be considered when delivering crosslink agent via sub-Tenon's injections (Garcia et al., 2017). Two groups have reported that scleral crosslinking using riboflavin and ultraviolet-A radiation can also slow progression of experimental myopia by increasing scleral biomechanical strength in guinea pigs (Dotan et al., 2016; Liu et al., 2016). Recently, Lin et al. showed successful slowing of experimental myopia using glycerinaldehyde for scleral crosslinking in rabbits (Lin et al., 2019). Interestingly, Chu et al. had earlier also performed sub-Tenon's injection using glycerinaldehyde in the guinea pig model of myopia (Chu et al., 2016) but, in contrast to the study by Lin et al., they reported that scleral crosslinking had no effect on the development of myopia despite biomechanical strengthening of the sclera. Chu et al. and Lin et al. used the same concentration of glycerinaldehyde, but Lin et al. injected the crosslinking agent every other day (seven times in total) compared to only one injection performed by Chu et al. The different number of injections may explain the disparity in the results between these two studies and stresses the importance of using multiple doses when studying the effect of scleral crosslinking. Recently, Grytz et al. reported the first investigation of dose-dependent effects of scleral crosslinking on myopia development (Grytz et al., 2018). This study used sub-Tenon's injections of genipin in tree shrews, confirming that scleral crosslinking can slow axial elongation in myopia and that the effect is dose dependent. Furthermore, a sham effect of sub-Tenon's injections on axial elongation was also seen in the study of Grytz et al., confirming the previous finding of Garcia et al. (2017).

Artificial crosslinking can be induced in multiple ways, where each method has its benefits and disadvantages. Maintaining a balance between minimising cytotoxic effects and invasive operative procedures, while preserving treatment efficacy, will be essential to identify and optimise a clinically deliverable method of scleral crosslinking. The classical approach is based on using ultraviolet A light-activated riboflavin. The clear advantage of a light activated crosslink agent is the ability to use the light to localise the treatment to the area of interest. A major challenge of this strategy remains the safe delivery of the light to the sclera, which currently requires the operative exposure of the sclera (Wollensak and Iomdina, 2009; Wollensak et al., 2005). Current scleral crosslinking techniques using riboflavin/ultraviolet A light were found to be not safe enough (Wang et al., 2015). To improve efficacy and reduce retinal toxicity, other light wavelengths such as blue light (Zhang et al., 2015b) have been proposed and continue to be evaluated.

An alternative approach is to use crosslink agents that don't require light activation. The most commonly used scleral crosslinking agents from this category are two low-cytotoxic compounds: glycerinaldehyde and genipin. Both agents have been successfully used to slow myopia progression, as mentioned above. Genipin is a naturally occurring organic compound and one of the best characterized low-cytotoxic crosslinking agents (Campbell et al., 2017; Fessel et al., 2014).

Campbell et al. have shown that a much lower concentration of genipin is required to achieve a comparable scleral stiffening effect to that obtainable using alternative low-cytotoxicity agents such as glycer-aldehyde (7-fold) or methylglyoxal (30-fold) (Campbell et al., 2017). The main advantage of using a crosslink agent that doesn't require light activation is the less invasive delivery of the agent via sub-Tenon's injections. However, there are also disadvantages in using non-light activated agents. For example, currently there is no method to limit the crosslinking procedure to the sclera alone. Grytz et al. reported that the genipin solution can diffuse across the limbal boundary during the sub-Tenon's injections, crosslinking not only the sclera but also the cornea (Grytz et al., 2018). All studies that showed successful slowing of myopia progression using glycer-aldehyde or genipin required repeated injections of the crosslink agents (typically 3 to 5 times or weekly injections). The development of an improved and sustained delivery strategy will be essential for a potential application in the clinic. Moreover, while no study has reported any major safety concerns or alarming adverse effects, the safety of these agents is still under evaluation.

Scleral crosslinking has also been proposed as a potential treatment strategy for glaucoma, but was found to increase glaucoma damage in a mouse model when the entire sclera was crosslinked (Kimball et al., 2014). However, Coudrillier et al. have shown that restricting scleral crosslinking to the PPS region can have a beneficial effect by reducing the magnitude of biomechanical strains within the LC (Coudrillier et al., 2016). Consequently, localised scleral crosslinking may find utilisation in glaucoma axonal neuroprotection, but this potential treatment modality requires further investigation and remains unproven.

## 6. Future directions and conclusions

The structure and biomechanical performance of the sclera is coming under increasing focus by researchers whose work is defining with more clarity the tissue's central importance in common, sight-threatening ocular pathologies such as glaucoma and progressive myopia. Classical views of the sclera as a largely static, quiescent tissue are being replaced by a growing awareness of its dynamic nature in terms of ECM growth and remodelling mechanisms and cellular biomechanical responses over wide-ranging time scales. Increasingly comprehensive understanding of the multiple, interacting biomechanical loads on the sclera (including eye movement forces and fluid pressures) is leading to more physiologically relevant combined experimental and computational models. Such models are required to investigate scleral-related disease and its association with ageing - a need that will become even more pressing as the global population continues to age.

Going forward it is certain that we will see more notable advances in the broad and fertile area of scleral research. It is likely that new imaging modalities will be leveraged to visualise further aspects of scleral hierarchical structure and cell-ECM interactions, similar to what we are seeing in corneal research with the recent application of methods such as third harmonic generation (Jay et al., 2015) and coherent anti-Stokes Raman scattering (Kaji et al., 2017) multiphoton imaging. We can also expect to see bioimaging methods increasingly combined with quantitative tools such as Fourier methods (Pijanka et al., 2019) to provide more representative ECM and cellular structural inputs for computational modelling (Fig. 34).

In the future there will likely be a continuation of the current trend towards 3D imaging techniques (Feneck et al., 2018; Yang et al., 2018b) and the unification of ocular structure data in an effort to gain a more holistic view of ocular behaviour through whole eye biomechanical modelling (Voorhees et al., 2017; Whitford et al., 2016; Zhou et al., 2019a, 2019b). It is possible that we will also see a future shift towards in vivo biomechanical modelling approaches, particularly if urgently needed progress can be made on characterisation of ECM structure in the living eye. Indeed, quantitatively mapping collagen fibre organisation in vivo in human subjects may prove critical to improve

glaucoma diagnosis and management. Recently, PSOCT has been used to evaluate the volumetric microstructural tissue organisation in rat PPS in vivo (Fig. 35). This was done by taking advantage of the birefringence caused by collagen fibres (Baumann et al., 2014). In that study, a PPS fibre ring was observed, which was validated against conventional histology and found consistent with other ex vivo studies (Girard et al., 2011a). Translating PSOCT to the clinic could become feasible in the future, however significant challenges such as loss of signal quality when imaging deep tissues must first be overcome.

The rise of artificial intelligence (AI) computing and its pervasion into vision research will likely accelerate in future, and this could result in further clinical benefits for scleral-related disease diagnosis and prognosis – perhaps most immediately in the glaucoma clinic. For instance, AI algorithms have already been developed to enhance, denoise, and automatically segment the PPS (along with other connective and neural tissues) in OCT images of the ONH in order to extract important in vivo structural information. The performance of such algorithms is already on a par with that of human experts (Fig. 36). Other AI algorithms have used the textural and structural information (Devalia et al., 2018a, 2018b; Girard et al., 2011b) of the sclera (along with that of other tissues) in OCT images of the ONH to provide a glaucoma diagnostic power that could challenge current gold-standard glaucoma parameters such as RNFL thickness (Girard et al., 2018). In the future, we are likely to see the emergence of other AI algorithms that will use structural and biomechanical information about the sclera to help predict which patients are at risk of developing visual field loss from glaucoma.

In terms of scleral treatments, an increasing emphasis on minimally invasive therapies is probable. The success of collagen crosslinking to treat corneal biomechanical problems (e.g. keratoconus) has provided incentive for research into scleral crosslinking (see s5.2). However, while notable progress has been made using animal models there remain many unanswered questions in terms of safety, efficacy and mode of delivery that are currently blocking clinical translation. Another potentially productive scleral therapeutic route currently still in its infancy is stem cell treatment. Scleral reinforcement via the application of mesenchymal stem cells is being evaluated as a potential treatment for progressive myopia (Janowski et al., 2015). Cell-mediated strategies involving both direct structural enhancement of the scleral stroma and indirect routes via stimulation of dopamine are being considered (Fig. 37). Meanwhile, increasing success in the search for novel myopia genes is coming from the widening use of big data analyses (Flitcroft et al., 2018). These studies are already providing potential targets that could be leveraged in future towards gaining control of myopic scleral elongation through, for example, gene therapy. Given the already substantial and growing burden of scleral-related eye disorder worldwide, the success of such approaches will become even more important in the future.

## Declarations of interest

None.

## Acknowledgements

The assistance of Petar Markov in preparation of figures for this document is gratefully acknowledged. The authors are thankful for funding support under the following grant numbers. CB: Fight For Sight Project Grant 1360, NIH Grant R01EY021500 (subaward 2003284605), MRC Program Grant MR/K000837/1 and various STFC Facility Access Awards; IAS: NIH grants R01-EY023966, R01-EY028662 and P30-EY008098; RG: NIH grants R01-EY026588, R01-EY027759, Eye Sight Foundation of Alabama and Research to Prevent Blindness; TDN: Public Health Service Research Grant EY021500 and NSF Grant CMMI-1727104; MJAG: MOE Singapore Academic Research Funds (Tier 2: R-397-000-280-112 & R-397-000-308-112, Tier 1: R-397-000-294-114), NMRC Grant NMRC/STAR/0023/2014.

## References

- Albon, J., Farrant, S., Akhtar, S., Young, R., Boulton, M.E., Smith, G., Taylor, M., Guggenheim, J., Morgan, J.E., 2007. Connective tissue structure of the tree shrew optic nerve and associated ageing changes. *Investig. Ophthalmol. Vis. Sci.* 48, 2134–2144.
- Ambati, J., Canakis, C.S., Miller, J.W., Gragoudas, E.S., Edwards, A., Weissgold, D.J., Kim, I., Delori, F.C., Adamis, A.P., 2000. Diffusion of high molecular weight compounds through sclera. *Investig. Ophthalmol. Vis. Sci.* 41, 1181–1185.
- Anderson, D.R., 1969. Ultrastructure of human and monkey lamina cribrosa and optic nerve head. *Arch. Ophthalmol.* 82, 800–814.
- Ashby, R., Ohlendorf, A., Schaeffel, F., 2009. The effect of ambient illuminance on the development of deprivation myopia in chicks. *Investig. Ophthalmol. Vis. Sci.* 50, 5348–5354.
- Austin, B.A., Coulon, C., Liu, C.Y., Kao, W.W., Rada, J.A., 2002. Altered collagen fibril formation in the sclera of lumican-deficient mice. *Investig. Ophthalmol. Vis. Sci.* 43, 1695–1701.
- Ayyalasmayajula, A., Park, R.I., Simon, B.R., Vande Geest, J.P., 2016. A porohyperelastic finite element model of the eye: the influence of stiffness and permeability on intraocular pressure and optic nerve head biomechanics. *Comput. Methods Biomech. Biomed. Eng.* 19, 591–602.
- Bachmann, B., Birke, M., Kook, D., Eichhorn, M., Lutjen-Drecoll, E., 2006. Ultrastructural and biochemical evaluation of the porcine anterior chamber perfusion model. *Investig. Ophthalmol. Vis. Sci.* 47, 2011–2020.
- Bailey, A.J., Paul, R.G., Knott, L., 1998. Mechanisms of maturation and ageing of collagen. *Mech. Ageing Dev.* 106, 1–56.
- Battaglioli, J.L., Kamm, R.D., 1984. Measurements of the compressive properties of scleral tissue. *Investig. Ophthalmol. Vis. Sci.* 25, 59–65.
- Baumann, B., Rauscher, S., Glosmann, M., Gotzinger, E., Pircher, M., Fialova, S., Groger, M., Hitzzenberger, C.K., 2014. Peripapillary rat sclera investigated in vivo with polarization-sensitive optical coherence tomography. *Investig. Ophthalmol. Vis. Sci.* 55, 7686–7696.
- Bekerman, I., Gottlieb, P., Vaiman, M., 2014. Variations in eyeball diameters of the healthy adults. *J. Ophthalmol.* 2014 503645.
- Bellezza, A.J., Hart, R.T., Burgoyne, C.F., 2000. The optic nerve head as a biomechanical structure: initial finite element modeling. *Investig. Ophthalmol. Vis. Sci.* 41, 2991–3000.
- Bellezza, A.J., Rintalan, C.J., Thompson, H.W., Downs, J.C., Hart, R.T., Burgoyne, C.F., 2003. Deformation of the lamina cribrosa and anterior scleral canal wall in early experimental glaucoma. *Investig. Ophthalmol. Vis. Sci.* 44, 623–637.
- Boote, C., Hayes, S., Jones, S., Quantock, A.J., Hocking, P.M., Inglehearn, C.F., Ali, M., Meek, K.M., 2008. Collagen organization in the chicken cornea and structural alterations in the retinopathy, globe enlarged (rge) phenotype—an X-ray diffraction study. *J. Struct. Biol.* 161, 1–8.
- Boote, C., Hayes, S., Young, R.D., Kamma-Lorger, C.S., Hocking, P.M., Elsheikh, A., Inglehearn, C.F., Ali, M., Meek, K.M., 2009. Ultrastructural changes in the retinopathy, globe enlarged (rge) chick cornea. *J. Struct. Biol.* 166, 195–204.
- Boote, C., Kamma-Lorger, C.S., Hayes, S., Harris, J., Burghammer, M., Hiller, J., Terrill, N.J., Meek, K.M., 2011. Quantification of collagen organization in the peripheral human cornea at micron-scale resolution. *Biophys. J.* 101, 33–42.
- Boubriak, O.A., Urban, J.P., Akhtar, S., Meek, K.M., Bron, A.J., 2000. The effect of hydration and matrix composition on solute diffusion in rabbit sclera. *Exp. Eye Res.* 71, 503–514.
- Bovee, C.E., Pasquale, L.R., 2017. Evolving surgical interventions in the treatment of glaucoma. *Semin. Ophthalmol.* 32, 91–95.
- Braunsmann, C., Hammer, C.M., Rheinlaender, J., Kruse, F.E., Schaffer, T.E., Schlotzer-Schrehardt, U., 2012. Evaluation of lamina cribrosa and peripapillary sclera stiffness in pseudoexfoliation and normal eyes by atomic force microscopy. *Investig. Ophthalmol. Vis. Sci.* 53, 2960–2967.
- Brown, C.T., Vural, M., Johnson, M., Trinkaus-Randall, V., 1994. Age-related changes of scleral hydration and sulfated glycosaminoglycans. *Mech. Ageing Dev.* 77, 97–107.
- Bron, A.J., Tripathi, A.C., Tripathi, B.J., 1997. The cornea and sclera. *Wolff's anatomy of the eye and orbit*, 8th. Chapman and Hall, London, pp. 233–277.
- Brown, D.J., Morishige, N., Neekhra, A., Minckler, D.S., Jester, J.V., 2007. Application of second harmonic imaging microscopy to assess structural changes in optic nerve head structure ex vivo. *J. Biomed. Opt.* 12 024029.
- Buch, H., Vinding, T., La Cour, M., Appleyard, M., Jensen, G.B., Nielsen, N.V., 2004. Prevalence and causes of visual impairment and blindness among 9980 Scandinavian adults: the Copenhagen City Eye Study. *Ophthalmology* 111, 53–61.
- Bushby, A.J., P'Ng K, M., Young, R.D., Pinali, C., Knupp, C., Quantock, A.J., 2011. Imaging three-dimensional tissue architectures by focused ion beam scanning electron microscopy. *Nat. Protoc.* 6, 845–858.
- Cabrera, F.J., Wang, D.C., Reddy, K., Acharya, G., Shin, C.S., 2019. Challenges and opportunities for drug delivery to the posterior of the eye. *Drug Discov. Today*(S1359-6446-1).
- Campbell, I.C., Coudrillier, B., Mensah, J., Abel, R.L., Ethier, C.R., 2015. Automated segmentation of the lamina cribrosa using Frangi's filter: a novel approach for rapid identification of tissue volume fraction and beam orientation in a trabeculated structure in the eye. *J. R. Soc. Interface* 12, 20141009.
- Campbell, I.C., Hannon, B.G., Read, A.T., Sherwood, J.M., Schwamer, S.A., Ethier, C.R., 2017. Quantification of the efficacy of collagen cross-linking agents to induce stiffening of rat sclera. *J. R. Soc. Interface* 14.
- Cazaux, S., Sadoun, A., Biarnes-Pelicot, M., Martinez, M., Obeid, S., Bongrand, P., Limozin, L., Puech, P.H., 2016. Synchronizing atomic force microscopy force mode and fluorescence microscopy in real time for immune cell stimulation and activation studies. *Ultramicroscopy* 160, 168–181.
- Chakraborty, N., Wang, M., Solocinski, J., Kim, W., Argento, A., 2016. Imaging of scleral collagen deformation using combined confocal Raman microspectroscopy and polarized light microscopy techniques. *PLoS One* 11, e0165520.
- Chakravarti, S., Paul, J., Roberts, L., Chervoneva, I., Oldberg, A., Birk, D.E., 2003. Ocular and scleral alterations in gene-targeted lumican-fibromodulin double-null mice. *Investig. Ophthalmol. Vis. Sci.* 44, 2422–2432.
- Chang, M.Y., Shin, A., Park, J., Nagiel, A., Lalane, R.A., Schwartz, S.D., Demer, J.L., 2017. Deformation of optic nerve head and peripapillary tissues by horizontal duction. *Am. J. Ophthalmol.* 174, 85–94.
- Chen, J., Gedde, S.J., 2018. New developments in tube shunt surgery. *Curr. Opin. Ophthalmol.* 30 (2), 125–131.
- Cheng, H.M., Singh, O.S., Kwong, K.K., Xiong, J., Woods, B.T., Brady, T.J., 1992. Shape of the myopic eye as seen with high-resolution magnetic resonance imaging. *Optom. Vis. Sci.* 69, 698–701.
- Chu, Y., Cheng, Z., Liu, J., Wang, Y., Guo, H., Han, Q., 2016. The effects of scleral collagen cross-linking using glycerolaldehyde on the progression of form-deprived myopia in Guinea pigs. *J. Ophthalmol* 2016, 3526153.
- Clayson, K., Pan, X., Pavlatos, E., Short, R., Morris, H., Hart, R.T., Liu, J., 2017. Corneal stiffening increases IOP spike magnitudes during rapid microvolumetric change in the eye. *Exp. Eye Res.* 165, 29–34.
- Cone-Kimball, E., Nguyen, C., Oglesby, E.N., Pease, M.E., Steinhart, M.R., Quigley, H.A., 2013. Scleral structural alterations associated with chronic experimental intraocular pressure elevation in mice. *Mol. Vis.* 19, 2023–2039.
- Cone, F.E., Gelman, S.E., Son, J.L., Pease, M.E., Quigley, H.A., 2010. Differential susceptibility to experimental glaucoma among 3 mouse strains using bead and viscoelastic injection. *Exp. Eye Res.* 91, 415–424.
- Costa, D., Leiva, M., Naranjo, C., Rios, J., Pena, M.T., 2016. Cryopreservation (-20 degrees C) of feline corneal tissue: histologic, microbiologic, and ultrastructural study. *Vet. Ophthalmol.* 19 (Suppl. 1), 97–104.
- Cotter, S.A., Varma, R., Ying-Lai, M., Azen, S.P., Klein, R., 2006. Causes of low vision and blindness in adult latinos: the los angeles latino eye study. *Ophthalmology* 113, 1574–1582.
- Coudrillier, B., Boote, C., Quigley, H.A., Nguyen, T.D., 2013. Scleral anisotropy and its effects on the mechanical response of the optic nerve head. *Biomechanics Model. Mechanobiol.* 12, 941–963.
- Coudrillier, B., Campbell, I.C., Read, A.T., Galdes, D.M., Vo, N.T., Feola, A., Mulvihill, J., Albon, J., Abel, R.L., Ethier, C.R., 2016. Effects of peripapillary scleral stiffening on the deformation of the lamina cribrosa. *Investig. Ophthalmol. Vis. Sci.* 57, 2666–2677.
- Coudrillier, B., Pijanka, J., Jefferys, J., Sorensen, T., Quigley, H.A., Boote, C., Nguyen, T.D., 2015a. Collagen structure and mechanical properties of the human sclera: analysis for the effects of age. *J. Biomech. Eng.* 137 041006.
- Coudrillier, B., Pijanka, J., Sorensen, T., Quigley, H.A., Boote, C., Nguyen, T.D., 2015b. Effects of age and diabetes on scleral stiffness. *J. Biomech. Eng.* 137.
- Coudrillier, B., Pijanka, J.K., Jefferys, J.L., Goel, A., Quigley, H.A., Boote, C., Nguyen, T.D., 2015c. Glaucoma-related changes in the mechanical properties and collagen micro-architecture of the human sclera. *PLoS One* 10 e0131396.
- Coudrillier, B., Tian, J., Alexander, S., Myers, K.M., Quigley, H.A., Nguyen, T.D., 2012. Biomechanics of the human posterior sclera: age- and glaucoma-related changes measured using inflation testing. *Investig. Ophthalmol. Vis. Sci.* 53, 1714–1728.
- Cruz Perez, B., Pavlatos, E., Morris, H.J., Chen, H., Pan, X., Hart, R.T., Liu, J., 2016. Mapping 3D strains with ultrasound speckle tracking: method validation and initial results in porcine scleral inflation. *Ann. Biomed. Eng.* 44, 2302–2312.
- Cruz Perez, B., Tang, J., Morris, H.J., Palko, J.R., Pan, X., Hart, R.T., Liu, J., 2014. Biaxial mechanical testing of posterior sclera using high-resolution ultrasound speckle tracking for strain measurements. *J. Biomech.* 47, 1151–1156.
- Cui, W., Bryant, M.R., Sweet, P.M., McDonnell, P.J., 2004. Changes in gene expression in response to mechanical strain in human scleral fibroblasts. *Exp. Eye Res.* 78, 275–284.
- Curtin, B.J., Iwamoto, T., Renaldo, D.P., 1979. Normal and staphylococcal sclera of high myopia. An electron microscopic study. *Arch. Ophthalmol.* 97, 912–915.
- Danford, F.L., Yan, D., Dreier, R.A., Cahir, T.M., Girkin, C.A., Vande Geest, J.P., 2013. Differences in the region- and depth-dependent microstructural organization in normal versus glaucomatous human posterior sclerae. *Investig. Ophthalmol. Vis. Sci.* 54, 7922–7932.
- Davidson, R.S., Dhaliwal, D., Hamilton, D.R., Jackson, M., Patterson, L., Stonecipher, K., Yoo, S.H., Braga-Mele, R., Donaldson, K., 2016. Surgical correction of presbyopia. *J. Cataract Refract. Surg.* 42, 920–930.
- Daxer, A., Misof, K., Grabner, B., Ettl, A., Fratzl, P., 1998. Collagen fibrils in the human corneal stroma: structure and ageing. *Investig. Ophthalmol. Visual Sci.* 39, 644–648.
- Demer, J.L., 2016. Optic nerve sheath as a novel mechanical load on the globe in ocular duction. *Investig. Ophthalmol. Vis. Sci.* 57, 1826–1838.
- Devalla, S.K., Chin, K.S., Mari, J.M., Tun, T.A., Strouthidis, N.G., Aung, T., Thiery, A.H., Girard, M.J.A., 2018a. A deep learning approach to digitally stain optical coherence tomography images of the optic nerve head. *Investig. Ophthalmol. Vis. Sci.* 59, 63–74.
- Devalla, S.K., Renukanand, P.K., Sreedhar, B.K., Subramanian, G., Zhang, L., Perera, S., Mari, J.M., Chin, K.S., Tun, T.A., Strouthidis, N.G., Aung, T., Thiery, A.H., Girard, M.J.A., 2018b. DRUNET: a dilated-residual U-Net deep learning network to segment optic nerve head tissues in optical coherence tomography images. *Biomed. Opt. Express* 9, 3244–3265.
- Dikici, A.S., Mihmanli, I., Kilic, F., Ozkok, A., Kuyumcu, G., Sultan, P., Samanci, C., Halit Yilmaz, M., Raffee, B., Tamcelik, N., Isik Hasiloglu, Z., Kantarci, F., 2016. In vivo evaluation of the biomechanical properties of optic nerve and peripapillary structures by ultrasonic shear wave elastography in glaucoma. *Iran. J. Radiol. : Q. J. Publ.*

- Radiol. Soc. Iran. 13, e36849.
- Dolgin, E., 2015. The myopia boom. *Nature* 519, 276–278.
- Dotan, A., Kremer, I., Gal-Or, O., Livnat, T., Zigler, A., Bourla, D., Weinberger, D., 2016. Scleral cross-linking using riboflavin and ultraviolet-A radiation for prevention of axial myopia in a rabbit model. *J. Vis. Exp.* 110, e53201.
- Downs, J.C., 2015. Optic nerve head biomechanics in aging and disease. *Exp. Eye Res.* 133, 19–29.
- Downs, J.C., Suh, J.K., Thomas, K.A., Bellezza, A.J., Hart, R.T., Burgoyne, C.F., 2005. Viscoelastic material properties of the peripapillary sclera in normal and early-glaucoma monkey eyes. *Investig. Ophthalmol. Vis. Sci.* 46, 540–546.
- Eilaghi, A., Flanagan, J.G., Tertinegg, I., Simmons, C.A., Wayne Brodland, G., Ross Ethier, C., 2010. Biaxial mechanical testing of human sclera. *J. Biomech.* 43, 1696–1701.
- Elsheikh, A., Anderson, K., 2005. Comparative study of corneal strip extensometry and inflation tests. *J. R. Soc. Interface* 2, 177–185.
- Elsheikh, A., Geraghty, B., Alhasso, D., Knappett, J., Campanelli, M., Rama, P., 2010. Regional variation in the biomechanical properties of the human sclera. *Exp. Eye Res.* 90, 624–633.
- Fazio, M.A., Clark, M.E., Bruno, L., Girkin, C.A., 2018. In vivo optic nerve head mechanical response to intraocular and cerebrospinal fluid pressure: imaging protocol and quantification method. *Sci. Rep.* 8, 12639.
- Fazio, M.A., Grytz, R., Morris, J.S., Bruno, L., Gardiner, S.K., Girkin, C.A., Downs, J.C., 2014a. Age-related changes in human peripapillary scleral strain. *Biomechanics Model. Mechanobiol.* 13, 551–563.
- Fazio, M.A., Grytz, R., Morris, J.S., Bruno, L., Girkin, C.A., Downs, J.C., 2014b. Human scleral structural stiffness increases more rapidly with age in donors of African descent compared to donors of European descent. *Investig. Ophthalmol. Vis. Sci.* 55, 7189–7198.
- Feneck, E.M., Lewis, P.N., Ralphs, J., Meek, K.M., 2018. A comparative study of the elastic fibre system within the mouse and human cornea. *Exp. Eye Res.* 177, 35–44.
- Feola, A.J., Coudrillier, B., Mulvihill, J., Gerdal, D.M., Vo, N.T., Albon, J., Abel, R.L., Samuels, B.C., Ethier, C.R., 2017. Deformation of the lamina cribrosa and optic nerve due to changes in cerebrospinal fluid pressure. *Investig. Ophthalmol. Vis. Sci.* 58, 2070–2078.
- Feola, A.J., Myers, J.G., Raykin, J., Mulugeta, L., Nelson, E.S., Samuels, B.C., Ethier, C.R., 2016. Finite element modeling of factors influencing optic nerve head deformation due to intracranial pressure. *Investig. Ophthalmol. Vis. Sci.* 57, 1901–1911.
- Fessel, G., Cadby, J., Wunderli, S., van Weeren, R., Snedeker, J.G., 2014. Dose- and time-dependent effects of genipin crosslinking on cell viability and tissue mechanics - toward clinical application for tendon repair. *Acta Biomater.* 10, 1897–1906.
- Flitcroft, D.I., Loughman, J., Wildsoet, C.F., Williams, C., Guggenheim, J.A., 2018. Novel myopia genes and pathways identified from syndromic forms of myopia. *Investig. Ophthalmol. Vis. Sci.* 59, 338–348.
- Franz-Odenaal, T.A., 2008. Scleral ossicles of teleostei: evolutionary and developmental trends. *Anat. Rec.* : 2007 291, 161–168.
- Friberg, T.R., Lace, J.W., 1988. A comparison of the elastic properties of human choroid and sclera. *Exp. Eye Res.* 47, 429–436.
- Fullwood, N.J., Hammiche, A., Pollock, H.M., Hourston, D.J., Song, M., 1995. Atomic force microscopy of the cornea and sclera. *Curr. Eye Res.* 14, 529–535.
- Funata, M., Tokoro, T., 1990. Scleral change in experimentally myopic monkeys. *Graefes Arch. Clin. Exp. Ophthalmol.* 228, 174–179.
- Garcia, M.B., Jha, A.K., Healy, K.E., Wildsoet, C.F., 2017. A bioengineering approach to myopia control tested in a Guinea pig model. *Investig. Ophthalmol. Vis. Sci.* 58, 1875–1886.
- Gawne, T.J., Siegwart Jr., J.T., Ward, A.H., Norton, T.T., 2017. The wavelength composition and temporal modulation of ambient lighting strongly affect refractive development in young tree shrews. *Exp. Eye Res.* 155, 75–84.
- Ge, P., Bottega, W.J., Prenner, J.L., Fine, H.F., 2017. On the behavior of an eye encircled by a scleral buckle. *J. Math. Biol.* 74, 313–332.
- Gentle, A., Liu, Y., Martin, J.E., Conti, G.L., McBrien, N.A., 2003. Collagen gene expression and the altered accumulation of scleral collagen during the development of high myopia. *J. Biol. Chem.* 278, 16587–16594.
- Geraghty, B., Jones, S.W., Rama, P., Akhtar, R., Elsheikh, A., 2012. Age-related variations in the biomechanical properties of human sclera. *J. Mech. Behav. Biomed. Mater.* 16, 181–191.
- Girard, M.J., Beotra, M.R., Chin, K.S., Sandhu, A., Clemo, M., Nikita, E., Kamal, D.S., Papadopoulos, M., Mari, J.M., Aung, T., Strouthidis, N.G., 2016. In vivo 3-dimensional strain mapping of the optic nerve head following intraocular pressure lowering by trabeculectomy. *Ophthalmology* 123, 1190–1200.
- Girard, M.J., Chin, K.S., Devalla, S.K., Aung, T., Jonas, J.B., Wang, Y.X., Thiery, A.H., 2018. Deep Learning Can Exploit 3D Structural Information of the Optic Nerve Head to Provide a Glaucoma Diagnostic Power Superior to that of Retinal Nerve Fibre Layer Thickness. Association for Research in Vision and Ophthalmology, Honolulu, pp. 4081.
- Girard, M.J., Dahlmann-Noor, A., Rayapureddi, S., Bechara, J.A., Bertin, B.M., Jones, H., Albon, J., Khaw, P.T., Ethier, C.R., 2011a. Quantitative mapping of scleral fiber orientation in normal rat eyes. *Investig. Ophthalmol. Vis. Sci.* 52, 9684–9693.
- Girard, M.J., Downs, J.C., Bottlang, M., Burgoyne, C.F., Suh, J.K., 2009a. Peripapillary and posterior scleral mechanics-Part II: experimental and inverse finite element characterization. *J. Biomech. Eng.* 131 051012.
- Girard, M.J., Downs, J.C., Burgoyne, C.F., Suh, J.K., 2009b. Peripapillary and posterior scleral mechanics-part I: development of an anisotropic hyperelastic constitutive model. *J. Biomech. Eng.* 131 051011.
- Girard, M.J., Strouthidis, N.G., Desjardins, A., Mari, J.M., Ethier, C.R., 2013. In vivo optic nerve head biomechanics: performance testing of a three-dimensional tracking algorithm. *J. R. Soc. Interface* 10 20130459.
- Girard, M.J., Strouthidis, N.G., Ethier, C.R., Mari, J.M., 2011b. Shadow removal and contrast enhancement in optical coherence tomography images of the human optic nerve head. *Investig. Ophthalmol. Vis. Sci.* 52, 7738–7748.
- Girard, M.J., Suh, J.K., Bottlang, M., Burgoyne, C.F., Downs, J.C., 2009c. Scleral biomechanics in the aging monkey eye. *Investig. Ophthalmol. Vis. Sci.* 50, 5226–5237.
- Girard, M.J., Suh, J.K., Bottlang, M., Burgoyne, C.F., Downs, J.C., 2011. Biomechanical changes in the sclera of monkey eyes exposed to chronic IOP elevations. *Investig. Ophthalmol. Vis. Sci.* 52 (8), 5656–5669.
- Glasser, A., 2008. Restoration of accommodation: surgical options for correction of presbyopia. *Clin. Exp. Optom.* 91, 279–295.
- Glasser, A., Troilo, D., Howland, H.C., 1994. The mechanism of corneal accommodation in chicks. *Vis. Res.* 34, 1549–1566.
- Gogola, A., Jan, N.J., Brazile, B., Lam, P., Lathrop, K.L., Chan, K.C., Sigal, I.A., 2018a. Spatial patterns and age-related changes of the collagen crimp in the human cornea and sclera. *Investig. Ophthalmol. Vis. Sci.* 59, 2987–2998.
- Gogola, A., Jan, N.J., Lathrop, K.L., Sigal, I.A., 2018b. Radial and circumferential collagen fibers are a feature of the peripapillary sclera of human, monkey, pig, cow, goat, and sheep. *Investig. Ophthalmol. Vis. Sci.* 59, 4763–4774.
- Grant, C.A., Thomson, N.H., Savage, M.D., Woon, H.W., Greig, D., 2011. Surface characterisation and biomechanical analysis of the sclera by atomic force microscopy. *J. Mech. Behav. Biomed. Mater.* 4, 535–540.
- Green, J.S., Bear, J.C., Johnson, G.J., 1986. The burden of genetically determined eye disease. *Br. J. Ophthalmol.* 70, 696–699.
- Grytz, R., 2018. Scleral remodeling in myopia. In: Roberts, C., Dupps, W.J., Downs, J.C. (Eds.), *Biomechanics of the Eye*, first ed. Kugler, Amsterdam, pp. 383–403.
- Grytz, R., El Hamdaoui, M., 2017. Multi-scale modeling of vision-guided remodeling and age-dependent growth of the tree shrew sclera during eye development and lens-induced myopia. *J. Elast.* 129, 171–195.
- Grytz, R., El Hamdaoui, M., Levy, A.M., Girkin, C.A., Samuels, B.C., 2018. Scleral Crosslinking Using Genipin Has a Dose-dependent Effect on Form-Deprivation Myopia in Tree Shrews. Association for Research in Vision and Ophthalmology Annual Meeting, Honolulu, pp. 708.
- Grytz, R., Fazio, M.A., Libertaux, V., Bruno, L., Gardiner, S., Girkin, C.A., Downs, J.C., 2014. Age- and race-related differences in human scleral material properties. *Investig. Ophthalmol. Vis. Sci.* 55, 8163–8172.
- Grytz, R., Meschke, G., 2009. Constitutive modeling of crimped collagen fibrils in soft tissues. *J. Mech. Behav. Biomed. Mater.* 2, 522–533.
- Grytz, R., Meschke, G., Jonas, J.B., 2011. The collagen fibril architecture in the lamina cribrosa and peripapillary sclera predicted by a computational remodeling approach. *Biomechanics Model. Mechanobiol.* 10, 371–382.
- Grytz, R., Siegwart Jr., J.T., 2015. Changing material properties of the tree shrew sclera during minus lens compensation and recovery. *Investig. Ophthalmol. Vis. Sci.* 56, 2065–2078.
- Guggenheim, J.A., McBrien, N.A., 1996. Form-deprivation myopia induces activation of scleral matrix metalloproteinase-2 in tree shrew. *Investig. Ophthalmol. Vis. Sci.* 37, 1380–1395.
- Guo, L., Frost, M.R., He, L., Siegwart Jr., J.T., Norton, T.T., 2013. Gene expression signatures in tree shrew sclera in response to three myopiagenic conditions. *Investig. Ophthalmol. Vis. Sci.* 54, 6806–6819.
- Hamanaka, T., 1989. Scleral spur and ciliary muscle in man and monkey. *Jpn. J. Ophthalmol.* 33, 221–236.
- Hamilton, D.R., Davidorf, J.M., Maloney, R.K., 2002. Anterior ciliary sclerotomy for treatment of presbyopia: a prospective controlled study. *Ophthalmology* 109, 1970–1976 discussion 1976–1977.
- Harper, A.R., Summers, J.A., 2015. The dynamic sclera: extracellular matrix remodeling in normal ocular growth and myopia development. *Exp. Eye Res.* 133, 100–111.
- Hayes, S., Boote, C., Tuft, S.J., Quantock, A.J., Meek, K.M., 2007. A study of corneal thickness, shape and collagen organisation in keratoconus using videokeratography and X-ray scattering techniques. *Exp. Eye Res.* 84, 423–434.
- Hipsley, A., Hall, B., Rocha, K.M., 2018. Scleral surgery for the treatment of presbyopia: where are we today? *Eye Vis.* 5, 4.
- Hipsley, A., Ma, D.H., Sun, C.C., Jackson, M.A., Goldberg, D., Hall, B., 2017. Visual outcomes 24 months after LaserACE. *Eye Vis.* 4, 15.
- Ho, L.C., Sigal, I.A., Jan, N.J., Squires, A., Tse, Z., Wu, E.X., Kim, S.G., Schuman, J.S., Chan, K.C., 2014. Magic angle-enhanced MRI of fibrous microstructures in sclera and cornea with and without intraocular pressure loading. *Investig. Ophthalmol. Vis. Sci.* 55, 5662–5672.
- Ho, L.C., Sigal, I.A., Jan, N.J., Yang, X., van der Merwe, Y., Yu, Y., Chau, Y., Leung, C.K., Conner, I.P., Jin, T., Wu, E.X., Kim, S.G., Wollstein, G., Schuman, J.S., Chan, K.C., 2016. Non-invasive MRI assessments of tissue microstructures and macromolecules in the eye upon biomechanical or biochemical modulation. *Sci. Rep.* 6, 32080.
- Hodson, S., 1997. Corneal stromal swelling. *Prog. Retin. Eye Res.* 16, 99–116.
- Holden, B.A., Fricke, T.R., Wilson, D.A., Jong, M., Naidoo, K.S., Sankaridurg, P., Wong, T.Y., Naduvilath, T.J., Resnikoff, S., 2016. Global prevalence of myopia and high myopia and temporal trends from 2000 through 2050. *Ophthalmology* 123, 1036–1042.
- Howlett, M.H., McFadden, S.A., 2007. Emmetropization and schematic eye models in developing pigmented Guinea pigs. *Vis. Res.* 47, 1178–1190.
- Hu, S., Cui, D., Yang, X., Hu, J., Wan, W., Zeng, J., 2011. The crucial role of collagen-binding integrins in maintaining the mechanical properties of human scleral fibroblasts-seeded collagen matrix. *Mol. Vis.* 17, 1334–1342.
- Hua, Y., Tong, J., Ghatge, D., Kedar, S., Gu, L., 2017. Intracranial pressure influences the behavior of the optic nerve head. *J. Biomech. Eng.* 139.
- Hua, Y., Voorhees, A.P., Sigal, I.A., 2018. Cerebrospinal fluid pressure: revisiting factors influencing optic nerve head biomechanics. *Investig. Ophthalmol. Vis. Sci.* 59, 154–165.
- Huang, Y., Meek, K.M., 1999. Swelling studies on the cornea and sclera: the effects of pH

- and ionic strength. *Biophys. J.* 77, 1655–1665.
- Ismail, E.N., Ruberti, J.W., Malek, G., 2017. Quick-freeze/deep-etch electron microscopy visualization of the mouse posterior pole. *Exp. Eye Res.* 162, 62–72.
- Izu, Y., Anson, H.L., Zhang, G., Soslow, L.J., Bonaldo, P., Chu, M.L., Birk, D.E., 2011. Dysfunctional tendon collagen fibrillogenesis in collagen VI null mice. *Matrix Biol.* 30, 53–61.
- Jan, N.J., Brazile, B.L., Hu, D., Grube, G., Wallace, J., Gogola, A., Sigal, I.A., 2018. Crimp around the globe; patterns of collagen crimp across the corneal shell. *Exp. Eye Res.* 172, 159–170.
- Jan, N.J., Gomez, C., Moed, S., Voorhees, A.P., Schuman, J.S., Bilonick, R.A., Sigal, I.A., 2017a. Microstructural crimp of the lamina cribrosa and peripapillary sclera collagen fibers. *Investig. Ophthalmol. Vis. Sci.* 58, 3378–3388.
- Jan, N.J., Grimm, J.L., Tran, H., Lathrop, K.L., Wollstein, G., Bilonick, R.A., Ishikawa, H., Kagemann, L., Schuman, J.S., Sigal, I.A., 2015. Polarization microscopy for characterizing fiber orientation of ocular tissues. *Biomed. Opt. Express* 6, 4705–4718.
- Jan, N.J., Lathrop, K., Sigal, I.A., 2017b. Collagen architecture of the posterior Pole: high-resolution wide field of view visualization and analysis using polarized light microscopy. *Investig. Ophthalmol. Vis. Sci.* 58, 735–744.
- Jan, N.J., Sigal, I.A., 2018. Collagen fiber recruitment: a microstructural basis for the nonlinear response of the posterior pole of the eye to increases in intraocular pressure. *Acta Biomater.* 72, 295–305.
- Janowski, M., Bulte, J.W., Handa, J.T., Rini, D., Walczak, P., 2015. Concise review: using stem cells to prevent the progression of myopia-A concept. *Stem Cells* 33, 2104–2113.
- Jay, L., Bourget, J.M., Goyer, B., Singh, K., Brunette, I., Ozaki, T., Proulx, S., 2015. Characterization of tissue-engineered posterior corneas using second- and third-harmonic generation microscopy. *PLoS One* 10, e0125564.
- Jin, Y., Wang, X., Zhang, L., Jonas, J.B., Aung, T., Schmetterer, L., Girard, M.J.A., 2018. Modeling the origin of the ocular pulse and its impact on the optic nerve head. *Investig. Ophthalmol. Vis. Sci.* 59, 3997–4010.
- Jonas, J.B., 2011. Role of cerebrospinal fluid pressure in the pathogenesis of glaucoma. *Acta Ophthalmol.* 89, 505–514.
- Jonas, J.B., Dai, Y., Panda-Jonas, S., 2016a. Peripapillary suprachoroidal cavitation, parapapillary gamma zone and optic disc rotation due to the biomechanics of the optic nerve dura mater. *Investig. Ophthalmol. Vis. Sci.* 57, 4373.
- Jonas, J.B., Holbach, L., Panda-Jonas, S., 2014. Scleral cross section area and volume and axial length. *PLoS One* 9, e93551.
- Jonas, J.B., Holbach, L., Panda-Jonas, S., 2016b. Histologic differences between primary high myopia and secondary high myopia due to congenital glaucoma. *Acta Ophthalmol.* 94, 147–153.
- Jones, H.J., Girard, M.J., White, N., Fautsch, M.P., Morgan, J.E., Ethier, C.R., Albon, J., 2015. Quantitative analysis of three-dimensional fibrillar collagen microstructure within the normal, aged and glaucomatous human optic nerve head. *J. R. Soc. Interface* 12.
- Kaji, Y., Akiyama, T., Segawa, H., Oshika, T., Kano, H., 2017. Raman microscopy: a noninvasive method to visualize the localizations of biomolecules in the cornea. *Cornea* 36 (Suppl. 1), S67–s71.
- Kamma-Lorger, C.S., Boote, C., Hayes, S., Moger, J., Burghammer, M., Knupp, C., Quantock, A.J., Sorensen, T., Di Cola, E., White, N., Young, R.D., Meek, K.M., 2010. Collagen and mature elastic fibre organisation as a function of depth in the human cornea and limbus. *J. Struct. Biol.* 169, 424–430.
- Kaufmann, C., Bachmann, L.M., Robert, Y.C., Thiel, M.A., 2006. Ocular pulse amplitude in healthy subjects as measured by dynamic contour tonometry. *Arch. Ophthalmol.* 124, 1104–1108.
- Keeley, F.W., Morin, J.D., Vesely, S., 1984. Characterisation of collagen from normal human sclera. *Exp. Eye Res.* 39, 533–542.
- Keyes, J.T., Yan, D., Rader, J.H., Utzinger, U., Vande Geest, J.P., 2011. A gimbal-mounted pressurization chamber for macroscopic and microscopic assessment of ocular tissues. *J. Biomech. Eng.* 133 095001.
- Killer, H.E., Laeng, H.R., Flammer, J., Groscurth, P., 2003. Architecture of arachnoid trabeculae, pillars, and septa in the subarachnoid space of the human optic nerve: anatomy and clinical considerations. *Br J Ophthalmol* 87, 777–781.
- Kimball, F.E., Nguyen, C., Steinhart, M.R., Nguyen, T.D., Pease, M.E., Oglesby, E.N., Oveson, B.C., Quigley, H.A., 2014. Experimental scleral cross-linking increases glaucoma damage in a mouse model. *Exp. Eye Res.* (in press).
- Kimura, S., Kobayashi, M., Nakamura, M., Hirano, K., Awaya, S., Hoshino, T., 1995. Immunoelectron microscopic localization of decorin in aged human corneal and scleral stroma. *J. Electron. Microsc.* 44, 445–449.
- Kokott, W., 1934. Das spaltlinienbild der sklera (Ein Beitrag zum funktionellen bau der sklera). *Klin Monbl Augenheilkd* 92, 177–185.
- Komai, Y., Ushiki, T., 1991. The three-dimensional organisation of collagen fibrils in the human cornea and sclera. *Investig. Ophthalmol. Visual Sci.* 32, 2244–2258.
- Kouchaki, B., Hashemi, H., Yekta, A., Khabazkhoob, M., 2017. Comparison of current tonometry techniques in measurement of intraocular pressure. *J. Curr. Ophthalmol.* 29, 92–97.
- Kramer, L.A., Sargsyan, A.E., Hasan, K.M., Polk, J.D., Hamilton, D.R., 2012. Orbital and intracranial effects of microgravity: findings at 3-T MR imaging. *Radiology* 263, 819–827.
- Krumspatzky, H.G., Ludtke, R., Mickler, A., Klaus, V., Selbmann, H.K., 1999. Blindness incidence in Germany. A population-based study from Wurttemberg-Hohenzollern. *Ophthalmologica. Journal international d'ophtalmologie. International journal of ophthalmology. Zeitschrift für Augenheilkunde* 213, 176–182.
- Kuchtey, J., Kuchtey, R.W., 2014. The microfibril hypothesis of glaucoma: implications for treatment of elevated intraocular pressure. *J. Ocul. Pharmacol. Ther. : Off. J. Assoc. Ocul. Pharmacol. Ther.* 30, 170–180.
- Lanchares, E., Del Buey, M.A., Cristobal, J.A., Calvo, B., Ascaso, F.J., Malve, M., 2016. Computational simulation of scleral buckling surgery for rhegmatogenous retinal detachment: on the effect of the band size on the myopization. *J. Ophthalmol* 2016, 3578617.
- Lari, D.R., Schultz, D.S., Wang, A.S., Lee, O.T., Stewart, J.M., 2012. Scleral mechanics: comparing whole globe inflation and uniaxial testing. *Exp. Eye Res.* 94, 128–135.
- Lee, A.G., Mader, T.H., Gibson, C.R., Tarver, W., 2017. Space flight-associated neuro-ocular syndrome. *JAMA Ophthalmol.* 135, 992–994.
- Lee, S.B., Geroski, D.H., Prausnitz, M.R., Edlhauser, H.F., 2004. Drug delivery through the sclera: effects of thickness, hydration, and sustained release systems. *Exp. Eye Res.* 78, 599–607.
- Leung, L.K., Ko, M.W., Ye, C., Lam, D.C., Leung, C.K., 2014. Noninvasive measurement of scleral stiffness and tangent modulus in porcine eyes. *Investig. Ophthalmol. Vis. Sci.* 55, 3721–3726.
- Levy, A.M., Fazio, M.A., Grytz, R., 2018. Experimental myopia increases and scleral crosslinking using genipin inhibits cyclic softening in the tree shrew sclera. *Ophthalmic Physiol. Opt.* 38, 246–256.
- Lewis, P.N., White, T.L., Young, R.D., Bell, J.S., Winlove, C.P., Meek, K.M., 2016. Three-dimensional arrangement of elastic fibers in the human corneal stroma. *Exp. Eye Res.* 146, 43–53.
- Lima, E.G., Tan, A.R., Tai, T., Marra, K.G., DeFail, A., Ateshian, G.A., Hung, C.T., 2009. Genipin enhances the mechanical properties of tissue-engineered cartilage and protects against inflammatory degradation when used as a medium supplement. *J. Biomed. Mater. Res. A* 91, 692–700.
- Lin, J.T., Mallo, O., 2003. Treatment of presbyopia by infrared laser radial sclerectomy. *J. Refract. Surg.* 19, 465–467.
- Lin, X., Naidu, R.K., Dai, J., Zhou, X., Qu, X., Zhou, H., 2019. Scleral cross-linking using glycerinaldehyde for the prevention of axial elongation in the rabbit: blocked axial elongation and altered scleral microstructure. *Curr. Eye Res.* 44, 162–171.
- Lin, X., Wang, B.J., Wang, Y.C., Chu, R.Y., Dai, J.H., Zhou, X.T., Qu, X.M., Liu, H., Zhou, H., 2018. Scleral ultrastructure and biomechanical changes in rabbits after negative lens application. *Int. J. Ophthalmol.* 11, 354–362.
- Linsenmayer, T.F., Gibney, E., Igoe, F., Gordon, M.K., Fitch, J.M., Fessler, L.I., Birk, D.E., 1993. Type V collagen: molecular structure and fibrillar organization of the chicken alpha 1(V) NH2-terminal domain, a putative regulator of corneal fibrillogenesis. *J. Cell Biol.* 121, 1181–1189.
- Liu, S., Li, S., Wang, B., Lin, X., Wu, Y., Liu, H., Qu, X., Dai, J., Zhou, X., Zhou, H., 2016. Scleral cross-linking using riboflavin UVA irradiation for the prevention of myopia progression in a Guinea pig model: blocked axial extension and altered scleral microstructure. *PLoS One* 11, e0165792.
- Liu, Y., Wildsoet, C., 2011. The effect of two-zone concentric bifocal spectacle lenses on refractive error development and eye growth in young chicks. *Investig. Ophthalmol. Vis. Sci.* 52, 1078–1086.
- Lu, J.L., Hall, L., Liu, J., 2018. Improving glaucoma surgical outcomes with adjunct tools. *J. Curr. Glaucoma Pract.* 12, 19–28.
- Luan, H., Roberts, R., Sniegowski, M., Goebel, D.J., Berkowitz, B.A., 2006. Retinal thickness and subnormal retinal oxygenation response in experimental diabetic retinopathy. *Investig. Ophthalmol. Vis. Sci.* 47, 320–328.
- Luesma, M.J., Gherghiceanu, M., Popescu, L.M., 2013. Telocytes and stem cells in limbus and uvea of mouse eye. *J. Cell Mol. Med.* 17, 1016–1024.
- Ma, Y., Pavlatos, E., Clayton, K., Pan, X., Kwok, S., Sandwisch, T., Liu, J., 2019. Mechanical deformation of human optic nerve head and peripapillary tissue in response to acute IOP elevation. *Investig. Ophthalmol. Vis. Sci.* 60, 913–920.
- Yu, S.W., Ma, A., Wong, J.K., 2019. Micropulse laser for the treatment of glaucoma: a literature review. *Surv. Ophthalmol.* 64 (4), 486–497.
- Mader, T.H., Gibson, C.R., Pass, A.F., Kramer, L.A., Lee, A.G., Fogarty, J., Tarver, W.J., Dervay, J.P., Hamilton, D.R., Sargsyan, A., Phillips, J.L., Tran, D., Lipsky, W., Choi, J., Stern, C., Kuyumjian, R., Polk, J.D., 2011. Optic disc edema, globe flattening, choroidal folds, and hyperopic shifts observed in astronauts after long-duration space flight. *Ophthalmology* 118, 2058–2069.
- Malecaze, F.J., Gazagne, C.S., Tarroux, M.C., Gorrard, J.M., 2001. Scleral expansion bands for presbyopia. *Ophthalmology* 108, 2165–2171.
- Malik, N.S., Moss, S.J., Ahmed, N., Furth, A.J., Wall, R.S., Meek, K.M., 1992. Ageing of the human corneal stroma: structural and biochemical changes. *Biochim. Biophys. Acta* 1138, 222–228.
- Markov, P.P., Eliasi, A., Pijanka, J.K., Htoon, H.M., Paterson, N.G., Sorensen, T., Elsheikh, A., Girard, M.J.A., Boote, C., 2018. Bulk changes in posterior scleral collagen microstructure in human high myopia. *Mol. Vis.* 24, 818–833.
- Marshall, G.E., 1995. Human scleral elastic system: an immunoelectron microscopic study. *Br. J. Ophthalmol.* 79, 57–64.
- Marshall, G.E., Konstas, A.G.P., Lee, W.R., 1993. Collagens in the aged human macular sclera. *Exp. Eye Res.* 12, 143–153.
- McBrien, N.A., Cornell, L.M., Gentle, A., 2001. Structural and ultrastructural changes to the sclera in a mammalian model of high myopia. *Investig. Ophthalmol. Vis. Sci.* 42, 2179–2187.
- McBrien, N.A., Jobling, A.I., Gentle, A., 2009. Biomechanics of the sclera in myopia: extracellular and cellular factors. *Optom. Vis. Sci.* 86, E23–E30.
- McBrien, N.A., Lawlor, P., Gentle, A., 2000. Scleral remodeling during the development of and recovery from axial myopia in the tree shrew. *Investig. Ophthalmol. Vis. Sci.* 41, 3713–3719.
- McBrien, N.A., Metlapally, R., Jobling, A.I., Gentle, A., 2006. Expression of collagen-binding integrin receptors in the mammalian sclera and their regulation during the development of myopia. *Investig. Ophthalmol. Vis. Sci.* 47, 4674–4682.
- McBrien, N.A., Norton, T.T., 1994. Prevention of collagen crosslinking increases form-deprivation myopia in tree shrew. *Exp. Eye Res.* 59, 475–486.
- Meek, K., Boote, C., 2004. The organisation of collagen in the corneal stroma. *Exp. Eye Res.* 78, 503–512.
- Meek, K.M., 2008. The cornea and sclera. In: *Fratzl, P. (Ed.), Collagen: Structure and*

- Mechanics. Springer, New York, pp. 359–396.
- Meek, K.M., Boote, C., 2009. The use of x-ray scattering techniques to quantify the orientation and distribution of collagen in the corneal stroma. *Prog. Retin. Eye Res.* 28, 369–392.
- Meller, D., Peters, K., Meller, K., 1997. Human cornea and sclera studied by atomic force microscopy. *Cell Tissue Res.* 288, 111–118.
- Midgett, D.E., Jefferys, J.L., Quigley, H.A., Nguyen, T.D., 2018. The contribution of sulfated glycosaminoglycans to the inflation response of the human optic nerve head. *Investig. Ophthalmol. Vis. Sci.* 59, 3144–3154.
- Moisseiev, E., Loewenstein, A., 2017. Drug delivery to the posterior segment of the eye. *Dev. Ophthalmol.* 58, 87–101.
- Morgan, W.H., Yu, D.Y., Cooper, R.L., Alder, V.A., Cringle, S.J., Constable, I.J., 1995. The influence of cerebrospinal fluid pressure on the lamina cribrosa tissue pressure gradient. *Investig. Ophthalmol. Vis. Sci.* 36, 1163–1172.
- Moring, A.G., Baker, J.R., Norton, T.T., 2007. Modulation of glycosaminoglycan levels in tree shrew sclera during lens-induced myopia development and recovery. *Investig. Ophthalmol. Vis. Sci.* 48, 2947–2956.
- Morris, H.J., Tang, J., Cruz Perez, B., Pan, X., Hart, R.T., Weber, P.A., Liu, J., 2013. Correlation between biomechanical responses of posterior sclera and IOP elevations during micro intraocular volume change. *Investig. Ophthalmol. Vis. Sci.* 54, 7215–7222.
- Munier, A., Gunning, T., Kenny, D., O'Keefe, M., 1998. Causes of blindness in the adult population of the Republic of Ireland. *Br. J. Ophthalmol.* 82, 630–633.
- Murienne, B.J., Chen, M.L., Quigley, H.A., Nguyen, T.D., 2016. The contribution of glycosaminoglycans to the mechanical behaviour of the posterior human sclera. *J. R. Soc. Interface* 13.
- Murienne, B.J., Jefferys, J.L., Quigley, H.A., Nguyen, T.D., 2015. The effects of glycosaminoglycan degradation on the mechanical behavior of the posterior porcine sclera. *Acta Biomater.* 12, 195–206.
- Myers, K.M., Cone, F.E., Quigley, H.A., Gelman, S., Pease, M.E., Nguyen, T.D., 2010a. The in vitro inflation response of mouse sclera. *Exp. Eye Res.* 91, 866–875.
- Myers, K.M., Cone, F.E., Quigley, H.A., Nguyen, T.D., 2011. The scleral inflation response of mouse eyes to increases in pressure. In: Proulx, T. (Ed.), *Mechanics of Biological Systems and Materials*. Springer, New York.
- Myers, K.M., Coudrillier, B., Boyce, B.L., Nguyen, T.D., 2010b. The inflation response of the posterior bovine sclera. *Acta Biomater.* 6, 4327–4335.
- Newton, R.H., Meek, K.M., 1998. Circumcorneal annulus of collagen fibrils in the human limbus. *Investig. Ophthalmol. Vis. Sci.* 39, 1125–1134.
- Nguyen, C., Cone, F.E., Nguyen, T.D., Coudrillier, B., Pease, M.E., Steinhart, M.R., Oglesby, E.N., Jefferys, J.L., Quigley, H.A., 2013. Studies of scleral biomechanical behavior related to susceptibility for retinal ganglion cell loss in experimental mouse glaucoma. *Investig. Ophthalmol. Vis. Sci.* 54, 1767–1780.
- Nguyen, C., Midgett, D., Kimball, E., Jefferys, J., Nguyen, T.D., Schaub, J., Pease, M., Quigley, H., 2018. Age-related changes in quantitative strain of mouse astrocytic lamina cribrosa and peripapillary sclera using confocal microscopy in an explant model. *Investig. Ophthalmol. Vis. Sci.* 59, 5157–5166.
- Nguyen, C., Midgett, D., Kimball, E.C., Steinhart, M.R., Nguyen, T.D., Pease, M.E., Oglesby, E.N., Jefferys, J.L., Quigley, H.A., 2017. Measuring deformation in the mouse optic nerve head and peripapillary sclera. *Investig. Ophthalmol. Vis. Sci.* 58, 721–733.
- Norman, R.E., Flanagan, J.G., Rausch, S.M., Sigal, I.A., Tertinegg, I., Eilaghi, A., Portnoy, S., Sled, J.G., Ethier, C.R., 2010a. Dimensions of the human sclera: thickness measurement and regional changes with axial length. *Exp. Eye Res.* 90, 277–284.
- Norman, R.E., Flanagan, J.G., Sigal, I.A., Rausch, S.M., Tertinegg, I., Ethier, C.R., 2010b. Finite element modeling of the human sclera: influence on optic nerve head biomechanics and connections with glaucoma. *Exp. Eye Res.* 29 (Sept).
- Norton, T.T., Amedo, A.O., Siegwart Jr., J.T., 2010. The effect of age on compensation for a negative lens and recovery from lens-induced myopia in tree shrews (*Tupaia glis belangeri*). *Vis. Res.* 50, 564–576.
- Norton, T.T., Rada, J.A., 1995. Reduced extracellular matrix in mammalian sclera with induced myopia. *Vis. Res.* 35, 1271–1281.
- Norton, T.T., Siegwart Jr., J.T., 1995. Animal models of emmetropization: matching axial length to the focal plane. *J. Am. Optom. Assoc.* 66, 405–414.
- Oglesby, E.N., Tezel, G., Cone-Kimball, E., Steinhart, M.R., Jefferys, J., Pease, M.E., Quigley, H.A., 2016. Scleral fibroblast response to experimental glaucoma in mice. *Mol. Vis.* 22, 82–99.
- Ohlendorf, A., Schaeffel, F., 2009. Contrast adaptation induced by defocus - a possible error signal for emmetropization? *Vis. Res.* 49, 249–256.
- Ohno-Matsui, K., Jonas, J.B., 2018. Posterior staphyloma in pathologic myopia. *Prog. Retin. Eye Res.* 70, 99–109.
- Olsen, T.W., Edelhauser, H.F., Lim, J.L., Geroski, D.H., 1995. Human scleral permeability. Effects of age, cryotherapy, transscleral diode laser, and surgical thinning. *Investig. Ophthalmol. Vis. Sci.* 36, 1893–1903.
- Overby, D.R., Bertrand, J., Schicht, M., Paulsen, F., Stamer, W.D., Lutjen-Drecoll, E., 2014. The structure of the trabecular meshwork, its connections to the ciliary muscle, and the effect of pilocarpine on outflow facility in mice. *Investig. Ophthalmol. Vis. Sci.* 55, 3727–3736.
- Palko, J.R., Morris, H.J., Pan, X., Harman, C.D., Koehl, K.L., Gelatt, K.N., Plummer, C.E., Komaromy, A.M., Liu, J., 2016. Influence of age on ocular biomechanical properties in a canine glaucoma model with ADAMTS10 mutation. *PLoS One* 11, e0156466.
- Palko, J.R., Pan, X., Liu, J., 2011. Dynamic testing of regional viscoelastic behavior of canine sclera. *Exp. Eye Res.* 93, 825–832.
- Park, C.Y., Marando, C.M., Liao, J.A., Lee, J.K., Kwon, J., Chuck, R.S., 2016. Details of the collagen and elastin architecture in the human limbal conjunctiva, Tenon's capsule and sclera revealed by two-photon excited fluorescence microscopy. *Investig. Ophthalmol. Vis. Sci.* 57, 5602–5610.
- Park, S.W., Lee, J.J., Lee, J.E., 2018. Scleral buckling in the management of rhegmatogenous retinal detachment: patient selection and perspectives. *Clin. Ophthalmol.* 12, 1605–1615.
- Pavlatos, E., Ma, Y., Clayton, K., Pan, X., Liu, J., 2018. Regional deformation of the optic nerve head and peripapillary sclera during IOP elevation. *Investig. Ophthalmol. Vis. Sci.* 59, 3779–3788.
- Pavlatos, E., Perez, B.C., Morris, H.J., Chen, H., Palko, J.R., Pan, X., Weber, P.A., Hart, R.T., Liu, J., 2016. Three-dimensional strains in human posterior sclera using ultrasound speckle tracking. *J. Biomech. Eng.* 138, 021015.
- Perez, B.C., Morris, H.J., Hart, R.T., Liu, J., 2013. Finite element modeling of the viscoelastic responses of the eye during microvolumetric changes. *J. Biomed. Sci. Eng.* 6, 29–37.
- Phillips, J.R., Khalaj, M., McBrien, N.A., 2000. Induced myopia associated with increased scleral creep in chick and tree shrew eyes. *Investig. Ophthalmol. Vis. Sci.* 41, 2028–2034.
- Phillips, J.R., McBrien, N.A., 2004. Pressure-induced changes in axial eye length of chick and tree shrew: significance of myofibroblasts in the sclera. *Investig. Ophthalmol. Vis. Sci.* 45, 758–763.
- Piez, K.A., Miller, A., 1974. The structure of collagen fibrils. *J. Supramol. Struct.* 2, 121–137.
- Pijanka, J.K., Abass, A., Sorensen, T., Elsheikh, A., Boote, C., 2013. A wide-angle X-ray fibre diffraction method for quantifying collagen orientation across large tissue areas: application to the human eyeball coat. *J. Appl. Crystallogr.* 46, 1481–1489.
- Pijanka, J.K., Coudrillier, B., Ziegler, K., Sorensen, T., Meek, K.M., Nguyen, T.D., Quigley, H.A., Boote, C., 2012. Quantitative mapping of collagen fiber orientation in non-glaucoma and glaucoma posterior human sclerae. *Investig. Ophthalmol. Vis. Sci.* 53, 5258–5270.
- Pijanka, J.K., Kimball, E.C., Pease, M.E., Abass, A., Sorensen, T., Nguyen, T.D., Quigley, H.A., Boote, C., 2014. Changes in scleral collagen organization in murine chronic experimental glaucoma. *Investig. Ophthalmol. Vis. Sci.* 55, 6554–6564.
- Pijanka, J.K., Markov, P.P., Midgett, D., Paterson, N.G., White, N., Blain, E.J., Nguyen, T.D., Quigley, H.A., Boote, C., 2019. Quantification of collagen fiber structure using second harmonic generation imaging and two-dimensional discrete Fourier transform analysis: application to the human optic nerve head. *J. Biophot.* 12, e201800376.
- Pijanka, J.K., Spang, M.T., Sorensen, T., Liu, J., Nguyen, T.D., Quigley, H.A., Boote, C., 2015. Depth-dependent changes in collagen organization in the human peripapillary sclera. *PLoS One* 10, e0118648.
- Pinsky, P.M., Van der Heide, D., Chernyak, D., 2005. Computational modeling of mechanical anisotropy in the cornea and sclera. *J. Cataract Refract. Surg.* 31, 136–145.
- Pitha, I., Oglesby, E., Chow, A., Kimball, E., Pease, M.E., Schaub, J., Quigley, H., 2018. Rho-kinase inhibition reduces myofibroblast differentiation and proliferation of scleral fibroblasts induced by transforming growth factor beta and experimental glaucoma. *Transl. Vis. Sci. Technol.* 7, 6.
- Poostchi, A., Wong, T., Chan, K.C., Kedzlie, L., Sachdev, N., Nicholas, S., Garway-Heath, D.F., Wells, A.P., 2010. Optic disc diameter increases during acute elevations of intraocular pressure. *Investig. Ophthalmol. Vis. Sci.* 51, 2313–2316.
- Poukens, V., Glasgow, B.J., Demer, J.L., 1998. Nonvascular contractile cells in sclera and choroid of humans and monkeys. *Investig. Ophthalmol. Vis. Sci.* 39, 1765–1774.
- Qu, J., Chen, H., Zhu, L., Ambalavanan, N., Girkin, C.A., Murphy-Ullrich, J.E., Downs, J.C., Zhou, Y., 2015. High-magnitude and/or high-frequency mechanical strain promotes peripapillary scleral myofibroblast differentiation. *Investig. Ophthalmol. Vis. Sci.* 56, 7821–7830.
- Quantock, A.J., Meek, K.M., 1988. Axial electron density of human scleral collagen. Location of proteoglycans by x-ray diffraction. *Biophys. J.* 54, 159–164.
- Quigley, H.A., Cone, F.E., 2013. Development of diagnostic and treatment strategies for glaucoma through understanding and modification of scleral and lamina cribrosa connective tissue. *Cell Tissue Res.* 353 (2), 231–244.
- Quigley, H.A., Dorman-Pease, M.E., Brown, A.E., 1991. Quantitative study of collagen and elastin of the optic nerve head and sclera in human and experimental monkey glaucoma. *Curr. Eye Res.* 10, 877–888.
- Rada, J.A., Achen, V.R., Penugonda, S., Schmidt, R.W., Mount, B.A., 2000. Proteoglycan composition in the human sclera during growth and aging. *Investig. Ophthalmol. Vis. Sci.* 41, 1639–1648.
- Rada, J.A., Achen, V.R., Perry, C.A., Fox, P.W., 1997. Proteoglycans in the human sclera. Evidence for the presence of aggrecan. *Investig. Ophthalmol. Vis. Sci.* 38, 1740–1751.
- Raiskup, F., Theuring, A., Pillunat, L.E., Spoerl, E., 2015. Corneal collagen crosslinking with riboflavin and ultraviolet-A light in progressive keratoconus: ten-year results. *J. Cataract Refract. Surg.* 41, 41–46.
- Robinson, P.N., Booms, P., 2001. The molecular pathogenesis of the Marfan syndrome. *Cell. Mol. Life Sci. : CMLS* 58, 1698–1707.
- Rohen, J.W., Futa, R., Lutjen-Drecoll, E., 1981. The fine structure of the cribriform meshwork in normal and glaucomatous eyes as seen in tangential sections. *Investig. Ophthalmol. Vis. Sci.* 21, 574–585.
- Roth, A., Muhlendyck, H., De Gottrau, P., 2002. [The frequency of Tenon's capsule revisited]. *J. Fr. Ophthalmol.* 25, 968–976.
- Rucker, F.J., Wallman, J., 2012. Chicks use changes in luminance and chromatic contrast as indicators of the sign of defocus. *J. Vis.* 12.
- Samuels, B.C., Siegwart, J.T., Zhan, W., Hethcox, L., Chimento, M., Whitley, R., Downs, J.C., Girkin, C.A., 2018. A novel tree shrew (*Tupaia belangeri*) model of glaucoma. *Investig. Ophthalmol. Vis. Sci.* 59, 3136–3143.
- Scarcelli, G., Pineda, R., Yun, S.H., 2012. Brillouin optical microscopy for corneal biomechanics. *Investig. Ophthalmol. Vis. Sci.* 53, 185–190.
- Schaeffel, F., Glasser, A., Howland, H.C., 1988. Accommodation, refractive error and eye growth in chickens. *Vis. Res.* 28, 639–657.
- Schultz, D.S., Lotz, J.C., Lee, S.M., Trinidad, M.L., Stewart, J.M., 2008. Structural factors that mediate scleral stiffness. *Investig. Ophthalmol. Vis. Sci.* 49, 4232–4236.

- Shao, P., Besner, S., Zhang, J., Scarcelli, G., Yun, S.H., 2016. Etalon filters for Brillouin microscopy of highly scattering tissues. *Opt. Express* 24, 22232–22238.
- Shelton, L., Rada, J.S., 2007. Effects of cyclic mechanical stretch on extracellular matrix synthesis by human scleral fibroblasts. *Exp. Eye Res.* 84, 314–322.
- Shen, L., You, Q.S., Xu, X., Gao, F., Zhang, Z., Li, B., Jonas, J.B., 2015a. Scleral thickness in Chinese eyes. *Investig. Ophthalmol. Vis. Sci.* 56, 2720–2727.
- Shen, L., You, Q.S., Xu, X., Gao, F., Zhang, Z., Li, B., Jonas, J.B., 2016. Scleral and choroidal volume in relation to axial length in infants with retinoblastoma versus adults with malignant melanomas or end-stage glaucoma. *Graefes Arch. Clin. Exp. Ophthalmol.* 254, 1779–1786.
- Shen, Z.M., Zhang, Z.Y., Zhang, L.Y., Li, Z.G., Chu, R.Y., 2015b. Posterior scleral reinforcement combined with patching therapy for pre-school children with unilateral high myopia. *Graefes Arch. Clin. Exp. Ophthalmol.* 253, 1391–1395.
- Sherman, S.M., Norton, T.T., Casagrande, V.A., 1977. Myopia in the lid-sutured tree shrew (*Tupaia glis*). *Brain Res.* 124, 154–157.
- Shin, A., Park, J., Demer, J.L., 2018. Opto-mechanical characterization of sclera by polarization sensitive optical coherence tomography. *J. Biomech.* 72, 173–179.
- Sibony, P., Kupersmith, M.J., Rohlf, F.J., 2011. Shape analysis of the peripapillary RPE layer in papilledema and ischemic optic neuropathy. *Investig. Ophthalmol. Vis. Sci.* 52, 7987–7995.
- Sibony, P.A., 2016. Gaze evoked deformations of the peripapillary retina in papilledema and ischemic optic neuropathy. *Investig. Ophthalmol. Vis. Sci.* 57, 4979–4987.
- Sieglwart Jr., J.T., Norton, T.T., 1999. Regulation of the mechanical properties of tree shrew sclera by the visual environment. *Vis. Res.* 39, 387–407.
- Sieglwart Jr., J.T., Norton, T.T., 2010. Binocular lens treatment in tree shrews: effect of age and comparison of plus lens wear with recovery from minus lens-induced myopia. *Exp. Eye Res.* 91, 660–669.
- Sieglwart Jr., J.T., Norton, T.T., 2011. Perspective: how might emmetropization and genetic factors produce myopia in normal eyes? *Optom. Vis. Sci.* 88, E365–E372.
- Sieglwart Jr., J.T., Strang, C.E., 2007. Selective modulation of scleral proteoglycan mRNA levels during minus lens compensation and recovery. *Mol. Vis.* 13, 1878–1886.
- Sigal, I.A., Flanagan, J.G., Ethier, C.R., 2005. Factors influencing optic nerve head biomechanics. *Investig. Ophthalmol. Vis. Sci.* 46, 4189–4199.
- Sigal, I.A., Flanagan, J.G., Tertinegg, I., Ethier, C.R., 2004. Finite element modeling of optic nerve head biomechanics. *Investig. Ophthalmol. Vis. Sci.* 45, 4378–4387.
- Sigal, I.A., Flanagan, J.G., Tertinegg, I., Ethier, C.R., 2007. Predicted extension, compression and shearing of optic nerve head tissues. *Exp. Eye Res.* 85, 312–322.
- Sigal, I.A., Flanagan, J.G., Tertinegg, I., Ethier, C.R., 2009. Modeling individual-specific human optic nerve head biomechanics. Part I: IOP-induced deformations and influence of geometry. *Biomechanics Model. Mechanobiol.* 8, 85–98.
- Sigal, I.A., Grimm, J.L., Jan, N.J., Reid, K., Minckler, D.S., Brown, D.J., 2014a. Eye-specific IOP-induced displacements and deformations of human lamina cribrosa. *Investig. Ophthalmol. Vis. Sci.* 55, 1–15.
- Sigal, I.A., Grimm, J.L., Schuman, J.S., Kagemann, L., Ishikawa, H., Wollstein, G., 2014b. A method to estimate biomechanics and mechanical properties of optic nerve head tissues from parameters measurable using optical coherence tomography. *IEEE Trans. Med. Imaging* 33, 1381–1389.
- Sigal, I.A., Wang, B., Strouthidis, N.G., Akagi, T., Girard, M.J., 2014c. Recent advances in OCT imaging of the lamina cribrosa. *Br. J. Ophthalmol.* 98 (Suppl. 2), ii34–39.
- Sigal, I.A., Yang, H., Roberts, M.D., Burgoyne, C.F., Downs, J.C., 2011a. IOP-induced lamina cribrosa displacement and scleral canal expansion: an analysis of factor interactions using parameterized eye-specific models. *Investig. Ophthalmol. Vis. Sci.* 52, 1896–1907.
- Sigal, I.A., Yang, H., Roberts, M.D., Downs, J.C., 2010. Morphing methods to parameterize specimen-specific finite element model geometries. *J. Biomech.* 43, 254–262.
- Sigal, I.A., Yang, H., Roberts, M.D., Grimm, J.L., Burgoyne, C.F., Demirel, S., Downs, J.C., 2011b. IOP-induced lamina cribrosa deformation and scleral canal expansion: independent or related? *Investig. Ophthalmol. Vis. Sci.* 52, 9023–9032.
- Soh, Y.B., 2016. Development of a Ring Implant for Glaucoma Department of Biomedical Engineering. National University of Singapore.
- Steinhart, M.R., Cone, F.E., Nguyen, C., Nguyen, T.D., Pease, M.E., Puk, O., Graw, J., Oglesby, E.N., Quigley, H.A., 2012. Mice with an induced mutation in collagen 8A2 develop larger eyes and are resistant to retinal ganglion cell damage in an experimental glaucoma model. *Mol. Vis.* 18, 1093–1106.
- Strouthidis, N.G., Fortune, B., Yang, H., Sigal, I.A., Burgoyne, C.F., 2011. Effect of acute intraocular pressure elevation on the monkey optic nerve head as detected by spectral domain optical coherence tomography. *Investig. Ophthalmol. Vis. Sci.* 52, 9431–9437.
- Strouthidis, N.G., Girard, M.J., 2013. Altering the way the optic nerve head responds to intraocular pressure—a potential approach to glaucoma therapy. *Curr. Opin. Pharmacol.* 13, 83–89.
- Tang, J., Liu, J., 2012. Ultrasonic measurement of scleral cross-sectional strains during elevations of intraocular pressure: method validation and initial results in posterior porcine sclera. *J. Biomech. Eng.* 134, 091007.
- Tektas, O.Y., Hammer, C.M., Danias, J., Candia, O., Gerometta, R., Podos, S.M., Lutjendrecoll, E., 2010. Morphologic changes in the outflow pathways of bovine eyes treated with corticosteroids. *Investig. Ophthalmol. Vis. Sci.* 51, 4060–4066.
- Teng, S., Tan, H., Peng, J., Lin, H.C., Kim, K.H., Lo, W., Sun, Y., Lin, W., Lin, S., Jee, S., So, P.T.C., Dong, C.Y., 2006. Multiphoton autofluorescence and second harmonic generation imaging of the ex-vivo porcine eye. *Investig. Ophthalmol. Vis. Sci.* 47, 1216–1224.
- Thale, A., Tillmann, B., 1993. The collagen architecture of the sclera—SEM and immunohistochemical studies. *Ann. Anat. = Anatomischer Anzeiger: Off. Organs Anat. Ges.* 175, 215–220.
- Thompson, F., 1990. Scleral Reinforcement, Myopia Surgery. Macmillan, New York, pp. 267–297.
- Tonge, T.K., Murienne, B.J., Coudrillier, B., Alexander, S., Rothkopf, W., Nguyen, T.D., 2013. Minimal preconditioning effects observed for inflation tests of planar tissues. *J. Biomech. Eng.* 135, 114502.
- Tun, T.A., Wang, X., Baskaran, M., Nongpiur, M.E., Tham, Y.C., Perera, S.A., Strouthidis, N.G., Aung, T., Cheng, C.Y., Girard, M.J.A., 2019. Variation of peripapillary scleral shape with age. *Investig. Ophthalmol. Vis. Sci.* 60, 3275–3282.
- Umihira, J., Nagata, S., Nohara, M., Hanai, T., Usuda, N., Segawa, K., 1994. Localization of elastin in the normal and glaucomatous human trabecular meshwork. *Investig. Ophthalmol. Vis. Sci.* 35, 486–494.
- Voorhees, A.P., Ho, L.C., Jan, N.J., Tran, H., van der Merwe, Y., Chan, K., Sigal, I.A., 2017. Whole-globe biomechanics using high-field MRI. *Exp. Eye Res.* 160, 85–95.
- Voorhees, A.P., Jan, N.J., Hua, Y., Yang, B., Sigal, I.A., 2018. Peripapillary sclera architecture revisited: a tangential fiber model and its biomechanical implications. *Acta Biomater.* 79, 113–122.
- Vurgese, S., Panda-Jonas, S., Jonas, J.B., 2012. Scleral thickness in human eyes. *PLoS One* 7, e29692.
- Wallman, J., Turkel, J., Trachtman, J., 1978. Extreme myopia produced by modest change in early visual experience. *Science* 201, 1249–1251.
- Wallman, J., Winawer, J., 2004. Homeostasis of eye growth and the question of myopia. *J. Neurosci.* 24, 447–468.
- Walls, G.S., 1942. The Vertebrate Eye and its Adaptive Radiation. Haffner, New York.
- Wang, B., Hua, Y., Sigal, I.A., 2018. Biomechanical Effects of Fiber Interweaving. Biomedical Engineering Society (BMES) Annual Meeting, Atlanta, Georgia, USA.
- Wang, F., Lee, H.P., Lu, C., 2007. Biomechanical effect of segmental scleral buckling surgery. *Curr. Eye Res.* 32, 133–142.
- Wang, J.K., Kardon, R.H., Ledolter, J., Sibony, P.A., Kupersmith, M.J., Garvin, M.K., 2017a. Peripapillary retinal pigment epithelium layer shape changes from acetazolamide treatment in the idiopathic intracranial hypertension treatment trial. *Investig. Ophthalmol. Vis. Sci.* 58, 2554–2565.
- Wang, M., Corpuz, C.C., 2015. Effects of scleral cross-linking using genipin on the process of form-deprivation myopia in the Guinea pig: a randomized controlled experimental study. *BMC Ophthalmol.* 15, 89.
- Wang, M., Zhang, F., Liu, K., Zhao, X., 2015. Safety evaluation of rabbit eyes on scleral collagen cross-linking by riboflavin and ultraviolet A. *Clin. Exp. Ophthalmol.* 43, 156–163.
- Wang, X., Beotra, M.R., Tun, T.A., Baskaran, M., Perera, S., Aung, T., Strouthidis, N.G., Milea, D., Girard, M.J.A., 2016a. In vivo 3-dimensional strain mapping confirms large optic nerve head deformations following horizontal eye movements. *Investig. Ophthalmol. Vis. Sci.* 57, 5825–5833.
- Wang, X., Fisher, L.K., Milea, D., Jonas, J.B., Girard, M.J., 2017b. Predictions of optic nerve traction forces and peripapillary tissue stresses following horizontal eye movements. *Investig. Ophthalmol. Vis. Sci.* 58, 2044–2053.
- Wang, X., Rumpel, H., Lim, W.E., Baskaran, M., Perera, S.A., Nongpiur, M.E., Aung, T., Milea, D., Girard, M.J., 2016b. Author response: peripapillary suprachoroidal cavitation, parapapillary gamma zone and optic disc rotation due to the biomechanics of the optic nerve dura mater. *Investig. Ophthalmol. Vis. Sci.* 57, 4374–4375.
- Wang, X., Rumpel, H., Lim, W.E., Baskaran, M., Perera, S.A., Nongpiur, M.E., Aung, T., Milea, D., Girard, M.J., 2016c. Finite element analysis predicts large optic nerve head strains during horizontal eye movements. *Investig. Ophthalmol. Vis. Sci.* 57, 2452–2462.
- Watson, P., Hazleman, B.L., McCluskey, P.M., Pavesio, C.E., 2012. The sclera and systemic disorders. 3rd. JP Medical Ltd, London.
- Watson, P.G., Young, R.D., 2004. Scleral structure, organisation and disease. A review. *Exp. Eye Res.* 78, 609–623.
- Wenstrup, R.J., Florer, J.B., Brunskill, E.W., Bell, S.M., Chervoneva, I., Birk, D.E., 2004. Type V collagen controls the initiation of collagen fibril assembly. *J. Biol. Chem.* 279, 53331–53337.
- Whitford, C., Joda, A., Jones, S., Bao, F., Rama, P., Elsheikh, A., 2016. Ex vivo testing of intact eye globes under inflation conditions to determine regional variation of mechanical stiffness. *Eye Vis.* 3, 21.
- Wildsoet, C.F., 1997. Active emmetropization—evidence for its existence and ramifications for clinical practice. *Ophthalmic Physiol. Opt.* 17, 279–290.
- Winkler, M., Jester, B., Nien-Shy, C., Massei, S., Minckler, D.S., Jester, J.V., Brown, D.J., 2010. High resolution three-dimensional reconstruction of the collagenous matrix of the human optic nerve head. *Brain Res. Bull.* 81, 339–348.
- Winkler, M., Shoa, G., Xie, Y., Petsche, S.J., Pinsky, P.M., Juhasz, T., Brown, D.J., Jester, J.V., 2013. Three-dimensional distribution of transverse collagen fibers in the anterior human corneal stroma. *Investig. Ophthalmol. Vis. Sci.* 54, 7293–7301.
- Wollensak, G., Iomdina, E., 2008a. Crosslinking of scleral collagen in the rabbit using glycerolaldehyde. *J. Cataract Refract. Surg.* 34, 651–656.
- Wollensak, G., Iomdina, E., 2008b. Long-term biomechanical properties after collagen crosslinking of sclera using glycerolaldehyde. *Acta Ophthalmol.* 86, 887–893.
- Wollensak, G., Iomdina, E., 2009. Long-term biomechanical properties of rabbit sclera after collagen crosslinking using riboflavin and ultraviolet A (UVA). *Acta Ophthalmol.* 87, 193–198.
- Wollensak, G., Iomdina, E., Dittert, D.D., Salamatin, O., Stoltenburg, G., 2005. Cross-linking of scleral collagen in the rabbit using riboflavin and UVA. *Acta Ophthalmol. Scand.* 83, 477–482.
- Wollensak, G., Spoerl, E., Seiler, T., 2003. Riboflavin/Ultraviolet-A-induced collagen crosslinking for the treatment of keratococcos. *Am. J. Ophthalmol.* 135, 620–627.
- Xue, A., Zheng, L., Tan, G., Wu, S., Wu, Y., Cheng, L., Qu, J., 2018. Genipin-crosslinked donor sclera for posterior scleral contraction/reinforcement to fight progressive myopia. *Investig. Ophthalmol. Vis. Sci.* 59, 3564–3573.
- Yamada, N., Olsen, T.W., 2016. Routes for drug delivery to the retina: topical, trans-scleral, suprachoroidal and intravitreal gas phase delivery. *Dev. Ophthalmol.* 55,

- 71–83.
- Yamamoto, S., Hashizume, H., Hitomi, J., Shigeno, M., Sawaguchi, S., Abe, H., Ushiki, T., 2000. The subfibrillar arrangement of corneal and scleral collagen fibrils as revealed by scanning electron and atomic force microscopy. *Arch. Histol. Cytol.* 63, 127–135.
- Yan, D., McPheeters, S., Johnson, G., Utzinger, U., Vande Geest, J.P., 2011. Microstructural differences in the human posterior sclera as a function of age and race. *Investig. Ophthalmol. Vis. Sci.* 52, 821–829.
- Yang, B., Brazile, B., Jan, N.J., Hua, Y., Wei, J., Sigal, I.A., 2018a. Structured polarized light microscopy for collagen fiber structure and orientation quantification in thick ocular tissues. *J. Biomed. Opt.* 23, 1–10.
- Yang, B., Jan, N.J., Brazile, B., Voorhees, A., Lathrop, K.L., Sigal, I.A., 2018b. Polarized light microscopy for 3-dimensional mapping of collagen fiber architecture in ocular tissues. *J. Biophot.* 11, e201700356.
- Yang, B., Lee, P.-Y., Brazile, B., Sigal, I.A., 2019. Snapshot-polarized Light Microscopy to Visualize and Quantify Collagenous Soft Tissue Microstructure at 156 Frames/second, SB3C - Summer Biomechanics, Bioengineering and Biotransport Conference. Seven Springs, Philadelphia, USA.
- Yang, H., Downs, J.C., Girkin, C., Sakata, L., Bellezza, A., Thompson, H., Burgoyne, C.F., 2007. 3-D histomorphometry of the normal and early glaucomatous monkey optic nerve head: lamina cribrosa and peripapillary scleral position and thickness. *Investig. Ophthalmol. Vis. Sci.* 48, 4597–4607.
- Yang, H., Downs, J.C., Sigal, I.A., Roberts, M.D., Thompson, H., Burgoyne, C.F., 2009. Deformation of the normal monkey optic nerve head connective tissue after acute IOP elevation within 3-D histomorphometric reconstructions. *Investig. Ophthalmol. Vis. Sci.* 50, 5785–5799.
- Yang, H., Thompson, H., Roberts, M.D., Sigal, I.A., Downs, J.C., Burgoyne, C.F., 2011. Deformation of the early glaucomatous monkey optic nerve head connective tissue after acute IOP elevation in 3-D histomorphometric reconstructions. *Investig. Ophthalmol. Vis. Sci.* 52, 345–363.
- Young, R.D., 1985. The ultrastructural organization of proteoglycans and collagen in human and rabbit scleral matrix. *J. Cell Sci.* 74, 95–104.
- Yuan, Y., Zong, Y., Zheng, Q., Qian, G., Qian, X., Li, Y., Shao, W., Gao, Q., 2016. The efficacy and safety of a novel posterior scleral reinforcement device in rabbits. *Mater. Sci. Eng. C Mater. Biol. Appl.* 62, 233–241.
- Yun, S.H., Chernyak, D., 2018. Brillouin microscopy: assessing ocular tissue biomechanics. *Curr. Opin. Ophthalmol.* 29, 299–305.
- Zhang, L., Albon, J., Jones, H., Gouget, C.L., Ethier, C.R., Goh, J.C., Girard, M.J., 2015a. Collagen microstructural factors influencing optic nerve head biomechanics. *Investig. Ophthalmol. Vis. Sci.* 56, 2031–2042.
- Zhang, L., Thakku, S.G., Beotra, M.R., Baskaran, M., Aung, T., Goh, J.C.H., Strouthidis, N.G., Girard, M.J.A., 2017. Verification of a virtual fields method to extract the mechanical properties of human optic nerve head tissues in vivo. *Biomechanics Model. Mechanobiol.* 16, 871–887.
- Zhang, M., Zou, Y., Zhang, F., Zhang, X., Wang, M., 2015b. Efficacy of blue-light cross-linking on human scleral reinforcement. *Optom. Vis. Sci.* 92, 873–878.
- Zhou, D., Abass, A., Eliasy, A., Studer, H.P., Movchan, A., Movchan, N., Elsheikh, A., 2019a. Microstructure-based numerical simulation of the mechanical behaviour of ocular tissue. *J. R. Soc. Interface* 16, 20180685.
- Zhou, D., Eliasy, A., Abass, A., Markov, P., Whitford, C., Boote, C., Movchan, A., Movchan, N., Elsheikh, A., 2019b. Analysis of X-ray scattering microstructure data for implementation in numerical simulations of ocular biomechanical behaviour. *PLoS One* 14, e0214770.
- Zhuola, Barrett, S., Kharaz, Y.A., Comerford, E., Akhtar, R., 2018. Nanostructural and mechanical changes in the sclera following proteoglycan depletion. *J. Model. Ophthalmol.* 2, 14–17.
- Zyablitskaya, M., Munteanu, E.L., Nagasaki, T., Paik, D.C., 2018. Second harmonic generation signals in rabbit sclera as a tool for evaluation of therapeutic tissue cross-linking (TXL) for myopia. *J. Vis. Exp.* 131. <https://doi.org/10.3791/56385>.
- Zyablitskaya, M., Takaoka, A., Munteanu, E.L., Nagasaki, T., Trokel, S.L., Paik, D.C., 2017. Evaluation of therapeutic tissue crosslinking (TXL) for myopia using second harmonic generation signal microscopy in rabbit sclera. *Investig. Ophthalmol. Vis. Sci.* 58, 21–29.

## Glossary of biomechanics

- Anisotropic material:** A material having different material properties in different directions
- Constitutive model:** A mathematical description of a material's stress-strain relationship – i.e. its deformation response to loading
- Creep rate:** Time-dependent strain response of a material subjected to constant load
- Deformation:** A description of the change in shape and size of a continuous body
- Elastic material:** A material that regains its original shape and size when the applied load is removed, without dissipating energy
- Elastic modulus:** A parameter used to define the stiffness of an elastic material
- Equilibrium behaviour:** A stable material state that does not vary in time.
- Finite element method:** Computational method in which Newton's second law is solved for the biomechanics of a complex body by subdividing the body into a number of simpler interconnected building blocks or *elements*. E.g. an FEM model can be used to predict the deformation response of a body given information about its geometry, loading and material properties
- Hyperelastic model:** A constitutive model for an elastic material whose stress-strain relationship can be described mathematically by a *strain energy density function* (a function relating the stored energy of an elastic material to its deformation). The term is often applied to material behaviour under large deformations
- Hysteresis:** A property of a material having different stress-strain curves under loading and unloading. The area bounded by the two curves (the so-called 'hysteresis loop' represents the energy dissipated)
- Inverse finite element method:** An inverse method that uses the finite element approach to calculate unknown parameters from a set of known observations
- Inverse method:** An iterative computational method used to estimate unknown parameters for a set of observations. E.g. unknown material properties of a tissue are computed from known geometry, loading and deformation data
- Isotropic material:** A material having identical material properties in all directions
- Material property:** A physical property of a material that is independent of the size and shape of the tissue
- Non-linear material:** A material whose deformation response is not linearly proportional to the applied load
- Normal force/stress:** Normal forces are applied perpendicular to the surface of a body. The normal stress is the normal force normalized by the surface area. IOP is an example of a normal stress
- Porohyperelastic model:** A model in which a material is described as a highly deformable, porous hyperelastic solid skeleton saturated by mobile fluid
- Shear force/stress:** Shear forces are forces applied parallel to a surface of a body. The shear stress is the shear force normalized by the surface area
- Stiffness:** Intrinsic property of a material describing its resistance to deformation under loading
- Strain:** A measure of local deformation in a material
- Stress:** The distribution of internal forces inside a body subjected to external forces
- Tensile force:** External load that leads to extension of a tissue along the load direction
- Virtual fields method:** An inverse method to extract mechanical parameters from full-field deformation maps
- Viscoelastic material:** Materials that exhibit both elastic behaviour of a solid and viscous behaviour of a fluid. Viscoelastic materials dissipate energy but can recover their original shape when unloaded